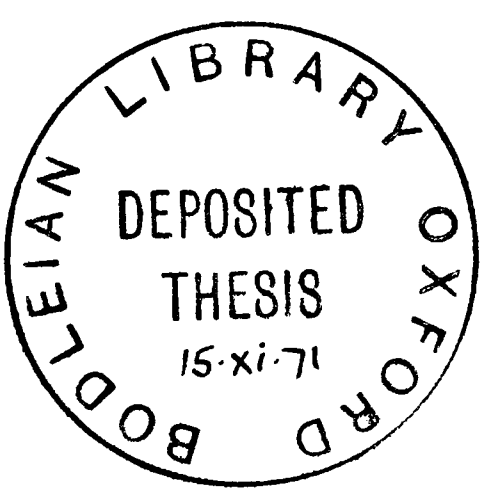
STUDIES OF SOLUTE DISTRIBUTION AT SOLID-LIQUID INTERFACES



R. M. Sharp, B.A.

St. Peter's College

A Thesis submitted for the Degree of Doctor of Philosophy

in the University of Oxford

Department of Metallurgy

Trinity Term 1971

ACKNOWLEDGMENTS

I should like to thank all those people, both inside and outside this Department who have expressed interest in this work. I am particularly grateful to Dr A. Hellawell for his sustained help and encouragement and to Professor P. B. Hirsch for providing laboratory facilities.

I am indebted to the British Steel Corporation for financial support.

Abstract

An attempt has been made in this thesis to put on a sound basis, the relation between interface morphology and distribution of solute in alloys solidifying in a cellular or dendritic manner.

Specimens have been grown under precisely known and regulated conditions and quenching by rapid withdrawal into water has ensured that the solute distribution existing in the liquid has been retained in the solid. Electron microprobe analysis coupled with optical microscopy studies have then been used to give information concerning the effect of growth variables on the nature of the interface.

The results of this work fall into two distinct parts. First, data are presented which relate to the tips of the cells or dendrites solidified under conditions involving convective flow or transport by diffusion only, and with both heavy and light solutes. Second, extensive annealing of the initial structure behind the tips has been investigated to establish the mechanism involved in post-solidification ripening.

It has been found that over the range of experimental conditions used, the amount of lateral segregation produced by cells and dendrites increases with increasing growth velocity and concentration and with a decrease in the value of the imposed temperature gradient. The results suggest that the solute segregation adjusts until the average gradient of liquidus temperature normal to the interface is equal to the imposed temperature gradient. At the same time as lateral segregation increases, there is a gradual change in morphology from simple cells to cells with branches and finally to crystallographic dendrites which have well-developed side arms. Increasing growth rate was found to cause a decrease in the size of branched cells and dendrites. However, the size of simple cells appears to be independent of growth velocity and alloy concentration but is linked to the magnitude of the concentration gradient at the tips.

In specimens in which there is convection in the melt, a boundary layer exists, inside which there is no stirring. Outside this layer the liquid is

fully mixed. The thickness of the layer was found to depend on alloy concentration. and temperature gradient, both variables which affect the magnitude of the density inversion.

Annealing of the cellular structure behind the growth front was found to occur by removal of solute-rich liquid from the cell walls to the cell corners. When the interface plane is (100) or (111) this takes place randomly, but if it is (110), then cell walls disappear preferentially in one direction. The reason for this has been discussed and the conclusion reached that the mechanism causing changes in cell structure is the reduction in surface area of the solute-rich liquid films.

Annealing in the branched cell and dendrite specimens takes place by the disappearance of branches or secondary arms behind the interface, the rate of disappearance depending on concentration and being essentially different for the two morphologies involved. The results presented give the spacing of arms as a function of time allowed for annealing.

CONTENTS

I Introduction 1

II A Review of Solid/Liquid Interface Studies in Metals

1. The Characteristics of a Moving Planar Solid-Liquid Interface 2
2. The Breakdown of a Planar Interface and the Production of Cells 5
3. The Cellular/Cellular Dendritic Transition 10
4. The Morphology and Size of Cells and Dendrites : Coarsening of Dendrites Behind the Interface 12
5. The Causes of Convection and its effect on the Planar/Cellular and Cellular/Dendritic Transitions 18
6. The Conditions Governing the Solute Distribution of Cells and Dendrites 20

III General Experimental Techniques

1. The Alloys Used 24
2. The Production of Quenched Interfaces in Directionally Solidified Rods of Alloy 26
3. Apparatus for Producing Convective Mixing in the Liquid 28
4. Acceleration of the Moving Interface 30
5. Electron-Probe Microanalysis 30
6. Preparation of Specimens for Microanalysis and Optical Microscopy 38
7. The Measurement of Temperature Gradients 39
8. Measurement of Sizes and Radii of Curvature of Cells and Dendrites 41
9. Measurement of Dendrite Coarsening Behind the Interface 44

IV Results

1. The Morphologies of Cells and Dendrites; r and L values 45
2. The Segregation occurring during the Growth of Cells and Dendrites under Conditions of No Liquid Mixing 47
3. The Effect of Liquid Convection 49
4. Acceleration of the Planar Interface through the Breakdown Conditions 53

5. The Coarsening of Cells 55

6. Coarsening of Secondary Dendrite Arms 58

V Discussion

1. Criteria of Growth of a Cellular or Dendritic Interface 61

2. The Effect of Liquid Convection on the Solute Segregation Pattern 64

3. The Scale and Morphology of Cellular and Dendritic Interfaces 68

4. The Coarsening of Cells Behind the Interface 72

5. The Coarsening of Branched Cells and Dendrite Arms Behind the Interface 75

VI Summary of Conclusions 78

VII References 80

I INTRODUCTION

Previous investigators have made exhaustive studies of the nature of solid-liquid interfaces under various conditions, but many of them have been concerned merely with observations rather than with any attempt to understand the underlying reasons why the conditions should have the effect they do. Moreover, much of the initial work was carried out by studying decanted interfaces or sections on specimens which were able to anneal at a high temperature for some time, and may therefore be unreliable.

It is the intention of this work to attempt to provide more information about the reasons why certain morphologies are preferred under given sets of conditions. In order to do this, the technique of electron probe micro-analysis has been used as far as possible to give much needed information concerning the solute distribution at interfaces. Simultaneous with the use of this technique, detailed optical microscopy studies have been carried out, since observed solute distribution and shape and scale of the interface structure are at the same time the cause and effect of each other.

In order to obtain reliable and meaningful quantitative results, specimens were produced under precisely regulated conditions by freezing unidirectionally, and, more important, by permitting only one growth parameter to vary in any series of experiments. In addition, the use of quenched interfaces removed the uncertainty due to using decanted interfaces or sections where extensive annealing had occurred.

This work was started as a Part II thesis, which demonstrated the efficacy of the technique in producing information concerning the growth of planar interfaces. Much of this thesis is concerned with a determination of the solute patterns round cellular and dendritic interfaces, under conditions involving both mixed and quiescent melts. The remainder of it examines the solute redistribution which takes place between the beginning and end of solidification, that is behind the cell or dendrite tips. This redistribution depends on equilibrium considerations and it has a considerable influence in determining what the final observed solidification sub-structure will be.

II A REVIEW OF STUDIES ON SOLID/LIQUID INTERFACES

1. The Characterisitcs of a moving planar solid-liquid interface

When a melt of impure metal or alloy is in contact with solid of the same alloy, the equilibrium concentration of the solute in the solid at the interface is different from the equilibrium concentration of solute in the liquid. This arises from the form of the phase diagram, examples of which are shown in figure 1. The ratio of solute concentration in the solid to that in the adjacent liquid is known as the distribution coefficient (k_o). This parameter can be either less than (figure 1(a)) or greater than (figure 1(b)) unity.

Movement of the interface into the liquid region, equivalent to freezing, involves the deposition of solid of one concentration from liquid of another. This necessitates redistribution of the solute and results in segregation of the solid formed. The segregation will depend on the amount of mixing in the melt but two extreme cases can be identified; that of complete liquid mixing and that of transport of solute being caused by diffusion only. In addition, a third case, that of partial liquid mixing, will be considered.

Freezing under conditions of transport by diffusion only

Tiller, Jackson, Rutter and Chalmers (1953) have considered the segregation of solute during normal freezing under conditions of no liquid mixing. They made the following assumptions.

1. Diffusion in the solid is negligible.
2. The value of the distribution coefficient (k_o) is constant.
3. Convective mixing in the liquid is negligible.

In the case where $k_o < 1$, rejection of the solute atoms into the liquid occurs when the solid freezes and the concentration of solute in the liquid therefore increases. If the initial concentration of the liquid is C_o, then the initial layer of solid freezes with a composition kC_o. Because the liquid concentration rises, the solid concentration must rise proportionately. This it does until a steady-state condition is reached, at the point when the solid concentration is equal to C_o.

Under steady-state conditions the amount of solute rejected from the interface is equal to that diffusing away from the interface into the bulk of the liquid. Consider a volume element bounded by planes of unit area at distances x and (x + dx) from the interface, as depicted in figure 2. Then the amount of solute diffusing into the face x is $D(^{\partial c}/\partial x)_x$ where D is the diffusion coefficient in the liquid at that temperature. The amount diffusing out of face (x + dx) is $D(^{\partial c}/\partial x)_{x + dx}$. The net increase due to diffusion is then $D^{\partial^2 c}/\partial x^2$. The net flow into the same volume element due to freezing is $V\partial c/\partial x$. Under steady-state conditions, and with the interface as the origin of the co-ordinates, these are equal, and $V^{\partial c}/\partial x + D^{\partial^2 c}/\partial x^2 = 0$.

This gives a solution $C_L = (C_I - C_o) \exp (^{-V}/D^x) + C_o$ (1)

where C_L is the concentration of solute in the liquid at point x, and C_I is the concentration in the liquid at the interface. Thus, figure 2 represents an exponential decay of solute concentration, the decay constant of which is V/D.

Steady-state conditions prevail during the solidification of a melt until the length of the enriched region is of the same order as the length of the unsolidified melt. The concentration of the solid then rises continuously as the liquid is progressively enriched.

Effect of Convection on Solute Segregation

If the liquid ahead of an advancing interface is fully mixed, then no solute enrichment peak can exist. The first solid to freeze still has the composition $C_o k_o$, where C_o is the alloy composition, but as solidification proceeds this rises only slightly. The final solute distribution along a bar solidified when there is complete mixing in the melt is given by curve (a) on figure 3. The solid concentration at any point has been calculated by Scheil (1939) to be

$$C_s = C_o k_o (1 - f_s)^{k_o - 1} \quad (2)$$

where f_s is the fraction of the melt already solidified. This equation holds reasonably well until about 80% of the bar has solidified, but clearly as f_s tends to unity, it predicts that the solute concentration should rise to infinity unless the expediency of a variable k_o is included.

Curve (b) of figure 3 shows the solute distribution expected for conditions where transport is by diffusion only and curve (c) shows an intermediate position where there is partial mixing of the melt. Burton, Prim and Slichter (1953a) have analysed this intermediate situation by assuming that mixing is complete in the bulk of the melt and up to a distance δ from the interface. Thus, in their model, the normal solute distribution occurs up to $x = \delta$ and from there the concentration is uniform (figure 4). An expression for k_e, the effective distribution coefficient, $(=C_L/C_o)$ is obtained in the following way.

At a distance $x = \delta$ from the interface the solute concentration is C_o. From equation (1)

$$(C_I - C_s) = (C_o - C_s)\, e^{V\delta/D}$$

$$C_s(1/k_o - 1) = C_s(1/k_e - 1)\, e^{V\delta/D}$$

$$k_e = \frac{1}{1 + (1/k_o - 1)\, e^{-V\delta/D}}$$

$$k_e = \frac{k_o}{k_o + (1 - k_o)\, e^{-V\delta/D}} \qquad (3)$$

A number of investigators have obtained values for the boundary layer thickness δ assuming that equation (3) holds true. They are given in the table below.

Boundary-layer Measurement

δ (μm)	Reference	Conditions
121	Burton et al (1953b)	Czochralski crystal growth
1635	Johnston and Tiller (1961)	Horizontal Tubes
500	Dean, Kerr and Hellawell (1961/2)	Horizontal Tubes
120	Cole and Winegard (1964/5)	Horizontal Tubes
2000	Hellawell (1965)	Horizontal Tubes

Experimental Observation of Segregation ahead of a Planar Interface

Weinberg (1963) has quenched rods of tin-antimony and tin-indium alloys containing radioactive traces, which had been directionally solidified. Each

rod was cut into 5 mm segments after quenching and its activity determined with a scintillation counter. The observed solute distributions were fitted by computer to theoretical expressions obtained for conditions of partial liquid mixing or conditions of no liquid mixing. The values of diffusion coefficient and distribution coefficient were variable in this computer programme in order to get the best fit for the curves. For specimens in which no convective mixing was assumed present, values of diffusion coefficient were of the order of 4×10^{-3} mm^2/sec. Forsten and Miekk-oja (1959) withdrew a crucible from a RF induction furnace at a rate of 45 mms/hour. X-ray absorption photographs were taken of the aluminium-gold alloy inside the crucible while solidification was proceeding. Micro-densitometer studies of these gave a measure of solute content and they estimated, on the basis that there was no convective mixing in the liquid, a diffusion coefficient of 8×10^{-3}mm^2/sec.

Sharp (1968) and Sharp and Hellawell (1969) quenched rods of aluminium-copper alloy during unidirectional solidification through a high temperature gradient. Electron microprobe analysis of these rods gave traces, as in figure 5 of the concentration of copper in front of a steady-state planar interface. For a number of different rates graphs were plotted of $\log(C_L - C_o)$ against x. By making use of equation (1), it can be shown that these should be straight lines whose slope is $(^{-V}/D)$.

$$C_L = C_o + (C_I - C_o) \exp (^{-Vx}/D)$$

$$\log (C_L - C_o) = \log (C_I - C_o) - {}^{Vx}/D$$

Figure 6 shows a number of such lines, for different rates. An average value for diffusion coefficient was given by this method as 3.0×10^{-3} mm^2/sec.

The values of diffusion coefficient as found by all these workers agree generally with those obtained by other methods and summarised by Edwards, Hucke and Martin (1968).

2. The Breakdown of a Planar interface: The Production of Cells

Under certain conditions of growth, it is observed that instead of an interface being planar, it consists of an array of hexagonal 'cells'(figure 7a).

Each cell is bounded by sheets of material which have been enriched in solute (for the case where $k_o < 1$) and thus in longitudinal section cells appear as in figure 7b.

In an attempt to explain the occurrence of this hexagonal array, Rutter and Chalmers (1953) described a possible cause of supercooling in the liquid ahead of a moving planar interface. For an alloy growing with a planar interface the distribution of solute in the liquid is found to be as in figure 5. Every point ahead of the interface has a different concentration of solute, and therefore, according to the phase diagram, a different liquidus temperature. The melt has a definite temperature gradient imposed on it by thermal conductivity considerations, so that under certain conditions it could be possible for the liquidus temperature at a particular point to be higher than the actual temperature. The liquid at that point will then be 'constitutionally supercooled'. Tiller et al (1953) have calculated the conditions under which constitutional supercooling occurs. Figure 8 shows liquidus temperatures as functions of distance ahead of the interface. The dotted lines represent actual temperatures and, it can be seen that a zone of constitutional supercooling (shaded areas) occurs when the tangent of the liquidus temperature curve at the interface is greater than the imposed temperature gradient. The liquidus temperature for any point in front of the interface is given by

$$T_L = T_o - mC_L$$

where m is the slope of the liquidus line on the phase diagram and T_o is the M.Pt. of the pure solvent.

From equation (1)

$$T_E = T_o - mC_o \left[1 + \frac{1 - k_o}{k_o} \exp\left(\frac{-Vx}{D}\right)\right]$$

$$\frac{dT_E}{dx} = mC_o \frac{(1 - k_o)}{k_o} \cdot \frac{V}{D} \exp\left(\frac{-Vx}{D}\right)$$

$$\text{At } x = 0 \quad \frac{dT_E}{dx} = mC_o \frac{(1 - k_o)}{k_o} \cdot \frac{V}{D}$$

For no constitutional supercooling to exist, this must be less than or equal to G_L, the temperature gradient in the melt.

$$\frac{dT_E}{dx} \lessapprox G_L$$

$$mC_o \frac{(1 - k_o)}{Dk_o} \lessapprox \frac{G_L}{V} \qquad (4)$$

Rutter and Chalmers attributed the formation of the cellular substructure to the presence of constitutional supercooling in that any projection at the interface would continue to grow, while rejecting solute laterally. However, Winegard and Chalmers (1954) have pointed out that the existence of a zone of supercooling is not a cause of the cellular substructure. For cells to develop, $^{dS}/dx$ must be positive (S is the amount of supercooling). This is so because if $^{dS}/dx$ is negative any part of the interface which advances ahead of the remainder enters a region of lower supercooling and therefore is retarded. The whole of the interface will in that case tend to advance at the same speed and thus be planar. These two criteria, viz $^{dS}/dx > 0$ and $S > 0$ do work out in practice to be identical since as S is zero at the interface, in order to have a zone of constitutional supercooling at all, it is necessary that $^{dS}/dx$ is positive.

Theories of Perturbation Analysis

The theory of constitutional supercooling, while it seems to predict the experimental phenomena accurately enough, was nevertheless derived from consideration of the interface as being in equilibrium. This is not however the case, as, although the interfacial region is in a steady-state, it is still an open system. The question is then, not which state, solid or liquid, is thermodynamically favourable in the liquid ahead of the interface, but which is state is achievable under the given conditions. To calculate this, it is necessary to take into account heat flow and the production of latent heat at the interface as the liquid freezes, as well as the capillarity effect caused by curving the interface. This latter term in all cases favours a planar interface. A number of workers have attempted to treat vigorously the stability with respect to arbitrary infinitesimal perturbations, of a moving planar interface.

Such perturbations can be of concentration (Delves 1966) or of interface shape (Mullins and Sekerka 1964). The problem is to consider the time evolution of the perturbation and the accompanying temperature and concentration fields, in order to determine whether it grows or decays. Delves shows that the results are exactly those obtained by Tiller et al in the theory of constitutional supercooling, though in some special cases there are deviations.

In the case that capillarity can be neglected, the results of Mullins and Sekerka's analysis lead to a modified constitutional supercooling relation, in good agreement with that of Tiller et al. The modified relation is

$$\frac{\frac{1}{2}\,(K_s G' + K_L G_L)}{K_s + K_L} > \frac{mC_o\,(1 - k_o)\,V}{k_o\,D}$$

where K_s and K_L are the thermal conductivities and G' and G_L the temperature gradients respectively of solid and liquid.

This resembles the original criterion in giving a straight line when the concentration of the solid at breakdown is plotted as a function of G/V. It differs, however, in having a slightly different slope and in having a finite intercept. The bending of the curve to give this intercept is due to the solid/liquid surface tension effect. Diagrams of these curves showing the comparison between constitutional supercooling and the stability theory of Mullins and Sekerka are shown in figure 9.

In the case where capillarity terms cannot be neglected, the analysis leads to the result that there is a critical velocity, which depends on the solid/liquid interface energy, above which instability is impossible whatever the amount of supercooling. Mullins and Sekerka have called this the condition of absolute stability. It can be thought of as occurring when the capillarity effect completely dominates the solute effect, this being true at very high velocities when the scale of transport of the solute is attenuated.

Experimental Studies of the Breakdown Conditions

A number of studies were made to test the original constitutional supercooling criterion. They were conducted by decanting the interface liquid off and examining the surface to see if cells were present. The results were

plotted on a $^{G}/_{V}$ against C_o graph, as in figure 9 (a). A straight line was drawn from the origin so as to separate the points which represented planar interfaces from those which represented cellular interfaces. From the slope of the line a value of diffusion coefficient could be found. These were considered reasonable values and thus the theory was thought satisfactory. Such studies were made on lead in tin by Walton et al (1955), lead, antimony and bismuth in tin by Plaskett and Winegard (1959) and tin, silver and gold in lead by Tiller and Rutter (1956).

These experiments, however, showed that a finite degree of constitutional supercooling was required before instability occurred. A larger degree of constitutional supercooling was found necessary to cause instability using zinc as solute than with lead and a much larger degree with germanium (Bolling, Rutter and Tiller 1956). Bolling and Tiller (1960) pointed out that the magnitude of constitutional supercooling necessary to produce the cellular structure was related to the solid/liquid interface energy, γ_{SL}. They suggested that this was because of a curvature effect, lowering the equilibrium melting point at the interface and therefore stabilising a planar morphology by an appropriate temperature depending on the interface energy. However, the experiments of Bardsley et al (1961) and Hunt, Spittle and Smith (1968) have not confirmed these results. They showed that cellular growth was initiated immediately constitutional supercooling occurred.

The discrepancy may be due to the difficulty of detecting whether the interface is planar or not on a decanted interface. It has been shown by Weinberg (1966) that results from decanted interfaces are not a reliable indication of the morphology of the growth front, though the method is to some extent vindicated as specimens which exhibited cells, elongated cells and no cells on decanted interfaces also showed similar segregation behind the interface.

The stability/instability boundary has not been sufficiently accurately determined to confirm the predictions of Mullins and Sekerka, though all the previous determinations could equally well support this theory as the constants

D and k_o are not known with any precision. One way of uniquely testing the Mullins and Sekerka theory would be to investigate the stability/instability boundary at low values of G/V. It should be possible to detect the variation from linearity of the G/V vs C plot as indicated in figure 9(b).

3. The Cellular/Cellular dendritic Transition

Under conditions corresponding to being well inside the unstable region of figure 9(b) it has been found experimentally that the array of simple hexagonal cells changes to give a structure in which branches appear in the cell boundaries. The branched cells develop into a cellular dendritic structure which will be discussed more fully in part 4, of this section.

The cellular/cellular dendrite transition has not been treated theoretically in the same way as the transition from a planar to a cellular structure, nor have there been the same number of experimental observations. Tiller and Rutter (1956), using alloys of tin in lead, were the first workers to study the transition, which they investigated as part of general observation on cells. They suggested, on the basis of their experimental results, that the transition was orientation-dependent and of the form

$$C_o = A\, G/V^{\frac{1}{2}}$$

where A is a constant which varies with orientation.

Holmes et al (1957) performed similar experiments using lead-silver alloys and found they were able to express both their own results and those of Tiller and Rutter so that the relevant parameters at the point of transition were related by the equation

$$C_o/K_o = A\, \frac{G_L}{V^{\frac{1}{2}}}$$

In 1959, Plaskett and Winegard, in a more extensive investigation using tin-base alloys containing lead, antimony and bismuth, found no orientation dependence of the transition and also that the relationship

$$C_o/K_o = G/V^{\frac{1}{2}}$$

was curved. They did, however, propose, without theoretical justification, that the cell size at transition was significant. The expression they

suggested was of the form

$$L_\theta C_o/k_o = A\, G/V^{\frac{1}{2}}$$

where A is a constant and L_θ is the cell size at transition for a particular orientation.

Coulthard and Elliott (1968) varied the growth rate and temperature gradient independently in alloys of tin and indium in lead and lead in tin. They found that G/V was a more appropriate parameter than $G/V^{\frac{1}{2}}$ and suggested a relationship of the form

$$L_\theta^{\,n}\ C_o/k_o \propto G/V$$

with n equal to 0.5 for the lead-tin system and 1.0 for the tin-lead system.

In order to resolve the apparent discrepancies between the results of these various workers, it is useful to consider the experimental methods involved. All of them used a directional solidification technique in a horizontal furnace and decanted the liquid off the interface after a suitable time.

Carruthers (1968) has shown that convective mixing always occurs when the temperature gradient is not aligned parallel to gravity. The liquid is divided up into convection cells whose length is dependent on the length of the unsolidified melt. Liquid movement perpendicular to the growth direction at the interface makes it difficult for the temperature gradient and growth rate to be measured accurately, as the interface is unlikely to be vertical. In addition, Cole and Winegard (1962) have shown that convective mixing in the liquid can influence the relationship governing the planar/cellular transition and therefore presumably the cell/cellular-dendrite transition.

The criterion for the transition having occurred was taken by all workers as being the first sign of branching in a cell boundary on a decanted interface. However, Weinberg (1966) has demonstrated that the decanted interface morphology is not a reliable indication of the morphology of the growth front.

Davies (1968) has used the experimental evidence available to determine by multiple regression analysis, the exponents b and c in the equation

$$C_o = a\ V^b G^c$$

He found a general lack of significance in his result and concluded that there is no simple criterion for the transition. This conclusion is to be contrasted with the most recent work on the subject, that of Morris and Winegard (1969), using lead alloys, which suggests that the cellular/cellular-dendritic transition is not abrupt, but that the morphology changes continuously.

4. The Morphology and Size of Cells andDendrites : Coarsening of Dendrite Arms

Morphology

The work of Walton et al (1955), Tiller and Rutter (1956) and Holmes et al (1957) showed that a finite "degree of constitutional supercooling" was necessary before cells develop. Tiller (1963) has postulated that there are transition morphologies which develop as a function of the degree of constitutional supercooling. These morphologies were based on observations by Tiller and Rutter.

As the planar/cellular boundary was approached, a pox-like structure, shown to consist of projections on the interface was observed. With more supercooling the interface developed a mixture of irregular cells and pox. As conditions changed further away from the transition, the pox-like projections disappeared and irregular cells increased in number, at the same time becoming more regular. The irregular cells subdivided into elongated cells which finally changed into an array of close-packed hexagonal cells. Figure 10 shows diagrammatic transverse sections of these various morphologies.

The pox-like structure seems to be unconnected with the cells since both could occur at the same time. Spittle, Hunt and Smith (1965) suggested that pox were artefacts due to freezing of the residual layer of liquid left on the interface after decanting, but this is unlikely since there were never seen in the region where a planar interface is stable. Biloni, Bolling and Cole (1966) suggest that the pox structure is an interim substructure not connected with cellular development. These authors have however described a structure of depressions in the interface which they refer to as an array of nodes. The nodes are in a roughly close-packed array and are found to be rich

in solute (in the case of alloys where $k_o < 1$). This is consistent with them being depressions on the interface but would not be consistent with projections. As the growth conditions change, the depressions elongate and join up to give elongated cells. The explanation of the depressions, according to Biloni et al is connected with dislocations emergent at the solid-liquid interface.

The observations of nodes on the interface were supported by the work of James (1966) who examined the morphology of the ice-water interface as it passed through the planar-cellular transition. He noted nodes arranged in wavy rows and observed these to change rapidly into an elongated cell structure. He did not however see any hexagonal cells.

The most recent work on this subject is due to Morris and Winegard (1969b). They solidified alloys of antimony in lead and decanted the liquid off the interface. They found that the crystallographic orientation of the interface had a marked effect on the stable interface morphology. When the growth direction was near <100> or <111>, nodes developed. When it was near <110> direction, elongated cells were present. The plane of the elongated cell boundaries was found to lie parallel to some plane on the {100} zone. As the growth velocity was increased, both the nodes and elongated cell boundaries joined up to form regular arrays of hexagonal cells.

Morris and Winegard observed that the distance between adjacent nodes decreased as the growth velocity increased, suggesting that their spacing was governed by diffusion. They therefore concluded that nodes were not connected with dislocations and would form even if no dislocations were present. They rationalised the observed orientation effect in terms of the influence of interface anisotropy on the initial perturbation. The perturbation most likely to develop would be bound by planes of low energy and low growth kinetics. These would be planes near {111}.

Increasing the concentration or growth rate or decreasing the temperature gradient causes the conditions to pass through the cellular/cellular dendritic transition discussed earlier. The cell walls tend to curve and branched develop. At the same time, Walton and Chalmers (1959) found that crystals of certain

orientation will grow in preference to others. At high temperature gradients, Coulthard and Elliott found that the first branched structure had a flat cell profile in contrast to the pointed tips of the dendrites. They called this a broken-cell structure and suggested that it only occurred when there was extensive mixing of the liquid. The mixing, they argued, would reduce the solute build-up ahead of the interface and increase the lateral diffusion of solute. This could produce an extra concentration of solute in the cell boundary which can only be relieved by branching of the boundaries and the production of broken cells.

Under conditions of more usual temperature gradients and growth rates pointed cellular-dendrites develop, having side-branches at definite crystallographic orientations. These branches are more or less continuous forming webs in the{100} planes. (Figure 11). The existence of the 'plate-like' morphology has been verified by Bowers, Brody and Flemings (1966). It is possible that this type of interface develops when the temperature gradient is small in the liquid so that the latent heat of fusion is conducted into the solid. Then the interconnecting planes would form a better heat-conducting path than would a rod-like array. Because the temperature gradient is small, orientation effects are more important than heat-flow consideration and the structure is strongly crystallographic (Chalmers 1964).

Free dendritic growth, comprising a rod-like arrangement is found when the latent heat is conducted outwards from the growing crystal into the melt. The rate of advance of the growing points is only determined by composition and temperature effects. If an external temperature gradient is imposed this favours conduction of latent heat through the solid and the rod-like arrangement will give way to the plate-like morphology.

Size of Cells

The size of cells on transverse sections has been the subject of a number of experimental investigations and theoretical analyses. The perturbation analysis of Mullins and Sekerka (1964) and extended by Hurle (1969) shows that the size of the first perturbation to grow should be given by the relation

$$\lambda \propto (GV)^{-1/3}$$

Bolling and Tiller (1960) suggest on the basis of their theoretical calculations that the relevant expression is of the form

$$\lambda \propto G^{-1_4} V^{-\frac{1}{2}}$$

Donaghey and Tiller have considered elongated cells only, and under conditions of high temperature gradient, they predict that cell size should increase with decreasing growth rate or concentration and with increasing temperature gradient.

The first experimental determination of cell size was made by Tiller and Rutter (1956), who showed that for lead-tin alloys the cell size is proportinnal to the function $^{L}/GV$. Plaskett and Winegard (1960) found a dependence on the function $^{G}/V^{\frac{1}{2}}$ in tin-base alloys. However, their results were replotted by Coulthard and Elliott (1967) in terms of the parameter $^{L}/GV$ in order to compare them with their own on the same system. The comparison proved difficult to explain as Plaskett and Winegard's cell sizes were up to a factor of four lower. However, all these investigations agreed on the role of compositional effects. Increase of concentration of solute increases the cell size.

Having regard to the variations in these observations, Jesse and Giller have attempted to rationalise the position. They have calculated correlation coefficients for the two possible expressions viz. $\lambda = {}^{a}/VG + b$ or $\lambda^2 V = K$, using the results of other workers. In addition they made measurements on transverse sections of cadmium-zinc alloys. They found that $\lambda^2 V = K$ was the more probable relation, but that this applied only to elongated cells and not to hexagonal cells.

The results of experimental investigations and theoretical predictions are summarised in the table below. A '+ve' dependence signifies an increase in cell spacing with increase in the parameter. A '-ve' dependence signifies the reverse.

Cell Size Dependence

Reference	Growth Rate	Temp Grad	Conc^{n}.	Remarks
Mullins and Sekerka	$1/V^{1/3}$	$1/G^{1/3}$	-	Cell size at breakdown
Donaghey and Tiller	-ve	+ve	-ve	High G. Elongated cells
Bolling and Tiller	$1/V^{\frac{1}{2}}$	$1/G^{1/4}$	-	Elongated cells
Tiller and Rutter	$1/V$	$1/G$	+ve	Horizontal furnaces
Plaskett and Winegard	$1/V^{\frac{1}{2}}$	G	none	Decanted interfaces
Coulthard and Elliott	$1/V$	$1/G$	+ve	Hexagonal Cells
Jesse and Giller	$1/V^{\frac{1}{2}}$	-	-	Elongated Cells on Transverse Sections

The lack of agreement between these results is self-evident.

It is useful at this stage to consider the experimental method of all these investigations. All except that of Jesse and Giller used decanted interfaces and grew specimens in a horizontal direction. The effects of these factors have already been discussed (page 11) Jesse and Giller grew specimens vertically and were careful to use crystals with a fixed orientation with respect to the growth direction. However, the photograph accompanying their work shows that the measurements were made at some distance back from the interface where extensive annealing of the segregation structure has taken place. Weinberg (1966) has shown that cell walls can disappear behind the interface and Hunt, Spittle and Smith (1968b) show extensive solute homogenisation leading to the development of super-cell boundaries associated with dislocation sub-boundaries.

Size of Dendrites

An investigation of dendrite spacing, analogous to those of cell spacings, in that it involved unidirectional solidification, was carried out by Bell and Winegard (1963/4). They varied temperature gradient, growth rate and composition in tin-lead alloys. The functional relation which they found was of the form

$$\lambda = (A - B \ln G)\ (V)^{-n} \qquad (n < 1)$$

where A, B and n increase with composition.

Thus the dendrite spacing, like cell spacing, increases with increase of concentration and with decrease of growth rate and temperature gradient. Adams points out, in a discussion of the paper by Bell and Winegard, that the results given by them can be more simply related by the expression

$$\lambda = \frac{2.43 + 2.01\ C_o}{1000\ \sqrt{CV}}$$

Other investigations into dendrite spacing relate to the spacings of castings which have solidified at a known cooling rate. The results are expressed in terms of cooling rate (equal to the product of growth rate and temperature gradient and expressed in ^{o}C/sec) rather than interface growth rate. They are measurements chiefly of secondary arm spacings, that is the distances between the lateral branches of the dendrite stalk. However, it is not always clear from the photographs accompanying the various papers which spacings are primary and which are secondary.

Michael and Bever (1954) have done the classic work on the measurement of arm spacings. They used aluminium-copper alloys with copper concentrations up to 4.82 wt% and cooling rates from 0.012 to 53^{o}C/sec. The specimens were cylindrical and sections were taken normal to the axes. However, their claim to measure secondary arm spacings is somewhat dubious as measurements were made between spheroidal particles or between divorced θ particles on specimens whose cooling rates were low.

Horwath and Mondolfo (1962) performed similar experiments and obtained agreement with the results of Michael and Bever. They proposed for dendrite spacing a formula

$$S = A\ (GV)^{B} + CM$$

where M is the mole fraction of copper, A, B, C are constants and GV is the cooling rate.

Bardes and Flemings correlated the data available with their own results expressing them as a function of the parameter 'local solidification time' (t) which is the time between the beginning and end of solidification. This is equivalent to the difference in temperature of the dendrite tip and the eutectic divided by the cooling rate.

$$t = \frac{T_{TIP} - T_{EU}}{GV} = \frac{m\,(C_E - C_{EU})}{GV}$$

The empirical relation they found was that

$$\text{arm spacing } \lambda = 7.5t^{0.39}$$

By carrying out isothermal holding experiments and verifying that the law still held for these, where t was the length of time of holding, Kattamis et al (1967a) concluded that the spacing of arms was a function purely of the time available for coarsening. The actual spacing of the arms at their formation was presumably negligible.

The empirical law as determined by them appeared to hold for aluminium-copper alloys over a factor of 10^9 in cooling rate and was only weakly dependent on alloy composition. A similar empirical law appeared to hold for magnesium-zinc alloys (Kattamis et al 1967b). Kattamis et al conclude that the driving force for coarsening is the reduction in surface area. This they show, should theoretically lead to a $t^{\frac{1}{3}}$ relationship. The reason for the value of the exponent being somewhat higher is not known.

5. The Causes of Convection and its effect on the Planar/Cellular and Cellular/Dendritic Transitions

Convection occurs because of density inversions in the liquid, caused by, for example, larger amounts of heavy solute being rejected at a higher position or by hotter and therefore lighter liquid vertically ~~above~~ below colder liquid. In vertical systems there are four possibilities regarding interaction of heat and solute effects causing convection. These are illustrated in figure 12. In (a) both heat and solute fields are directed in such a way as to cause no liquid mixing. In (b) both effects are such as to stabilise convection and steady convective flow will be observed. In (c) the solute field is in a direction so as to cause convection while the temperature distributions tends not to. This situation has been observed by oceanographers and is known as salt fingering (Turner and Stommel 1964, Stern and Turner 1969). Plumes of heavy liquid tend to move downwards through the lighter medium. They lose both heat and solute by diffusion on their way down until they become stable. Such convection gives rise to a layer structure in the liquid, each layer having its

own system of solute fingers. In the case of (d) solute effects tend to stabilise a non-stirred melt, but temperature differences give rise to convection. Hot liquid rises but as heat is lost to its surroundings quicker than solute is, the position is soon reached where the liquid is heavier than the surrounding liquid. Thus vertical convection cells are formed, and as these vary slightly in position, the temperature oscillates. Such temperature oscillations have been observed in metals by Cole and Winegard (1964/5).

In horizontal systems, Carruthers (1968) has shown mathematically that convection always occurs. The liquid is split up into horizontal convection cells whose spacing depends on the length of the melt.

Experimental work by several sets of workers (Cole and Winegard 1964/5), Weinberg (1963), Davis and Fryzuk (1965) has confirmed that convection occurs when temperature inversions are present and begins at a critical value of the temperature gradient. They did not, however, find a marked dependence of the amount of convective mixing on the solute contribution to the density inversion.

Effect of Convection on Planar/Cellular and Cellular/Dendritic Transition

The arguments of the constitutional supercooling theory for planar/cellular breakdown still apply in the case of a melt in which there is partial or complete mixing. However, the appropriate concentration to use in equation (4) is now C_s rather than C_o, the bulk concentration of the melt. This quantity is, of course, variable along the length of the specimens and therefore constitutional supercooling may exist towards the end of a solidifying bar, when it did not exist at the beginning. Hurle (1961) has treated the subject mathematically by combining the Burton et al expression for k_e (equation 3) with the criterion for constitutional supercooling (equation 4).

Delves (1968) has shown by mathematical analysis based on perturbation theory that effective convection in the melt may stabilise a planar interface in the presence of a small amount of constitutional supercooling. Hurle (1969) reworked Mullins and Sekerka's perturbation treatment for stirred melts. He found that in the case where δ is much greater than the breakdown cell size the convection has no effect at all. Where δ is much smaller than the breakdown cell size the analysis predicts the same conditions for breakdown except that the

condition of absolute stability which exists for non-stirred melts is not now found. The cell size dependence predicted bythis theory changes from a $(GV)^{-1}{}_3$ dependence to a $(GV)^{-1}$ dependence, but no correlation with experimental results has been found. However, this is not surprising since the lowest value of δ which has been observed is 120 μmand not smaller than the values of cell size normally encountered.

Ihe influence of convection on the cellular/cellular dendritic transition has never been investigated and since the criterion for the transition is not understood it is difficult to conjecture whether or not the presence of stirring in the melt will make any difference.

6. The Conditions Governing the Solute Distribution of Cells and Dendrites

The solute distribution of cells and dendrites is a complicated mathematical problem which has not yet been successfully solved. A comprehensive review of the subject is outside the scope of this work but it may be useful to consider the principles involved in the analysis. There are two distinct aspects of dendritic growth; firstly the initial growth of the tip, and secondly the thickening of the dendrite arms.

Growth of the Tip

We must first consider in general terms the growth of the dendrite tip, The pure bulk material has a melting point T_o (figure 13). Because the tip is curved, its melting point is lowered by an undercooling due to curvature equal to $2\gamma_{SL}/r\Delta s$ where r is the radius of curvature of the tip and Δs the entropy of fusion. There is then some undercooling, δT due to solute accumulation, lowering the interface temperature to T_I. The value of δT will depend in some way on the radius of curvature of the tip since this will control the efficiency of lateral segregation. It is possible to consider an undercooling due to the difficulty of actually incorporating atoms into the solid. This, so called kinetic undercooling, is, however, very small for metals. T_B is the bath temperature, the bath/^{under}cooling ΔT^* controlling the rate of removal of latent heat into the liquid.

One of the difficulties in the analysis of dendritic growth is that

assumptions must be made concerning the shape of the dendrite tip. The earliest model was that of Ivantsov (1947), who chose as his shape a stick of solid with a tip in the form of a paraboloid. The dendrite tip was assumed to be all at the same temperature and growth was controlled by the rate of transfer of heat away from the interface. Ivantsov produced an expression for growth velocity but his analysis prediced that any radius could apparently exist in a given situation, clearly unsatisfactory.

Since then, mathematical models have had to make a further assumption based on intuition rather than proof, in order to produce a unique solution. Temkin (1960) repeated Ivantsov's treatment using the assumption that dendrites grow at the fastest rate possible in a given environment. He realised that curvature at the tip of a dendrite implied that there must be a variation in temperature round it, and that Ivantsov's assumption of an isothermal dendrite was incorrect.

Kirkaldy's (1959) assumption is that the interface grows so as to maintain the minimum rate of entropy production. This, however, is not correct in that it presents the optimum thermodynamic state of the system but does not indicate the probability of reaching it in a finite time. It would for example never predict planar interface growth (Tiller 1959).

Bolling and Tiller manipulate the contributions in the total undercooling (figure 13) in terms of the growth conditions, tip shape and dendrite dimensions and make the assumption that the interface temperature will be a maximum. This enables them to predict a value for the effective distribution coefficient at the dendrite tip. Kotler and Tarshis (1968) have lately, however, pointed out that there are a number of mathematical errors in the treatment of Bolling and Tiller. They themselves have applied the Temkin analysis successfully to the results of Lindenmayer (1959) on ice-water systems.

Oldfield (1968) has studied the growth of dendrites numerically using computer solutions, by dividing the region round a dendrite into compartments and solving a heat-flow conservation equation for each. Diffusion of solute can, in principle be incorporated by superimposing a network of compartments

for solute conservation, but that has not yet been done. Oldfield found that there is no unique growth velocity for a particular tip radius. He predicts an oscillatory mode of growth of the tip leading to dendrite arms being produced. The development of these branches has not yet been successfully studied.

Horvay and Cahn (1961) have produced equations derived for the steady-state growth of a parabolic platelet. They, like Ivantsov, assume a simple model in which the dendrite is isothermal. Glicksman and Schaefer (1968) have shown that by substituting in these, measured values of radii of curvature of the tips at a given growth velocity, they could obtain excellent agreement between theory and experiment for the velocity of dendrites as a function of melt supercooling. Apart from these results, the various dendrite growth analyses have not been verified experimentally.

Thickening of Dendrites

The theoretical treatment for the thickening of dendrite arms is due to Brody and Flemings (1968). They consider a 'volume element' positioned as in figure 14, so that the bottom side is coincident with the centre of a primary dendrite arm and the top side coincident with the line equidistant between two dendrites. In the time between passage of the dendrite tip and the end of freezing, this volume element will have solidified from bottom to top. They apply equation (2) to the volume element and can thus give values of concentration of the solid and liquid at points down the dendrite stalk

$$C_s = C_o K_o (1 - f_s)^{k_o - 1}$$

The assumptions implicit in the use of the above equation include a requirement that no solute flows into or out of the volume element and that diffusion inside it is complete.

The second of these assumptions has been open to some contention, because it is believed by some workers that there are concentration gradients between dendrite arms. Kohn and Philibert (1960) have quenched solidifying castings and made micro-analysis measurements across the solid-liquid interfaces. Both their results and similar results of Doherty and Melford (1966) show solute

enrichment and an exponential decay of solute. However Subramanian et al (1966) have quenched ingots where no segregation would be expected and still obtained enrichment. They suggest that transient acceleration of the growth front caused by the quench has produced the solute distribution. The existence of the transient solute distribution at quenched interfaces has also been discussed by Sharp and Hellawell (1969).

Bower, Brody and Flemings (1966) have calculated the weight fraction of eutectic expected by application of their analysis and compared this with the experimental results of Michael and Bever. They find good agreement.

Cell Growth

In the case of the growth of cells, most of the solidification takes place at the cell tips and the subsequent growth of the enriched groove regions is of lesser importance. Kramer, Bolling and Tiller (1963) have obtained experimental results concerning the solute distribution at the tips of the cells. They used thermocouples in specimens of tin lead alloy. Measurement of the temperature at the tips gave solute concentration by reference to the phase diagram. They calculated the solute concentration expected by conservation of solute principles for a given value of the parameter $^{G}/_{VC}$ and a given cell geometry. Cell geometry was determined experimentally by decanting the liquid off the interface. Reasonable agreement was obtained between the predicted values of solute concentration and the experimental values, though there was a considerable scatter in the points. Results were expressed in terms of k_e, the effective distribution coefficient (equal to the concentration of solute at tips of the cells divided by the bulk liquid concentration). k_e was found to vary between k_o and 1 over a factor of about 10^2 in the value of the parameter $^{G}/_{VC}$.

III EXPERIMENTAL TECHNIQUES

1. Alloys Used

The alloys used in these investigations were taken from three binary alloy systems; aluminium-copper, aluminium-silver and aluminium-magnesium. The materials used were as follows, given with their densities in the liquid state.

			ρ (Smithells 1962)
Aluminium	'Super. raffinol'	99.999% Al	2.37
Copper	'Specpure' rod	99.999% Cu	8.96
Silver	Silver foil	99.999% Ag	10.5
Magnesium	'Specpure' crystals	99.999% Mg	1.57

Portions of the relevant phase diagrams are shown in figure 15 (Hansen 1958). A number of observations and comments on these systems are given below.

(a) Aluminium-copper system

The phase diagram shows the liquidus and solidus lines as straight, thereby giving a constant value for k_o. The limit of solid solubility is 5.7 wt% and the composition of eutectic, 33.0 wt%. The eutectic temperature is 548°C.

Values for the slope of the liquidus line (m) and the distribution coefficient as estimated from the phase diagram are:

$$m = 3.24^{\circ}C/wt\%$$

$$k_o = 0.17$$

(b) Aluminium-silver system

The phase diagram (figure 15b) for Al-Ag has curved liquidus and solidus lines, leading to variable values for liquidus slope and distribution coefficient. However, plotting the phase diagram in terms of weight percentage gives a straight liquidus line (figure 16) whose slope is

$$m = 1.3^{\circ}C/wt\%$$

The solidus line of the phase diagram was thought to be probably incorrect and values of k_o were determined by electron microprobe analysis of a number of alloys of various compositions in which liquid and solid in equilibrium were

produced at either side of a quenched interface. Calculations to position the solidus line in this system were also made by substituting numerical values into Van t'Hoff's expression. This expression is strictly only applicable at low values of composition, but, for interest, higher values were also substituted in it.

Van t'Hoff's expression is:

$$\frac{dx_l}{dT} - \frac{dx_s}{dT} = \frac{L}{RT_o^2}$$

in which L is the latent heat of fusion, T_o is the melting point of the pure solvent (in degrees absolute), R is the gas constant, dx_s dx_l are the concentrations of solid and liquid respectively which produce a lowering of the melting-point equal to dT.

Assuming that the liquidus line of the phase diagram was correct, values of dx_s were obtained using this equation. These gave a position for the solidus which agreed fairly well with the experimental results produced by microprobe analysis. Figure 17 shows k_o values for the aluminium-silver system obtained over a range of compositions, both by calculation and by experimental determination. Where values for k_o were required, they were taken from this plot.

(c) Aluminium-magnesium system

Aluminium-magnesium alloys were used for specimens in which it was required that the solute was lighter than the solvent (cf densities given previously).

The phase diagram (figure 15c) gives a value for the solid solubility limit of magnesium in aluminium as 17.4 wt% Mg. If the phase diagram is assumed to be essentially correct, then the liquidus slope and distribution coefficient are given by

$$m = 5.0^{o}C/wt\%$$

$$k_o = 0.3$$

2. The Production of Quenched Interfaces in Directionally-Solidified Rods of Alloy

(a) Filling of tubes with alloy

In order to obtain rods of alloy inside thin-walled, small diameter alumina tubes, a vacuum technique of filling them was employed. The components of the alloy were weighed out in the appropriate proportions and heated under vacuum for some hours in an alumina crucible at about 800°C. The melt was then allowed to cool down and solidify. Alumina tubes (inside diameter 2mms, outside diameter 4mms) were made to rest vertically on the alloy with their open ends downwards, by passing them through holes on a specially drilled stainless steel block. This block was positioned on top of the crucible, the whole apparatus being fitted together as in figure 18.

Crucible, block and tubes were suspended inside an evacuated furnace at 800°C. When the alloy melted, the tubes slipped down into it and opening of the furnace tube to air forced metal up into them. The apparatus was then lifted out of the furnace and the tubes removed before the alloy resolidified. Filling the tubes by this method ensured that there were, by and large, no air gaps which would have led to the formation of large bubbles in the alloy.

(b) High Temperature Gradient Apparatus

High temperature gradients were required in order to obtain cellular and dendritic specimens at reasonable traction rates and also to produce an interface which was flat on a macroscopic scale. They were produced by positioning the alumina tube which contained the alloy so that it was surrounded by water just below the hottest part of the furnace. The apparatus which was used initially to do this is shown in figure 19 and the details of the top part of it in figure 20. The brass water-jacket cools the water in the inside tube. This water is kept at a constant height using a constant head supply and it is intended to cool the lower end of the specimen, with which it is in contact. A brass cone is fitted in the top of the water-jacket, to reflect heat into the furnace and thus to prevent the water from boiling.

The specimen tube itself fits into the top of a silver steel rod which passes through the middle of a threaded brass tube. Tube and rod are clamped together at the lower end and rotation of the tube with a synchronous motor, as shown, causes it to move up and down at a regulated and known speed through a tapped P.T.F.E. plug. The whole assembly is mounted under a vertical platinum resistance furnace.

This piece of apparatus was successful for moving the solid-liquid interface at low rates, but for high rates of growth, the synchronous motors available were found to have insufficient power to turn the screw thread evenly. A larger motor was therefore subsequently employed, using a flexible drive shaft to transmit the drive and worm reduction gear-boxes which were interchangeable to vary the rate of movement of the interface.

Eventually it was decided to rebuild the apparatus in order to accommodate a larger motor which had a continuously variable speed. The new apparatus was also designed to prevent precession of the specimen which is inevitable if the specimen tube is slightly bent and is made to rotate.

This modified apparatus and drive mechanism are illustrated in figure 21. The steel rod in which the specimen is fixed passes through the middle of a steel tube and is clamped to the base-plate. The steel tube is clamped to a threaded brass tube and O-rings prevent water leakage. These two tubes are quite free to rotate without the steel rod or specimen doing so. At the lower end of the steel tube a gear wheel is fixed and this is driven by a worm. A further worm reduction gear-box transmits the drive from an Evershed and Vignoles motor. The motor is mounted on the base-plate and, on account of its size, is balanced by using a pulley system and a large steel counterweight. Employing this set-up, the speed of up and down movement of the threaded brass tube is continuously variable up to a speed of 0.7 mms/sec. As in the initial piece of apparatus, the brass tube was driven through a P.T.F.E. plug, but this latter was found to wear easily. As a substitute, nylon was tried since it has much more strength than P.T.F.E. However it was not possible to obtain a tight fit round the thread without the nylon sticking and seizing up. P.T.F.E. was there-

fore still used, but it had to be replaced at intervals.

A more general view of the apparatus is shown in figure 22. The furnace was mounted vertically upside-down and equipped with two platinum windings in order to give a long and uniform hot zone. Its maximum temperature was 1500°C and it was controlled by means of an Ether temperature controller. The circuit was arranged so that if the temperature was above the required value, then the furnace was supplied with about two thirds of the full current. The box above the temperature controller contained electronic equipment necessary for regulating the motor speed. Its construction and function will be explained in part 4 of this section.

(c) Growth and Quenching of Specimens

Specimen tubes were fitted into the top of the steel rod and pushed up into the furnace. After allowing a few minutes for equilibrium to be reached inside the specimen, the motor was switched on so that growth of solid proceeded at a particular rate. The specimens were quenched after growth of between two and four centimetres.

Quenching was effected in both the later and earlier apparatus by loosening the screw clamping together the brass tube and its insert and pulling the latter down so that the specimen came quickly into contact with the water already surrounding its lower end. The efficiency of this method of quenching, in retaining in the quenched liquid the solute distribution as it existed in the liquid, has already been demonstrated (Sharp 1968).

3. Apparatus for producing Convective Mixing in the Melt

Convective mixing was produced in the melt by two methods. One of these was to use a solute which was lighter than aluminium (viz. magnesium) and the other involved using a heavier solute (copper) but reversing the direction of growth of the interface.

(a) Lighter Solute

When using magnesium as a solute, exactly the same procedure and apparatus were used as previously described. Filling the tubes, however, required that nearly an atmosphere of argon was used when the metal was molten, in order to

reduce the vaporisation of magnesium.

Wider tubes (4mms internal diameter, 6.5mms external diameter) were used in these experiments, since the maximum velocity of convective flow is known from Poiseuille's equation to increase as the square of the tube diameter.

(b) Reversal of Growth Direction

The purpose of reversing the growth direction was to cause hotter liquid to lie below cooler liquid and also to have heavier solute rejected from a downward moving interface. The apparatus required is equivalent to an inverted form of the assembly used for experiments in which no convective mixing was required in the melt. However, since water could obviously not be used in such a position, an alternative method had to be devised which gave high temperature gradients and also an efficient quench.

The apparatus used is shown diagrammatically in figure 23. It fitted into the top of the same platinum resistance furnace used previously and specimens were made to slide inside a closely fitting, thin-walled copper tube. This tube was surrounded by a brass water-jacket. It was found that the alumina tubes supplied are often somewhat bent at their sealed-off ends and it was necessary, therefore, to use their other ends in order to be able to slide them easily through the tight-fitting copper tube. Accordingly, the open ends of the tubes were sealed by carefully heating them in a very hot oxy-coal gas flame, so that they kept their straightness right to the end. The end which had been closed in this way was pushed down through the apparatus into the furnace and fitted tightly into a long shaft which was connected to the traction device previously described. The shaft was made of an alumina tube so as to withstand the high furnace temperature without distortion.

Growth of the interface was produced by driving the specimen tube in an upward direction. Quenching of specimens in this apparatus was carried out by pulling them out through the copper tube. Surprisingly, this seemed to produce almost as efficient a quench as pulling them down into water, as evidenced by the scale of the dendritic segregation in the quenched region.

4. Acceleration of the Moving Interface

It has already been mentioned (page 27) that the motor used was capable of maintaining accurately any speed, giving continuously variable specimen traction rates of up to 0.7 mm/sec. The method of keeping the number of revolutions per second of the motor constant depends on balancing the output from a generator, whose shaft is integral with that of the motor, against a stable potential. A stabilised D.C. potential is produced by a power supply and the magnitude of this potential is variable up to 63v, being controlled by a potentiometer. If the output from the generator has a lower potential than the stabilised power supply then the current to the motor is stepped up by a servo-mechanism. If the potential output from the generator is higher, then the motor current is decreased. Thus a steady speed is maintained which is directly proportional to the generator voltage and can thus easily be measured.

In order to accelerate the specimen, it is necessary to change the position of the potentiometer controlling the magnitude of the stabilised D.C. potential. Linear movement of this potentiometer gives constant acceleration. An attachment was therefore devised to give constant acceleration by driving the shaft of the potentiometer with a synchronous motor. By interchanging different synchronous motors, acceleration rates could be made to vary between 5×10^{-3} $\mu m/_{sec^2}$ and 2.5×10^{-1} $\mu m/_{sec^2}$.

5. Electron-Probe Microanalysis Techniques

(a) Description of the Instrument

It was Castaing (1951) who first investigated the possibility of using a high energy (up to 50 keV) beam of electrons to analyse the surfaces of materials. Subsequently, Duncumb and Melford (1959) improved this technique by incorporating facilities which made it possible to scan the electron beam over an area on the specimen.

When an electron beam is incident on a surface, some of the electrons are absorbed and some are backscattered, the ratio of these being dependent on the atomic number of the material of the surface. A current can then be

measured between the specimen and earth which will depend on the composition of the specimen. Scanning the focussed beam over an area which contains different phases gives a variable current and, if this is backed off, amplified, and made to modulate the intensity of an oscilloscope beam whose scan is linked to the beam scan, then a picture of the specimen surface is built up. Such a picture will have a magnification which depends on the area of the specimen which is scanned. The resolution of the picture will be of the order of the size of the scatter of the electron beam in the specimen, about 1 μm.

Electrons of high kinetic energy striking atoms cause the inner atomic electrons to move into higher energy levels. As these electrons drop back into their low energy positions, X-rays are produced, the wavelengths (λ) of which are linked to the atomic number (z) of the atoms by Moseley's Law.

$$1/\lambda = k(Z - \sigma)^2$$

where k is a constant which depends on the electron shells involved in the transition and σ is a constant incorporated to take account of the screening of the unaffected electrons.

Thus, for any particular electron transition, there is a unique wavelength for each element of the periodic table. Taking into account other possible electronic transitions, each element will have a spectrum containing a number of peaks at different X-ray wavelengths.

The electron probe X-ray microanalyser is equipped with spectrometers to pick out the wavelength of X-rays which it is required to investigate. A number of crystals of differing interplanar spacings are necessary in order to cover the range of possible wavelengths. Even so, for higher atomic number elements (Rb upwards) the inner shell transitions (K lines) are at too low a wavelength, and higher shell transitions (L and M lines) are employed.

The required wavelength is diffracted by the selected crystal into a gas flow proportional counter. This consists of a tube with a wire down its centre, the potential difference between these being of the order of 2kV. Gas (90% argon; 10% methane) is circulated through these counters at a

pressure of one or two atmospheres depending on the energy of the X-rays. Hard X-rays require a higher pressure to absorb them than do soft X-rays. Windows separate the counters from the evacuated chambers in which they are placed, while allowing the X-rays through. Such windows are made of thin beryllium sheet for high energy X-rays and mylar film for those of low energy. For the elements below oxygen in the periodic table, a 200 mμm collodion film is used.

Each X-ray photon which is absorbed by the gas produced an "avalanche" of argon ions. This allows a current to pass between the tube and wire, the amplitude of the pulse being a measure of the energy and therefore the frequency of the photon. The pulse lasts for only a few ~~milli~~micro seconds, its energy being curtailed by the molecules of methane present as a quenching agent.

Since the pulse height is a measure of the wavelength of the X-rays, it is possible to discriminate further to cut out electronic noise and pulses from X-rays of different wavelengths. This is done by amplifying the pulses and electronically selecting only pulses of a given height range, using a pulse height analyser.

Pulses can be counted using a scalar counting device, or integrated to give readings on a rate-meter or pen recorder. Alternatively they can be made to give points of light on an oscilloscope screen. Using this method it is possible to build up a scanning picture whose contrast is produced by difference in emission of X-rays of a particular wavelength over the area covered.

(b) The Interpretation of X-ray Intensities

In order to obtain a quantitative estimate of the concentration of any given element in a specimen, it is necessary to have a standard of known concentration (usually 100%) to compare it with. Then, approximately, the ratio of the numbers of counts per second produced from the specimen to that from the standard under the same conditions is equal to the ratio of their concentrations. By making a number of corrections, this approximate connection can be improved. These corrections are set out below.

i) Correction for background

Not all of the X-rays produced are formed from electron re-arrangement inside atoms. There is a continuous spectrum, the so-called 'white radiation' which arises from elastic collisions between electrons and atoms. In addition, noise and cosmic rays contribute to the observed number of counts per second. It is important to subtract these contributions from the peak reading to obtain only the 'characteristic radiation', i.e. that produced from the electronic transitions. This can be done by moving the X-ray spectrometer off the characteristic peak for both specimen and standard and thus measuring the number of counts per second produced as background intensity. Alternatively, background count rates may be determined by taking measurements on the pure standard of a secondary component of the specimen (e.g. on a standard of pure aluminium when analysing for copper in Al-Cu alloys). This latter method is probably less accurate but has the advantage that spectrometer settings do not need to be disturbed.

ii) Correction for dead-time

The counting mechanism has a dead-time inherent in it of ten micro-seconds. This means that when one X-ray photon has entered the counter then no other can be counted inthe next ten microseconds. Thus, if N_A is the number of counts per second counted, the amount of time in one second during which the counter is not receptive is $N_A \times 10^{-6} \times 10$ seconds. The observed count-rate must therefore be corrected for this dead period as follows

Length of time of counting = 1 second

Length of time counter is receptive = $1 - (N_A \times 10^{-5})$ seconds

$$\text{True count rate} = \frac{N_A}{1 - 10^{-5} N_A}$$

Thus, if the apparent count rate is 10,000 c.p.s., there will be a 10% loss of counts because of the effects of dead time.

iii) Atomic number correction

The correction for atomic number differences between specimen and standard arises for two reasons. Firstly, at elements of high atomic number a smaller number of electrons are back-scattered than from those of low atomic number.

This means that more electrons are effective in causing excitation in a matrix of a heavy element. However, this effect is offset by the second contribution to the atomic number correction, which is connected with the depth of penetration of the electrons into the material. Light elements are unable to slow down electrons as quickly as can heavy elements. Thus, where the matrix consists predominantly of a light element, the electrons can penetrate in further and retain the energy necessary for exciting X-rays for a longer distance.

Castaing (1963) has shown a treatment for the quantitative treatment of atomic number effects. He considers the penetration of an electron into a target. For an element i, of density ρ_i , the energy loss experience by an electron as it moves along a path of length dx is

$$dE = S_i \rho_i f(E)\, dx$$

where S_i is the 'stopping power coefficient' which varies with atomic number, and f(E) is a function of the energy of the electron. For an alloy of average density ρ, the energy loss is given by

$$dE = S_{alloy}\, \rho\, f(E)\, dx$$

where $S_{alloy} = \Sigma\, C_i S_i$

C_i is the concentration of element i.

He shows that the relative X-ray intensity (i.e. the ratio of the intensity of X-rays from the element A in the specimen to the intensity from a standard of pure A) is related to concentration of A in the specimen by the formula

$$\text{Relative X-ray Intensity} = \frac{I_A}{I(A)} = \frac{S_A C_A}{\Sigma S_i C_i}$$

This expression assumes, however, that all electrons are absorbed and will therefore excite X-rays. If R is the fraction of the beam which is not back-scattered then a corrected relationship is

$$I_A/_{I(A)} = \frac{C_A S_A}{R_A} \div \Sigma \frac{S_i C_i}{R_i}$$

The ratio $\alpha = S/R$ is known as the 'effective current factor' and was approximated to unity by Castaing, though others have shown that this is not valid, and that the deceleration (s) term is predominant.

iv) Absorption Correction

Different elements absorb X-rays to a different extent so that a correction must be made to account for the variation in the proportion of X-rays absorbed in different matrices. The calculation must take into consideration the X-ray take off angle variation between different microanalysers and also the depth of penetration which depends on atomic number.

Castaing has defined a factor, on which absorption depends. This is applicable at only one accelerating potential, but it does take into account the take-off angle of the X-rays, (θ). The factor is given by $f(\chi)$ where

$$\chi = (\mu/\rho) \text{ cosec } \theta$$

where μ/ρ is the mass absorption coefficient.

Then the mass concentration C_A can be expressed in terms of a function of this parameter χ. For a binary system

$$C_A = \frac{I_A}{I(A)} = \frac{f_A(\chi_A)}{f_{AB}(\chi_{AB})}$$

Philibert (1963) has shown that the function of χ ($f_{(\chi)}$) can be approximately expressed by the formula

$$f(\chi) = \frac{1}{\left[1 + \chi/\sigma\right]\left[1 + h(1 + \chi/\sigma)\right]}$$

where $h = \sigma/K$

$K = 0.58 \times 10^{-6} \; Z^2/A \cdot 1/V^2$

σ = Lenard coefficient (varies with accelerating potential V)

A = atomic weight

Z = atomic number

The parameter h is found to be approximately given by $h = 1.2 \, A/Z^2$

Substituting a parameter u, defined as $\mu = (1 + \chi/\sigma)$, Philibert's expression becomes $1/f(\chi) = u(1 + hu)$.

This treatment of Philibert's does not take into account the variation in depth of penetration of electrons caused by atomic number dependence and its effect on the absorption correction. Thomas (1964) has modified the χ factor to incorporate these effects of atomic number variation. She does this by summing the absorption factors for all the components to give a composite χ- value.

$$\chi = \frac{(\mu/\rho)_i \, C_i \, \text{cosec}\, \theta}{C_i \, \alpha_i/\alpha}$$

with α defined as before.

i.e. for a binary system

$$\chi = \frac{(\mu/\rho)_A \, C_A + (\mu/\rho)_B \, C_B \, \text{cosec}\, \theta}{C_A\alpha_A/\alpha_A + C_B\alpha_B/\alpha_B}$$

$$= \frac{(\mu/\rho)_A \, C_A + (\mu/\rho)_B \, C_B \, \text{cosec}\, \theta}{C_A + C_B/\bar{\alpha}}$$

where $\bar{\alpha} = \alpha_B/\alpha_A$

Then for the absorption correction above

$$I_A/I(A) = \frac{f(\chi)_{specimen}}{f(\chi)_{standard}}$$

For both atomic number and absorption effects (iii and iv)

$$I_A/I(A) = \frac{f(\chi)_{specimen}}{f(\chi)_{standard}} \times \frac{C_A}{C_A + C_B/\bar{\alpha}}$$

v) Fluorescence correction

X-ray fluorescence is caused when X-rays excite atoms in the same way as electrons do, thus stimulating production of X-rays characteristic to the transitions of the excited atom. Fluorescence can be caused by either continuous or characteristic radiation and it can be produced from a volume much larger than that penetrated by the electron beam. The true intensity of X-rays can be reduced or enhanced by fluorescence effects, depending on the relative characteristic wavelengths of the component elements of the specimen. Castaing (1951) has shown that the magnitude of the fluorescence effect for a particular component depends on the ratio of its mass absorption coefficient at the characteristic wavelength of another component to the mass absorption coefficient of the alloy at the same wavelength. This ratio is particularly high when the two component elements involved are next to each other in the periodic table.

For most pairs of elements, however, the fluorescence correction is small

compared with the absorption and atomic number effects previously described and can often be ignored.

c) Techniques employed in Microanalysis

All the microanalysis described in this work was carried out on a Cameca Mk II MS 46 instrument. This particular microanalyser has the following standard facilities, which were made use of as the occasion demanded.

Point Counts: The specimen was placed under a well-focussed beam of electrons (about $\frac{1}{2}$ μm diameter) and the number of pulses which were counted by the scalar counter in ten seconds recorded. In general, this measurement was repeated a number of times and then compared with similar measurements made on a standard. The standards used were the pure metals, copper, silver and magnesium.

Line Counts: Where an average intensity of X-rays was required, as for instance over a two-phase region, the electron beam was made to scan over a line in the Y-direction. Scanning in this way is caused by deflecting the beam electrostatically so that it changes direction with a frequency of 100 cps. The length of the line can be controlled manually up to a maximum of 300 μm. Deflecting the beam in the Y-direction in this way does not defocus the spectrometers as it would if the beam were defocussed in the X-direction or if it were simply increased in size. Line counts obtained by recording scalar readings over periods of ten seconds were compared with point counts on standards in the same way as previously.

Point and Line Scans: It is possible to drive the specimen at a fixed rate in either X or Y directions using an external motor-drive attachment. This can be done with the beam either as a spot or a line and continuous records of intensity are produced as functions of distance by integrating the pulses and connecting the rate-meter to a pen recorder. With a fixed chart speed and a fixed rate of movement of the specimen, a distance scale can be calculated for the chart. Point scans and line scans do not give the accuracy which is obtained from counting pulses in a given time interval, but they do provide a permanent visual record of analysis over large distances.

In the following sections, when microanalysis results are quoted, these four terms, point counts, line counts, point scans and line scans will be used without further definition.

Correction Procedure: Correction of the intensity ratio values as described in part (b) was carried out using the procedure of Thomas (1964). According to the survey of correction procedures carried out by Poole (1967), this procedure gives reliable results. The expression for this was developed into a computer programme and data tapes giving values of the constants involved were punched out for each system (Al-Cu; Al-Mg; Al-Ag). The expression is simplest when working from a true value of concentration to the uncorrected value:-

$$C_A = \frac{k}{(1-k)\alpha + k}$$

where

$$k = \frac{I_A}{I(A)} \times \frac{f(\chi)_{standard}}{f(\chi)_{specimen}}$$

If it is done the other way round, then a process of successive approximations is necessary.

True values, at intervals of 0.01% over the composition range involved, were therefore inserted into the programme and the computer was instructed to prepare tables showing corrected and uncorrected values side by side.

Thus, for a point count or a line count, when the intensity ratio had been determined, and background and dead time effects corrected for, the true value of concentration could be found by simply consulting these tables.

6. Preparation of Specimens for Microanalysis and Optical Microscopy

(a) Mounting

When the alumina tubes containing the alloy rods had been quenched and removed from the apparatus used for pulling them at a fixed rate, they were broken up in order to remove the specimens of alloy. These were inserted into a bath of acid so that the position of the quenched interface would show up. A portion of the rod about twenty millimetres long was cut out from the interface region and mounted in plastic resin. In the case of specimens required for microanalysis, it was necessary to use resin which contained copper powder to prevent them charging up under the electron beam. Otherwise specimens

were mounted in a clear non-conducting resin.

(b) Polishing and Etching

The mounted specimens were polished on four silicon carbide papers of successively finer grades and finally on diamond wheels. The finish obtained was that produced from polishing on a wheel using 1 μm diamond paste. Specimens which were intended for microanalysis were not etched. This was for two reasons. Firstly, the action of an etchant is to dissolve parts of the surface preferentially and this would mean that an incorrect value for concentration would be obtained at the surface. Secondly, etching produces a rough surface, parts of which may consequently be out of the focus of the spectrometers of the X-ray analysis system.

However, for optical microscopy, after polishing to a 1 μm diamond finish, etching is obviously necessary. It was found that the most satisfactory etchant for all three alloy systems was Keller's etch, the constituents and proportions of which are:-

HNO_3	3.0%
HF	0.5%
HCl	2.0%
water	94.5%

The effect of this etch is to darken the intermetallic phases (e.g. $CuAl_2$), $AgAl_2$). Etching times varied from one or two seconds to a few minutes, depending on the concentration of the alloy.

7. Measurement of Temperature Gradients

When a specimen is placed in a thermal gradient as in the apparatus used for unidirectional solidification, a temperature gradient is set up inside it. The magnitude of this depends on the equilibrium existing between net radiation absorbed and conduction of heat out at the cold end. This equilibrium depends on the thermal conductivity of the alloy.

Measurement of temperature gradients inside the specimen is made difficult by the fact that replacement of the specimen or part of it by a thermocouple, changes the thermal conductivity and therefore alters the

temperature gradient, One must therefore accept that results measured in this way are liable to some distortion. However, this method of measurement was carried out, using a thermocouple doubled up so that the junction of the metals was at some position half-way up the specimen tube. This allowed a temperature gradient to be set up through the thermocouple wire. Measurement of the potential difference between the thermocouple leads were made at 5 mm intervals as the tube containing them was withdrawn. The table below shows the temperatures as measured over the relevant temperature range.

Furnace at 1000°C	mms	°C
	0	488
	5	530
	10	567
	15	587
	20	606
	25	626
	30	638
	35	652
Furnace at 1250°C	mms	°C
	0	495
	5	688
	10	821

A more reliable way of estimating temperature gradients was later devised which obviated the need for thermocouples and their consequent inaccuracy. After a dendritic alloy has been quenched, it is possible to see the position of the interdendritic eutectic front at the time of quenching, by the difference in lamella spacing caused by the rapid increase in growth rate. The distance between this position and the position of the tips of the dendrites can be measured microscopically. The temperature of the tips can be estimated from the phase diagram if the concentrations are determined by microanalysis, and the temperature of the eutectic can also be obtained from the phase diagram. Thus, as depicted in figure 24, a temperature gradient can be estimated. Values obtained in

this way for four different furnace temperatures are:-

Furnace Temperature (^{o}C)	Temp. Gradient (^{o}C/mm)
1450	163
1250	160
1000	75
850	48

Temperature gradient measurements obtained in this way suffer from two disadvantages. Firstly, the value applies to a range of temperature, from the tip temperature to the eutectic temperature, a range of about 100^{o}C. Thus, an average temperature gradient is obtained over this range. Secondly, in a solidifying melt, it is generally true that the temperature gradient in the solid is smaller than that in the liquid because of the higher thermal conductivity in solids. The temperature gradient value obtained in this method is neither that of the solid, nor that of the liquid, but corresponds to a liquid + solid region and, as such, is likely to be some average of the two.

However, the values given in the table above, do have some relative meaning, even if they are not correct on an absolute scale, and, with this reservation, they are used where required.

8. Measurement of Sizes and Radii of Curvature of Cells and Dendrites

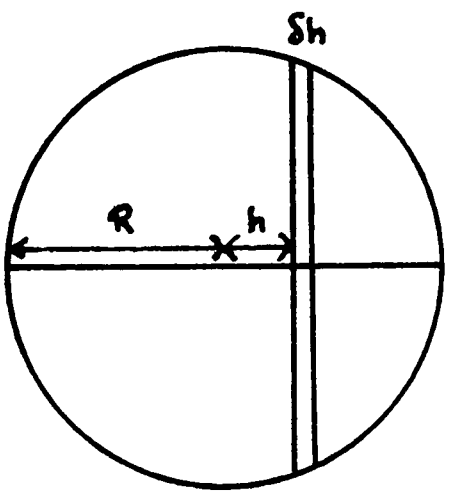
(a) Sizes

Cell sizes can be measured on longitudinal or transverse sections, though if the former used, some correction must be applied because of the fact that random and not diametric sections are taken through the cells.

(i) Longitudinal Sections

The method employed when measuring sizes on longitudinal sections was to count the number of cells or dendrites which fitted into a given number of divisions of a microscope eyepiece graticule and then to calibrate the eyepiece graticule against a stage micrometer. This gives a measurement of the size of the mean section viewed. A correction by a factor of 1.275 was necessary to give a value for the actual size. This was arrived at in the following way.

A round cell in transverse section is considered. This cross-section is cut into slices of thickness δh at a distance h from the centre of the cell, as in the accompanying diagram. The true length of the cell is 2R and the size of the slice is $2(R^2 - h^2)^{\frac{1}{2}}$. The average radius is given by adding the total for all the slices and dividing by the number of slices.



We take the total for all the slices as

$$2\sum_{h=-R}^{h=+R}(R^2 - h^2)^{\frac{1}{2}}$$ summing over all possible values of R

The number of slices is equal to the total width divided by the width of each slice, $= {}^{2R}/_{\delta h}$

Thus, the observed cell size 2R' is given by

$$2R' = 2\sum_{h=-R}^{h=+R}(R^2 - h^2)^{\frac{1}{2}} \div {}^{2R}/_{\delta h}$$

$$= \sum_{h=-R}^{h=+R}\frac{(R^2 - h^2)^{\frac{1}{2}}.\delta h}{R}$$

For $\delta h \rightarrow 0$

$$2R' = \int_{-R}^{+R}\frac{(R^2 - h^2)^{\frac{1}{2}}}{R}\,dh$$

$$= \frac{1}{R}\left[\tfrac{1}{2}h(R^2 - h^2)^{\frac{1}{2}} + \tfrac{1}{2}R^2 \sin^{-1} {}^{h}/_{R}\right]_{-R}^{+R}$$

$$= \frac{1}{R} \times \tfrac{1}{2} \times R^2 \times \pi$$

$$= \frac{\pi R}{2}$$

$$R = R' \times 1.275$$

It was observed that when a cell size value was obtained by correction in this way, it was approximately equivalent to the largest cell present on the longitudinal section (i.e. to a diametric section).

(ii) Transverse Sections

Cell sizes were measured on transverse sections either by a line intercept method or by an area method. In the first case, the number of cell boundaries which intercepted a line of given length was measured. This was repeated several times on the same specimen and an average taken. In the area method, a photograph was taken of a given area, with approximately a hundred cells on it. The number of cells was counted on the photograph and the average area of each cell thus determined. The square-root of this gave a measure of average cell size. The area method was used when it was necessary to detect small changes of cell size in specimens grown at different rates.

In the case of branched cell and dendrite sizes, the line intercept method was used as a check on the size obtained by taking the largest cells visible on a longitudinal section. The agreement between these two estimates was satisfactory. The table below shows some values for 3% alloys.

Rate of growth μm/sec	L (intercept method)	L (longitudinal) (corrected)
444	100	92
111	133	135
55.5	168	167

(b) Curvatures

The curvatures at the tips of cells are not easy to measure and are not accurately reproducible from specimen to specimen. An attempt was made to estimate them by tracing on to paper the profiles of the tips as seen on a projection microscope (figure 25). It was found that the largest cells on a longitudinal section of a given specimen had the largest curvatures, since they were closest to being diametric sections. A set of circles of different radii was drawn on a sheet of paper and the largest cell profile on the tracing paper superimposed on these circles in order to find the one which it fitted best. This method then gives the radius of curvature of the image of the cell right at its tip and this must be scaled down by a factor which depends on the magnification of the projection microscope.

Results obtained by this method were not accurate, but they did enable a

general trend in change of radius of curvature with changing growth variables to be observed.

9. Quantitative Measurement of Branched Cell and Dendrite Coarsening behind the Interface

Longitudinal sections do not, in general, give diametric sections through dendrites. However, this should not seriously affect the spacing of secondary dendrite arms which come out at right angles to the primary stalk. One way of measuring the change in secondary dendrite arm spacing is to select a dendrite and measure each arm size from the tip back. These sizes can be plotted against distances back from the tip. This produces a graph as in figure 26. However, in order to minimise statistical fluctuations in sizes, it is more accurate to take averages over many dendrites on the same longitudinal section.

The basic method used was to fix a band of known width on the microstructure and to count the number of arms inside that band, together with the number of primary arm sides considered. Division of the latter into the former gives the average number of side branches per dendrite, in the band, and thus the width of each branch can be obtained. This method of counting is shown diagrammatically in figure 27.

In the case of branched cells, where coarsening in a given distance is fast, the specimens were examined under a television microscope. This was set up so that only a band of width 120 μm was observable. The band was moved progressively along the specimen, so that a measurement was made every 120 μm.

Where coarsening was slow for more concentrated alloys, a microscope with a micrometer eyepiece was used. The distance between the wires of the eyepiece was set to 100 μm and readings of secondary arm spacing were taken at intervals of 500 μm along the specimen. In both cases graphs were obtained giving secondary dendrite arm size plotted against the distance back from the tips of the dendrites.

IV RESULTS

1. The Morphologies of Cells and Dendrites

The various morphologies of interfaces moving under different growth conditions and with different solute concentrations are illustrated in the figures 28, 29, 30. Planar interfaces were observed to break down into simple cells (figure 28) at the transition conditions predicted by the constitutional supercooling or perturbation analysis theories. These simple cells had a curvature at their tips which caused lateral solute rejection, and therefore the intercellular walls were rich in solute, whereas the intracellular solid was depleted.

The sizes of the cells did not seem to vary significantly with growth rate or alloy composition, though it was found that they did vary with temperature gradient. Precise area method (see page 43) cell size measurements were made on alloys containing 0.2% Cu. These were specimens grown at different rates but using the same furnace temperatures. Temperature gradients in these specimens were therefore the same. The total area over which cells were counted for each specimen was 500 μm x 400 μm. Results are given in the table below.

0.2% Cu alloys	Growth Rate V	Cell Size L
G = 7.5°C/mm	(μm/sec)	(μm)
	11.1	114
	16.7	90
	22.2	81
	27.8	90
	33.3	79
	38.9	78
	44.4	69
	50.0	80
		Average = 85 μm

No sensible variation appears to exist. The average value was found to be 85 μm.

Averaged values of cell size over many different growth rates are shown

below for Al - 2% Cu specimens grown at four different temperature gradients. These values show the dependence of cell size on temperature gradient and were made on longitudinal sections.

2% alloys	Temperature Gradient G (^{o}C/mm)	Cell size (Averaged) (μm)
	4.8	185
	7.5	85
	16.0	70
	16.3	60

It is noticeable that in these two tables the value for averaged cell size at a temperature gradient of 7.5^{o}C/mm is 85 μm notwithstanding that there is a factor of ten difference in the concentration of the alloys. This suggests that cell sizes are not dependent on alloy concentration.

At certain values of concentration and velocity of growth and a given temperature gradient, the simple cells of figure 28 branch at their tips to give a morphology as shown in figure 29. At the same time there is a larger increase in cell size, though with increasing growth rate this gradually decreases. Figure 31 shows how this cell size varies with velocity, the abrupt increase corresponding to the onset of branching, and figure 32 shows the results of cell size measurements for branched cells plotted as a function of $V^{-\frac{1}{2}}$.

The branched cell morphology is not easy to visualise, though it can be seen from figure 33, which is a transverse section through branched cells, that the tendency is for arms to come off in two directions at right angles. Figure 34 is a photograph of a plasticine model of such a branched cell, through this has been considered as a cylindrical cell growing alone and free from the impingement of others.

Branched cells do not grow in the dendrite direction, <100>, but they are pulled into that direction from the heat flow direction more than cells are. Thus, it can be seen (figure 35) that at the point of quenching, the fine dendrites, produced by the sudden increase in growth rate, grow at more of an

angle to the heat flow direction than the branched cells do. It can be assumed that the direction of dendrite growth is <100>.

Increase of concentration gives dendrites whose growth direction is exactly aligned parallel to <100>. These have well developed side-branches which are crystallographic and are at right-angles to the primary stalk (figure 28).

Curvature of cells and branched cells were measured using the technique described on page 43. Values were estimated for curvatures in aluminium-copper and aluminium-silver alloys. Specimens of the former were grown at two different temperature gradients and curvatures are shown in figure 36 plotted against the parameter $(VC)^{-\frac{1}{2}}$. The range of compositions and growth rates were as follows:

$$C = 2\% - 20\%$$

$$V = 1.67 - 50\ \mu m/sec$$

The form of this graph suggests that curvatures do not undergo a discontinuity at the cell/branched-cell transition and that they are dependent on temperature gradient. The points are re-plotted on a graph (figure 37) together with curvature values from specimens containing 15% and 25% of silver as solute. Two alternative empirical relationships which could satisfy all these various results from both alloy systems but are given at present with no justification are

$$r \propto G^{-1} \left(VC/_{k_o}\right)^{-\frac{1}{2}}$$

$$r \propto G^{-1} (mVC)^{-\frac{1}{2}}$$

2. The Segregation occurring at the tips of cells and dendrites under conditions of no liquid mixing

(a) Al-Cu Alloys

When a planar interface breaks down, the curvature of the cells causes redistribution of solute rejected at the interface laterally as well as parallel to the growth direction. This lowers the concentration of solute at the tips of the cells both in the solid, and, proportionately, in the liquid. The results of the curvature can be observed using electron probe microanalysis, by measuring the solute concentration C_s immediately behind the tips inside the

cells and relating these to bulk liquid concentrations C_o. Figure 38(a) shows a diagram giving the positions where the measurements of these concentrations were taken. Point counts at positions such as A, and 300 μm wide line counts in the quenched liquid at BC gave C_s and C_o respectively. Line scans OPQR gave traces on the pen-recorder as shown in (b), where the concentration in the intracellular solid is less than C_o, the bulk liquid concentration. The overall solid concentration $\overline{C}_s$ is still however equal to C_o and the solidification is thus taking place under steady-state conditions. A typical line trace taken over a cellular interface is shown in figure 39, with the appropriate concentrations indicated.

The efficiency of longitudinal versus lateral solute rejection at a cellular interface can be expressed by an effective distribution coefficient k_e which is given by the ratio of C_s to C_o

$$k_e = C_s/C_o$$

Obviously, the value of k_e at a planar front is unity and at an interface which rejects all its solute laterally k_e is equal to k_o. Figure 40 shows the observed variation of k_e between these two limits for alloys grown through two different temperature gradients. Thus, it approaches k_o assymptotically and rises rapidly to unity in the vicinity of the breakdown growth conditions. Alloys used for figure 40 have copper concentrations from 2% to 20% and it was found experimentally that they would all fit on the same curve if k_e was plotted against the parameter (VC).

(b) Al-Ag Alloys

Similar measurements to those described for aluminium-copper alloys were made on aluminium-silver alloys containing 15% and 25% silver, using a temperature gradient of 16.0°C/mm. k_e values were again obtained from point and line counts. These were plotted (figure 41) on the same graph as aluminium-copper results, but an attempt was made to normalise the results by plotting on the y-axis the function $(k_e - k_o)/k_o$ and on the x-axis, VC/VC^* where VC* is the product of critical velocity of growth and concentration necessary to cause breakdown from a planar to cellular interface. Because

of uncertainty in the value of temperature gradient, these VC* values were estimated from the observed values of breakdown viz.

$$VC^*\ (Al - Cu) = 2.22\ \mu m.wt\%/_{sec}$$

$$VC^*\ (Al - Ag) = 11.7\ \mu m.wt\%/_{sec}$$

As can be seen, these curves have similar characteristics and both give $(k_e - k_o)/k_o$ tending to zero as (VC) goes to infinity. It seems from these results that the range of values of (VC) over which $(k_e - k_o)/k_o$ decreases is approximately independent of the alloy system.

3. The Effect of Liquid Convection

The results described in the last chapter were made in apparatus which was designed to produce no convection in the liquid. That there was no convection was known from the form of figure 5, which was the solute distribution ahead of a planar interface. When liquid mixing occurs there is a change in the pattern of solute redistribution and C_s is not equal to C_o.

(a) Aluminium-magnesium system (positive temperature gradient)

A lighter solute, such as magnesium, cause convection of the 'salt-fingering' type to occur (page 18). Alloys of aluminium containing 4% Mg were made up and cast into thicker tubes than used previously in order to promote convection. Line scans through the interface region produced solute profiles like that illustrated in figure 42. The significance of these is difficult to understand, and for this reason, and also because of practical difficulties in using the alloy, only a few of such line scans were produced. These difficulties in using the alloy arose because of the high vapour pressure of magnesium. Bubbles of vapour were formed in the tubes and these often caused the tubes to crack and thus to allow metal to exude out of them, as shown in figure 43.

(b) Aluminium-copper system (negative temperature gradient)

Steady convection was observed in specimen tubes containing Al-2%Cu alloys solidified vertically downwards. A typical diffusion profile produced on a pen-recorder by a line scan on the microanalyser is shown in

figure 44. This was produced by scanning through a planar interface, as represented in figure 45. The length of line of the scan was of the order of 50μm in the cell but in the liquid it was expanded to 300μm. This expansion was necessary to average over the microsegregation in the quenched region, which was less fine in these specimens owing to the slower quench obtained. Superimposed on figure 44 are the relevant compositions. C_L, the liquid concentration was obtained by line counts in the liquid at such position as DE in figure 45. Point counts at positions such as A gave cell tip concentrations C_s and line counts over 300μm lines BC gave average solid compositions $\bar{C}_s$. In the case of growth under such circumstances, steady-state conditions are not maintained and the liquid concentration rises steadily from the beginning to the end of solidification with no concentration plateau.

It is necessary to consider these concentrations and the relations between them. From figure 44 it can be seen that the bulk liquid is fully mixed and of a composition C_L at a distance from the interface. This distance is known as the boundary layer thickness and given the symbol δ. The liquid concentration C_L determines the values of C_s, $\bar{C}_s$ and C_I in the following way. A diffusion profile can be drawn from C_L upwards with the correct value of decay constant ($^V/_D$) and this produces a concentration in the liquid at the interface of C_I. The concentration at the tips of the cells is then equal, in the solid, to $k_o C_I = C_s$. Average compositions in the solid are dependent on the efficiency of lateral rejection of solute, i.e. on the tip curvature. $C_s/\bar{C}_s$ is equivalent to the effective distribution coefficient in the case of non-stirred melts, since $C_s \neq C_L$ as it is under steady-state conditions. To distinguish it, in this case, we give it the symbol k_s, the lateral solute segregation coefficient. Then k_e in this case is, as before, C_s/C_L, the effective distribution coefficient.

To summarise

$k_o = C_{s/C_I}$ equilibrium distribution coefficient

$k_s = C_{s/\bar{C}_s}$ lateral solute segregation coefficient

$k_e = C_{s/C_L}$ effective distribution coefficient

Burton, Prim and Slichter (1953) assumed a model which involved complete mixing in the liquid further away from the interface than a distance δ, and transport by diffusion only at distances less than δ. Then, using equation (1) (page **3**) for a planar interface.

At distance δ, the concentration in the liquid is C_L

$$(C_L - C_s) = (C_I - C_s)\ e^{-R\delta/D}$$

$$\left(\frac{C_L}{C_s} - 1\right) = \left(\frac{C_I}{C_s} - 1\right)\ e^{-R\delta/D}$$

$$\left(\frac{1}{k_e} - 1\right) = \left(\frac{1}{k_o} - 1\right)\ e^{-R\delta/D}$$

$$k_e = \frac{k_o}{k_o + (1 - k_o)\ e^{-R\delta/D}}$$

This can be extended to cellular interfaces as follows

At distance δ

$$(C_L - \bar{C}_s) = (C_I - \bar{C}_s)\ e^{-R\delta/D}$$

$$\left(\frac{C_L}{C_s} - \frac{\bar{C}_s}{C_s}\right) = \left(\frac{C_I}{C_s} - \frac{\bar{C}_s}{C_s}\right)\ e^{-R\delta/D}$$

$$\left(\frac{1}{k_e} - \frac{1}{k_s}\right) = \left(\frac{1}{k_o} - \frac{1}{k_s}\right)\ e^{-R\delta/D}$$

This expression becomes identical to that of Burton, Prim and Slichter when $k_s \to 1$ i.e. when there is no lateral segregation corresponding to a planar front. When dendrites become increasingly sharp $k_s \to k_o$ and $k_e \to k_o$.

Using values of concentration determined as described, and assuming the validity of the Burton, Prim and Slichter model, values were obtained for δ, the boundary layer thickness. These values showed some scatter because of the difficulty of measuring $\bar{C}_s$ owing to the coarseness of the cellular structure. However the values of δ showed no overall dependence on rate of growth.

Twenty-three specimens were examined and each analysed completely twice. The specimens were grown through two different temperature gradients

whose magnitudes were determined as previously described. Two alloy compositions (2% and 10%) were used. The resulting 46 values of δ were averaged in three categories. These averages are shown in the accompanying table.

Concentration (wt%)	Temperature Gradient (^{o}C/mm)	δ (μm)
2	16.0	320
2	7.5	420
10	16.0	250

It is of interest to compare the values of δ obtained by this method with the traces produced, as in figure 44, by line scans across the interface. Superimposition of traces and δ-values are shown for the three groups of values on figure 46. All the specimens whose traces are shown were grown at a velocity of 16μm/sec so as to more readily facilitate comparison.

The results given so far have elucidated the effect of mixing in the liquid on the pattern of solute redistribution which is the direct consequence of the presence of the boundary layer. The question then arises as to whether mixing has any influence on the interface apart from this. The graph in figure 47 shows values of k_s, the solute segregation coefficient plotted as functions of log VC. The composition taken for this graph was $\bar{C}_s$ which would be the equivalent of C_o for non-stirred interfaces. Superimposed on the same diagram is the line of figure 40, for the variation of k_e. (k_e is the equivalent parameter in the case of interfaces where no stirring is present in the liquid.)

Cell size determinations were also carried out on specimens which had mixed liquid. The values were averaged over a number of different growth rates and are given in the table below. Also in the table are the values obtained under conditions of no liquid mixing.

Temperature Gradient (^{o}C/mm)	Cell size (mixed) (μm)	Cell size (no mixing) (μm)
16.0	67	70
7.5	80	85

4. Acceleration of a Planar Interface through the Breakdown Conditions

Specimens of Al-2% Cu alloys were accelerated both instantaneously and gradually in the pulling apparatus using the motor set-up described in chapter 4 of section III. All these experiments were carried out under such conditions that there was no liquid mixing. At given times after the start of acceleration, the specimens were quenched and subsequently sectioned for examination by microanalysis and optical microscopy.

(a) Instantaneous Accelerations

A number of specimens were accelerated instantaneously from a growth rate just below the growth rate necessary to cause planar interface breakdown to one which was higher by a factor of fifteen i.e. from 1.11 to 16.7 μm/sec. It was found that about 30 seconds growth at the higher rate was necessary before breakdown to cells occurred. The microstructure of a specimen grown for such a time is shown in figure 48(a). A perturbation is starting to grow and will eventually spread over the whole interface. The solute concentration profile corresponding to this specimen is figure 48(b). As can be seen, the solute gradient at the tip has become steeper since the velocity has increased and the sum of the areas of the two shaded regions will be equal to the area between the full and dotted lines.

At a little distance in front of the interface, the diffusion profile was characteristic of a slow growth rate, indicating that this specimen has not adjusted to steady-state conditions.

Fifteen seconds after this position was reached, the microstructure appears as in figure 49. There is now, at the interface, a cellular structure, whose spacing is smaller than that observed in specimens which are growing under steady-state conditions. The measured spacing is 26μm. However, some of the cells seem to grow faster than others and some of the original ones to appear are being overgrown. This is more marked after 60 seconds (figure 50(a)) when the observed spacing is more nearly equal to observed equilibrium spacings. The diffusion profile corresponding to

this photograph is shown in figure 50(b). The lower solute level is that inside the cells; the upper is the mean solute concentration. As in the previous solute profile, (figure 48(b)), the area of the shaded region should be equal to that of the region between the full and dotted lines.

An investigation was made into the possibility that the breakdown was delayed for 30 seconds because acceleration of the interface lagged markedly behind the acceleration of the traction device. It was noted that the planar interface before breakdown appeared, as in figure 51 to be curved towards the edge of the specimen. Obviously the edge of the specimen had not adjusted to the new speed of growth and was therefore hotter than the middle. The distance, taken in the direction of growth, between the interface position at the edge and that in the middle of specimens was measured as a function of time after start of acceleration, and the results are given below.

Time after start of acceleration (seconds)	Distance (μm)	Apparent Growth Rate (μm/sec)
15	280	18.6
20	295	14.8
30	560	18.6
	Average apparent growth rate =	17.3 μm/sec

Clearly, the interface was moving at the increased traction rate in the centre of the tube.

The conclusion of this set of measurements is also backed up by reference to the microprobe traces of figures 48(b), 50(b). The distances from the dotted to the full lines represent the distances moved during the time after instantaneous acceleration began. Since the interface appears to have moved nearly a millimetre in 60 seconds or 16.7μm/sec, it can be assumed that, in the middle of the specimens, increase of traction rate produces a nearly equivalent increase of interface growth rate.

(b) Gradual Accelerations

If the planar interface is accelerated at a constant rate instead of instantaneously, then the incubation period before it breaks down to give a cellular interface is longer. For example, at an acceleration rate of 5×10^{-3} μm/sec^2, the incubation period is 210 seconds, as compared with 30 seconds for an instantaneously accelerated specimen. However because of differences in acceleration rate the velocity at which breakdown occurs does decrease as specimens are accelerated more slowly. This coincides with a larger initial spacing of the cells.

Specimens were quenched at the point when the interface had just become cellular, and the spacings of these cells measured. The voltage output of the motor generator was recorded at the moment of quenching and the velocity of traction calculated from this. These experiments were carried out using specimens of alloys containing 2% copper in aluminium and using two different temperature gradients (7.5°C/mm and 16°C/mm).

Figure 52 shows how the initial spacing is related to the breakdown velocity. The steady-state spacings are plotted on the same graph with their breakdown velocities taken to be those given by constitutional supercooling theory, (i.e. the effect is the same as acceleration at an infinitesimally slow rate). As can be seen the results show no apparent dependence on temperature gradient.

5. The Coarsening of Cells behind the Interface

After the cells have been formed at the interface, redistribution of the intercellular liquid occurs. This is most easily observed in low concentration alloys which have been grown at low rates. A longitudinal section displaying the effect of liquid movement is shown in figure 53. Transverse sections from a specimen which was successively polished back from the interface also show the effect (figure 54). A diagrammatic representation of a cell which includes the transverse sections is shown in figure 55. From this it can be seen that the intercellular liquid is pulled into the nodes or corners of the cells and subsequently, when the

walls break, channels of liquid remain. These have a circular cross-section.

This phenomenon was examined in detail for aluminium alloys containing 0.2 wt% copper, in order to understand what causes the solute to change from being a hexagonal array of plates to being a set of cylindrical channels. The results are described here under three headings; morphology, solute distribution and effect of orientation.

(a) Morphology

The transverse sections of figure 54 show the general morphology changes observed on polishing back from the interface. Cell sizes at the interface, as previously explained, are not dependent on rate of growth over the range of growth velocities studied. However, it was found that some way behind the interface a complete, but larger, cell structure was visible. The sequence of changes in cell walls leading to this is shown in figure 56. As can be seen, this coarsening of the structure proceeds by preferential disappearance of some walls before others. The size of the coarsened cell array was measured and figure 57 shows how it relates to the velocity of growth. In figure 58, the straight line corresponds to the proportionality,

$$L \propto V^{-\frac{1}{2}}$$

Thus, it can be seen, that the higher the growth rate, the smaller is this coarsened structure and, as such, it could be thought that its size might be merely related to the time available for coarsening.

In order to investigate this possibility, a number of specimens were held in the furnace for different lengths of time up to 12 seconds before quenching. It was found that the size of the coarsened cell structure was not affected at all by such treatment. It was therefore primarily determined by the initial morphology of the interface and only secondarily by the time allowed for coarsening.

(b) Solute segregation

Microanalysis was carried out as depicted diagrammatically in figure 59(a). Line scans were made across cell walls at regular intervals on successive transverse sections, from the interface back. These produced traces on the pen-recorder as shown and the area under these was taken to give a measurement of the product of width and concentration of the cell walls. This measurement was of necessity a product, since the quenching causes a transient peak of solute everywhere at the interface including the grooves between cells, and this is not identical to the liquid solute distribution prior to quenching. Thus, it is shown by Sharp (1968), that a thin skin of $CuAl_2$ is formed on quenching. Cell walls therefore contain $CuAl_2$ when beforehand they could not have done. An additional uncertainty which is also removed by using the product of width and concentration arises from the fact that the cell walls after quenching are probably thinner than they were before.

The areas under the traces (the shaded areas of the figure) were plotted against distance along the cell wall for each transverse section (figure 59(b)). Coarsening times were estimated by measuring the thickness of material polished off behind the interface, using a dial gauge, and dividing this by the velocity of growth.

The microanalysis results of figure 59(b) confirm that the width of the cell wall decreases in the centre and increases at the corners. However figure 60 shows an alternative pattern of solute redistribution, in which the width of the wall in the centre is not disappearing significantly. Presumably this cell wall is adjacent to rapidly thinning walls and the increase in size of the corners is being completely accounted for by liquid provided by them.

(c) Effect of orientation

The pattern of cell coarsening shown in the previous diagrams is that obtained from specimens whose growth directions are close to <100>or <111>. In them, it appears that coarsening is independent of orientation on trans-

verse sections (figure 61(a)). However, where the cell growth direction was close to <110>, the resulting coarsening pattern appeared as in figure 61(b), the remaining cell walls being approximately lined up in one direction such that they are parallel to (100) planes. The size of the coarsened structure is still given by the graph in figure 58 i.e.

$$L \propto V^{-\frac{1}{2}}$$

Figure 62 shows the distribution of growth directions on a standard projection, indicating which coarsened to give patterns as in figure 61(a), and which, as in figure 61(b).
These orientation determinations were made using the back-reflection Laue technique of X-ray diffraction.

Microanalysis investigations of specimens where coarsening took place in specific directions were carried out in the same way as described in part (b). However, in this case, scans were made on cell walls in two directions at right angles (i.e. parallel and perpendicular to the elongated cell structure). The results of these investigations are shown on the graph in figure 63. They indicate that this uneven thinning of cell walls starts immediately behind the interface. We are concerned then with a mechanism of cell wall thinning which has some dependence on orientation.

6. The Coarsening of Secondary Dendrite Arms

In much the same way as cell walls grow thinner and disappear, secondary dendrite arms can coalesce behind the interface. This leads to a change in spacing behind the dendrite tips as the interface moves forward. Spacings of secondary dendrite arms were measured according to the techniques already described (page 44).

The results are presented here in two sections, because it was found that, for high and low concentration alloys, two essentially different coarsening dependences were found.

(a) Low Concentration Alloys

Examined in this category were aluminium-copper alloys with copper concentrations of 2%, 3% and 4%. The morphologies associated with these alloys at the rates of growth used were of the branched cell type

(figures 29, 33, 34). Data has already been given concerning the sizes of the primary stalks of these structures (figures 31, 32) and we now consider the sizes of the side projectsion.

Spacings as measured, λ, were plotted against the distance from the quenched interface. Such a graph for alloys containing 3% copper is shown in figure 64. The spacing appears to change linearly with distance and the gradients of these lines can be measured. They are given below for all the specimens which were obtained, expressed in dimensionless units - i.e. the change in spacing (in microns) as the distance behind the interface (1) changes by one micron.

Al-2% Cu Temp Gradient = 7.5^{o}C/mm

V(μm/sec)	55.5	111	166.5	222	333	444
Gradient	.047	.035	.027	.032	.027	.033

Temp Gradient = 16^{o}C/mm

V(μm/sec)	27.8	55.5	111	222
Gradient	.096	.111	.090	.074

Al-3% Cu Temp Gradient = 7.5^{o}C/mm

V(μm/sec)	55.5	111	222	444
Gradient	.052	.033	.043	.031

Al-4% Cu Temp Gradient = 7.5^{o}C/mm

V(μm/sec)	55.5	111	222	444
Gradient	.024	.025	.0185	.0185

It should be noted from figure 64, that the initial spacings are dependent on the rate of growth, varying, as would be expected, in the same way as the radii of curvature of the tips (i.e. larger for lower growth rates).

The representation of spacing changes as a function of distance behind the branched cell tips is not satisfactory, as coarsening would be more

likely to depend on the time and temperature available for it to take place. Conversion of the distance behind the tip to the time available for coarsening can easily be made by dividing it by the growth velocity. When this is done, the straight lines of figure 64 appear as in the straight lines of figure 65 - these are for 2% Cu alloys. Coarsening rates, in terms of microns per second appear to be highly dependent on growth rates.

(b) High Concentration Alloys

At higher concentrations, dendrite tips become more spiked and have well-developed side branches as shown in figure 30. Under these conditions, a completely different dependence was found to exist between coarsening rates and growth rates.

Figure 65 shows the results that were obtained for Al-10% Cu alloys. These specimens were grown at different rates between 50$\mu m/_{sec}$ and 444$\mu m/_{sec}$ yet all the points lie within the reproducibility of measurement on the same curve. It is noticeable also that coarsening does not take place with a linear dependence on time, and, compared with the lower concentration alloys, it takes place more slowly. There is, no doubt, a variation in initial secondary-arm spacings in these alloys, but this is fairly small over the range of rates employed.

Aluminium - 5% Copper alloys behave in a similar way, but their initial secondary-arm spacings are higher because their radii of curvature are higher. The results are given below.

Temperature Gradient = 7.5°C/mm

Growth rate 222$\mu m/_{sec}$

l(mm)	0	0.5	1.0	1.5	2.0
λ(μm)	14.2	23.1	27.0	28.1	30.0

Growth rate 111$\mu m/_{sec}$

l(mm)	0	0.5	1.0	1.5	2.0
λ(μm)	17.6	28.5	31.3	30.8	42.0

Growth rate 55.5$\mu m/_{sec}$

l(mm)	0	0.5	1.0	1.5	2.0
λ(μm)	21.4	36.0	42.0	53.0	54.0

V DISCUSSION

1. The Criterion of Growth of Cellular and Dendritic Interfaces

We must first evaluate the microanalysis data which concerns the lateral redistribution of solute at a cellular or dendritic interface. It has been observed (page 47 and figure 40) that this lateral redistribution gradually increases from zero at a planar front to being almost complete at very large values of growth rate and concentration. The decrease in k_e is brought about by decreasing the radius of curvature of the tips.

The data of figure 40 can be plotted in terms of $\log \frac{k_e - k_o}{k_o}$ vs $\log VC$ and this graph (figure 66) shows that the results can be expressed according to the equation

$$\log VC = A - \log \frac{k_e - k_o}{k_o} \quad \text{where A is a constant}$$

$$VC = A \times \frac{k_o}{k_e - k_o}$$

At the critical conditions for planar interface breakdown

$$VC = (VC)^* \qquad k_e = 1$$

From constitutional supercooling theory

$$\frac{G}{(VC)^*} = \frac{m(1 - k_o)}{Dk_o}$$

$$(VC)^* = \frac{k_o D G}{m(1 - k_o)}$$

$$A = DG/m$$

$$VC = \frac{D G k_o}{m(k_e - k_o)}$$

$$k_e = \frac{D G k_o}{mVC} + k_o$$

This simple criterion for k_e is equivalent to the statement that the average gradient of the liquidus temperature in front of the interface is always made equal to the imposed temperature gradient. This means that the concentration at the tips is fixed by the conditions as represented by figure 67 for various temperature gradients and growth velocities. If the steady-state

cellular interface is smeared out so as to have an average liquid composition C_I at the interface and a concentration at an infinite distance away from the interface of C_o, then the average composition gradient at the interface is

$$\frac{dC}{dx} = (C_I - C_o)\ {}^{V}/D$$

$$= (\frac{k_e}{k_o} - 1)\ {}^{VC}/D$$

The slope of the average liquidus temperature is

$$= \frac{mVC}{D}\ (\frac{k_e}{k_o} - 1)$$

and if this is equal to the applied temperature gradient then

$$G = \frac{mVC}{D}\ (\frac{k_e}{k_o} - 1)$$

$$k_e = \frac{DG}{mVC}\ k_o + k_o$$

While this treatment cannot be considered rigorous, it does provide a simple criterion to the effect that taking the interface as a whole, the adjustment of radii of curvature of the tips of the cells or dendrites is such as to eliminate constitutional supercooling. It should be noted that elimination of constitutional supercooling at the tips of the cells would produce the relation

$${}^{dC}/_{dx} = (C_I - C_s)\ {}^{V}/D = {}^{G}/m$$

$$\frac{GD}{mVC} = ({}^{1}/k_o - 1)\ k_e$$

$$k_e = \frac{DG}{mVC}\ \frac{k_o}{(1 - k_o)}$$

This leads to the erroneous result that as $VC \to \infty$ $k_e \to 0$.

The applicability of the derived empirical criterion can be tested for all the results obtained at different concentrations, in the different systems. In figure 68, the data are given as ${}^{VC}/(VC)^*$ plotted against the parameter $(k_e - k_o)/(1 - k_o)$. The dotted line is derived from the equation

$$\frac{(VC)^*}{VC} = \frac{k_e - k_o}{1 - k_o}$$

which corresponds to our empirical equation

$$k_e = \frac{DG}{mVC} k_o + k_o$$

The two assumptions involved in this treatment, namely that the average liquidus gradient is equal to the temperature gradient and that the problem can be treated as though the average liquid composition over the interface is equal to C_I, the composition at the tips, have already been made by Bower et al (1966). They are not, however, satisfactorily explained in that work. The second assumption is said to be true if all solute rejection is in the X-direction (i.e. perpendicular to the interface), yet plainly this can not be the case if dendrites are formed.

The impression gained from this work is that, although there is no particular justification for the second assumption, the results obtained for different systems, compositions, temperature gradients and rates of growth appear to fit in with it.

The effect of the foregoing conclusion is that cells and dendrites grow at the lowest temperature they can do in these experiments (i.e. with as large a solute pile-up as possible). We must consider what part in the total undercooling the undercooling due to curvature takes. The radius of curvature values in Al - 2% Cu alloys at the highest growth rates used in these experiments were of the order of 20 μm. Curvature undercooling can be calculated from the equation

$$\Delta T_c = \frac{2\gamma}{r\Delta s}$$ where Δs is the entropy of fusion

Taking a value of 300 ergs/sq cm for the surface energy, γ, this gives a figure for ΔT_c of

$$\Delta Tc = \frac{2 \times 300 \times 933}{4.2 \times 10^7 \times 10^{-4} \times 20 \times 250} \ ^oC$$

$$= .026^oC$$

For comparison, a typical solute undercooling (ΔT_s) for a similar specimen

would be

$$\Delta T_s = (C_I - C_o)m$$

$$= 3.24\ (^1/k_o - {}^1/k_e)\ C_s$$

$$= 3.24 \times 2 \times 0.9$$

$$= 6^o$$

Thus, for the conditions under which these experiments were carried out, it is possible to say assuming the equation for curvature undercooling to be correct that the curvature undercooling is negligible compared to the undercooling due to the accumulation of solute in front of the tips. The growth of cellular structures may not therefore governed by a minimum undercooling criterion but possibly by ~~it is rather~~ a criterion of maximum undercooling, consistent with there being no average constitutional supercooling.

2. The Effect of Liquid Convection on the Solute Segregation Pattern

(a) Steady Convection

In the specimens where there was convection in the melt, a static boundary layer existed in front of the interface, as has been described. This layer can be thought of as being a zone where transport by diffusion is greater than transport by convection. Convective flow in liquids decreases parabolically as surfaces are approached, because of frictional forces. In front of a moving interface, the magnitude of the diffusional flux decreases exponentially away from the interface. At some distance (δ) from the interface, the transport by convection and diffusion are equal. Although the transition from one to the other is gradual, the Burton, Prim and Slichter (1953) theory assumes, for mathematical convenience, that it is an abrupt changeover.

We consider first of all the effect of the boundary layer on the pattern of solute segregation. It has already been shown, in the results section, that the existence of a boundary layer reduces the concentration of solid deposited at a growing interface. For boundary layers in specimens such as those corresponding to figure 44, the thicknesses were found to be

dependent on the temperature gradient and the concentration, but not on the growth rate. This is probably what would be expected under the circumstances because convection in these specimens arises from density inversions caused by rejection of a heavy solute above lighter liquid and by having a temperature gradient with hot liquid below cold. Increasing the effect of either of these causes of convection should decrease the boundary layer thickness. It is interesting to note that variation in growth rate does not influence the thickness of the boundary layer.

The superimposition of boundary layer limits and probe traces (figure 46) suggests that the model of Burton et al (1953) is a highly satisfactory approximation to the actual conditions. The boundary layer thicknesses vary, in the results from both methods, in the same sense, and, in terms of absolute values of δ, they concur fairly accurately.

Convection does not, according to the results of the experiments described, have any other effect on the interface. Cell sizes remain unchanged and values of lateral solute segregatin coefficients are the same for both stirred and non-stirred melts. These latter measurements unfortunately, show a considerable scatter because of the necessity of analysing over the coarse cellular structure.

These conclusions are not unexpected, and it is easy to see that as long as the boundary layer is reasonably thick, the interface has no method of knowing whether the liquid is stirred or not. It can be assumed that if the boundary layer is so thin that the concentration gradient in the mixed zone would not have been zero in a direction at right angles to the growth direction, then the pattern of solute segregation will be markedly affected. This will take place if the boundary layer thickness becomes of the same order of the cell size.

This conclusion was also reached by Hurle (1969) in a mathematical analysis considering the effect of convection on the planar interface breakdown conditions. He found that for $2\pi\delta \gg L$ the effect was negligible but that when $2\pi\delta \ll L$, the Mullins and Sekerka predictions will be changed.

Estimates of δ from other studies have ranged from 120 μm to 2000 μm, and in this work from 250 μm to 420 μm, so that it may be that the condition $2\pi\delta \ll L$ has never been fulfilled.

(b) Salt-fingering

In the case of aluminium-magnesium alloys, the convective flow patterns are much more complex and it is difficult to analyse the results. Graphs of the type shown in figure 42 show that the solute is split up into some kind of layer system and will probably give a striated effect in the solid. It is possible to calculate values of boundary layer thickness from the concentrations estimated from microanalysis results, but it must be emphasised that such values are quite meaningless, since they have no relevance to the actual microsegregation involved.

It should be noted that it is possible to have the conditions set up for this type of convection and yet for no density inversion to exist. Density inversion is caused by solute effects and the temperature gradient stabilises a non-stirred melt. Whichever of these is greatest in magnitude is dominant. It is of interest to calculate the relative contributions of the two effects at a planar interface.

Then, density gradient caused by temperature effects is $(\frac{d\rho}{dx})_T$ where

$$(\frac{d\rho}{dx})_T = (\frac{d\rho}{dT}) \cdot (\frac{dT}{dx}) = (\frac{d\rho}{dT}) \cdot G$$

Density gradient caused by solute accumulation is

$$(\frac{d\rho}{dx})_c = (\frac{d\rho}{dc}) \cdot (\frac{dc}{dx}) = (\frac{d\rho}{dc}) \cdot (\frac{1}{k_o} - 1) \frac{VC}{D}$$

Substituting values into these equations

$$(\frac{d\rho}{dc}) \simeq 8 \times 10^{-3} \text{ gms}/\text{cc}/\% \qquad (\frac{d\rho}{dT}) \simeq 10^{-4} \text{ gms}/\text{cc}/^{o}\text{C}$$

$$(\frac{d\rho}{dx})_c \simeq 8 \times 10^{-3} \cdot \frac{VC}{D} (1/k_o - 1) \qquad (\frac{d\rho}{dx})_T \simeq 10^{-4} G$$

When these gradients are equal and opposite, the conditions are such as to just stabilise a non-stirred melt. This happens when:

$$10^{-4} G = 8 \times 10^{-3} \frac{VC}{D} (^1/k_o - 1)$$

$$^G/VC = \frac{80}{D} (^1/k_o - 1)$$

Thus it can be seen that convection is important in planar interface growth at velocities well below the velocity necessary to cause breakdown to cells. It can be estimated that the value of the parameter $^{VC}/G$ for the onset of convection in the liquid is of the order of $^1/16 = {}^m/80$ of the value at breakdown. This conclusion is, of course, only valid at the interface since the concentration gradient diminishes away from the interface. Convection will cease when the two contributions become equal. It is possible, therefore, to obtain a band of liquid close to the interface in which there is convection while liquid further up the tube is stabilised by the positive temperature gradient. For example, consider the width of a convection band at the planar interface breakdown conditions. The band width is x, and at that position the contributions $(^{d\rho}/dx)_T$ and $(^{d\rho}/dx)_c$ are equal.

$$\text{At } x \quad (\frac{dc}{dx}) = (^1/k_o - 1) \frac{V}{D} e^{\frac{-Vx}{D}}$$

$$(\frac{d\rho}{dx}) = (^1/k_o - 1) e^{\frac{-Vx}{D}} . 8 \times 10^{-3}$$

$$(\frac{d\rho}{dx}) = G. 10^{-4}$$

Equating these

$$80 (^1/k_o - 1) \frac{V}{D} e^{\frac{-Vx}{D}} = G$$

At breakdown conditions

$$\frac{G}{VC} = (^1/k_o - 1) \frac{m}{D}$$

$$e^{Vx/D} = \frac{80}{m} = 16$$

$$^{Vx}/D = 2.8$$

The width of the convection layer (x) is 2.8 times the characteristic distance of the diffusion profile and the melt is therefore effectively fully stirred. Between the values of the parameter $^{VC}/G$ for planar interface breakdown and for no convection, there exists the possibility of small convection bands,

in front of the interface, leading to partial and localised stirring.

3. The Scale and Morphology of Cellular and Dendritic Interfaces

(a) The Size of Cells

The results have shown that simple cell sizes do not vary to a large extent with either alloy composition or growth rate. We must then ask the question - what causes a variation in cell size? In order to answer this, it is necessary to evaluate the conditions in which they have been found to vary.

(i) Non-stirred melts

Cell size in non-stirred melts depends on temperature gradient but not growth rate or alloy composition. According to measurements of k_e-values discussed on p.61, the average concentration gradient in front of cell tips is also dependent on the imposed temperature gradient but not on composition or growth rate, since

$$\frac{dC}{dx} = \frac{G}{m}$$

Thus, it is possible to say that the size of cells, grown under steady-state conditions, is primarily connected with the average concentration gradient in front of their tips.

(ii) Stirred melts

In systems where there is convective mixing in the liquid, no change in cell size is observed. This is known to be true only for cases where the thickness of the boundary layer is larger than the diameter of the cells.

(iii) Planar interface breakdown

When a planar interface breaks down, investigations have shown that there is an incubation period, which can be as long as 3.5 minutes, before cells appear. The reason for this is not known, but the effect of it is to increase the concentration gradient in the liquid above its normal cellular steady-state value (i.e. $^{dC}/_{dx} > {}^{G}/_{m}$). The solid concentration remains almost unchanged. As figure 52 shows, the initial cell size has a dependence which is completely different from steady-state conditions, in that it is markedly dependent on the actual velocity at breakdown but not on the imposed

temperature gradient. This breakdown velocity, however, determines the concentration gradient in front of the first cells to appear, since, at a planar interface

$$\frac{dc}{dx} = \frac{VC}{D}\left({}^{1}/k_o - 1\right)$$

Note that the imposed temperature gradient does not influence the concentration gradient in this equation.

When the cells have grown for some time, they regain steady-state conditions and the average concentration gradient in the liquid at the tips becomes equal to ${}^{G}/m$. At the same time, the cells take the size which we have found to be characteristic of steady-state growth.

The evidence thus points to the dependence of cell size on the average concentration gradient in the liquid. This means that equilibrium cell sizes as predicted by perturbation theories must always be given by breakdown cell sizes at the breakdown conditions appropriate for that temperature gradient.

It is possible to solve Mullins and Sekerka's central equation for cell size at various growth conditions in order to predict the initial cell sizes which were produced according to the methods involved in this investigation. Such a solution is not strictly correct, because the Mullins and Sekerka equation is only applicable rigorously when the condition ${}^{\dot{\delta}}/\delta = 0$ is fulfilled. This is equivalent to having no constitutional supercooling. The condition ${}^{\dot{\delta}}/\delta = 0$ is solved with the equation given below so as to obtain a maximum value of ${}^{\dot{\delta}}/\delta$.

$$\frac{\dot{\delta}}{\delta} = \frac{Vm\left\{-2Tm\Gamma w^2\left[w^* - \left({}^{V}/D\right)p\right] - (G' + G)\left[w^* - \left({}^{V}/D\right)p\right] + 2mGc\left[w^* - {}^{V}/D\right]\right\}}{(G' - G)\left[w^* - \left({}^{V}/_{D}\right)p\right] + 2\,wmG_c}$$

where ${}^{\dot{\delta}}/_{\delta}$ is the rate of growth of a perturbation

w frequency of the perturbation

Tm melting point of the solvent

$w^* = {}^{V}/2D + \left[\left({}^{V}/2D\right)^2 + w^2\right]^{\frac{1}{2}}$

$p = (1 - k_o)$

$\Gamma = {}^{\gamma}/L$ where γ is the solid-liquid interface energy and L is the latent heat

G_c is the solute concentration gradient

G' and G are the thermal gradients in solid and liquid respectively adjusted by a suitable conductivity ratio.

Using this equation at conditions not equivalent to breakdown conditions (i.e. when $\dot{\delta}/\delta \neq 0$) will produce uncertainty in the validity of the result, but it is possible that the essential form of the dependence may be unchanged.

Values for the parameters were inserted in a computer solution of this equation, to obtain values of w which corresponded to the maximum in the $\dot{\delta}/\delta$ vs w curve. In the absence of reliable data, γ was taken to be 300 ergs/cm^2. The results showed negligible dependence on temperature gradient, and they are plotted as the line on figure 69. Also plotted on this graph are the points from figure 52, corresponding to initial spacings measured as a function of velocity at breakdown. Steady-state cell sizes are shown with velocities corresponding to breakdown under conditions of no constitutional supercooling. All these points are shown multiplied by a constant factor of 0.6 which it was found empirically was required. This factor could be the result of uncertainty in the values of the variables used in the solution of the Mullins and Sekerka equation or it may be caused by the errors in using the equation under conditions where ($\dot{\delta}/\delta \neq 0$). An alternative possibility is that cells do not form immediately from a planar interface, but that there is an intermediate stage. If, for example, there were an array of close-packed nodes, as has been reported, then cells which formed from these would have a spacing of $\sqrt{3}$ x the spacing of the nodes - according to the relation between nodes and cells shown in figure 70. This would involve a disappearance of a proportion of the nodes.

(b) Curvatures

Radius of curvature decreases, and more solute is rejected laterally, as the product VC increases. However radii of curvature for lower temperature gradient specimens are higher, even though, at the same composition and growth velocity, the amount of lateral rejection is greater. Presumably

this is connected in some way with the change in spacing of the cells, but it is difficult to understand exactly how it would occur.

The effect of curvature on the solute undercooling must be of the form shown in figure 71, for three different velocities. As the radius of curvature increases, for a given velocity, the undercooling rises because less solute is rejected laterally. This situation for a planar interface, when ΔT is given by

$$\Delta T = mC_o \left(^1/k_o - 1\right)$$

is approached asympotically. For a given undercooling, increasing the velocity requires a lower radius of curvature in order to cope with the faster lateral distribution which is necessary. The apparent radii of curvature observed are those shown by the crosses on the diagram. These are not positioned at the minima in the total undercooling curves. It should be noted that increasing the growth velocity lowers the radius of curvature at the tips not merely to keep pace with the lateral redistribution but to enhance it, thereby reducing the undercooling.

However, this situation must change when the dotted line represented on the diagram comes at high velocities to the position of the minima of undercooling. This is equivalent to the position where further decreaase of radius of curvature causes rapid increase in curvature undercooling, and, as such, applies only at extremely high tip curvatures. At this point, two courses can be considered. Either the radius of curvature decreases only to maintain the minimum in undercooling. This would mean an increase in solute pile-up. On the other hand, the radius could decrease further so as to lower the solute accumulation in the same way as previously. Both of these require an increase in undercooling with increasing growth rate, and detection of this could be possible with precise temperature measurements. Doherty and Feest (1971) have measured such an increase in undercooling and Burden (1971) has undertaken more precise and quantitative work on the same line.

(c) Branching of Simple Cells

Branching of simple cells was found to occur at specific values of growth velocity for a given alloy rather than being a gradual process. The onset of branching may correspond to the situation where the tip radius of curvature equals or is some function of half the cell spacing (i.e. until the cell tips are approximately hemispherical). The dependences of size and curvature on the growth variables are respectively, given by

$$L \propto G^{-\frac{1}{2}}$$

$$r \propto G^{-1}V^{-\frac{1}{2}}$$

If the onset of branching occurs when these are equal then it depends on the parameter r/L which is given by

$$r/L \propto \frac{G}{V^2}$$

This dependence has been widely reported in studies of the cell to dendrite transition.

When cells start to branch at their tips, then their size appears to change rapidly to somewhat higher values, but further increases of growth velocity causes a decrease in size. Possibly this sudden increase in size coincident with the onset of branching is caused by the increased efficiency of a branched cell in lateral solute rejection. This has the effect of not requiring such small diffusion distances and therefore the cells can take larger dimensions.

4. The Coarsening of Cells behind the Interface

(a) Mechanism of Re-arrangement of Intercellular Liquid

The results of investigations of transverse sections of cellular specimens behind the interface showed that rearrangement of intercellular liquid occurs. This was found to occur very quickly and to be orientation dependent. It is thought that the driving force for the effect is the reduction of surface area of solid-liquid interfaces - interfaces between the solid cells and the intercellular liquid.

A hexagonal cell, in reducing its solid-liquid interface free energy will tend to become rounded. This produces, as figure 72 shows, an

enlargement of the cell corners at the expense of the cell walls. Cell walls thus become thinner and eventually break. Comparison of figure 72(b) can be made with figure 73(b) which shows the thinning and breaking of an actual cell wall. Once a cell wall actually breaks, the surface tension holding both sides together as a sheet of liquid is no longer present and further reduction of the solid-liquid interface area causes rapid contraction of the broken walls into cylindrical channels. The cylindrical channels are now stable, since they cannot reduce their interface area any more. They do not therefore change either in number or size, unless it be by the much slower process of diffusion into the solid. The process of contraction into cylinders is shown diagrammatically in figure 72(c) and can be seen on the transverse sections of figure 54.

The orientation effect is observed only on transverse sections of specimens whose interface plane is close to (110). The unique characteristic of this plane as distinct from (111) or (100) in that the <100>and <110> directions are at right angles. Cell walls which are the slowest to break appear to be planes parallel to the (100) zone. We must consider the anisotropy of solid-liquid interface free energy values.

Crystal-liquid surface free energies are not known, but we can assume that variation of these is in the same direction though not of the same magnitude as free energies of free crystal faces. Polar surface energy variations (or γ-plots) have been determined for face-centred cubic crystals by Sundquist (1964) and have been theoretically predicted by Mackenzie et al (1962). They show that $\gamma_{110} > \gamma_{100}$ and the range of variation is of the order of 17%.

A variation in free energy values of this type will give rise to a tendency to obtain oval rather than round cells in transverse sections behind the interface. This will occur in order to minimise the area of the walls parallel to (110) - the plane which has the maximum γ-value. Because the oval cells are elongated in the <110> direction the walls in the (110) plane will break first. As soon as a wall has broken, its quick contraction will

feed the remaining walls with liquid and thereby reduce the likelihood of their breaking through. Thus, a structure of cell walls, continuous in the <110> direction will be left, even though the difference of surface energies in the different directions is very small.

(b) Mechanism of Coarsening

Figure 56 shows the coarsening of cells which is observed behind the interface, and it can be seen that this takes place by the regular disappearance of some cell walls before others. Obviously, the breaking of a cell wall and subsequent contraction of the liquid into the corners stabilises adjacent walls, but it is not easy to see why a regular pattern should be obtained nor why the scale of this pattern should depend ongrowth rate.

Cells grown at low growth rates have the same spacing at their tips as those grown at high rates, yet their shapes are not the same. The higher the rate, the more intercellular liquid is present and therefore the larger the separation between the cells (figure 74). We can explain the difference in the ability of the cellular structure to coarsen by the greater driving force arising from the more angular cells formed at low rates as compared with the more rounded solid formed at high growth rates. However this theory does not fully explain why such a coarsened structure is so perfectly formed.

(c) Implications of Cell Coarsening

The implications of cell coarsening are to render suspect all determinations of cell size made on transverse sections behind the interface. The speed with which coarsening takes place also casts doubts on the reliability of decanted interface measurements. Since there is appreciable liquid rearrangement in the intercellular regions after only 2 seconds in Al-0.2% Cu alloys, it may be that coarsening can occur during solidification of the residual liquid layer formed on the surface after decanting, especially when alloys with very low concentrations of solute are used.

These suspicions are increased by a consideration of the influence of orientation. The orientation dependence of elongated cells of Morris and Winegard (1969) is exactly that observed in this work and their photographs

of elongated cells are somewhat similar to the rearranged structures of, for example, figure 75. It suggests that elongated cells may not be a growth morphology which is found at the interface, except in the case of faceted crystals, in which they have been seen to exist in place of hexagonal cells (James 1966).

It is also considered relevant that cell size measurements at cell tips in these experiments show no variation with growth rate and yet the coarsened structures have cell sizes which depend on $V^{-\frac{1}{2}}$ - typical of cell size measurements in previous investigations.

5. The Coarsening of Branched Cell and Dendrite Arms behind the Interface

The dependence of the coarsening process of secondary arms being so linked to alloy composition, it is convenient to deal with high and low concentration alloys separately in this section.

(a) Low Concentration 2%, 3%, 4% copper.

These alloys show branched cell morphologies in the ranges studied. We suppose that the driving force for branched cell coarsening is much the same as causes the rearrangement of intercellular liquid in cellular growth - i.e. the reduction of solid-liquid interface free energy. This can be seen from the appearance of channels of liquid, a few seconds after the interface has passed. They are shown, in longitudinal section (figure 76), for an arm of a branched cell where the liquid is broken into droplets and is being pulled out of the positions between the arms.

It was noted in the results section that the coarsening rate for these low concentration alloys was dependent on rate of growth. It is found that the spacing can be given by an empirical relationship

$$\lambda = \lambda_o + kt$$

where λ is the time available for coarsening, λ_o is the initial spacing and k is a proportionality constant which depends on growth rate. The constant k varies with the primary spacing as shown in the graph in figure 77. This gives a relationship which is independent of the rate of growth of the interface

$$\lambda = \lambda_o + \frac{At}{L^2}$$

A is a proportionality constant which is not dependent on the growth rate. L is the primary spacing.

Although this relationship is obeyed satisfactorily, it is not completely clear what relevance the primary spacing has in determining the coarsening rate. It is, however, possible that the primary spacing is the characteristic diffusion distance involved in the liquid re-arrangement. Then

$$d\lambda/dt \propto D/L^2$$

$$= \lambda_o + \frac{BDt}{L^2}$$

where B is a constant of proportionality.

(b) High Concentration 5%, 10% copper.

High Concentration alloys coarsen more slowly and the rate of coarsening is not affected by the growth rate. Bardes et al (1966) and later investigators found that secondary arm spacing measurements on aluminium-copper alloys can be given by the formula

$$\lambda = 7.5 t_s^{0.39}$$

where t_s is the 'local solidification time'

The expression gives $\lambda \to 0$ as $t_s \to 0$, which is correct, because the local solidification time is a function of growth variables as well as being indicative of the time available for coarsening.

$$t_s = \frac{m(C_{EU} - C_I)}{GV} = \frac{m\Delta C}{GV}$$

C_{EU} is the eutectic composition and C_I the concentration of liquid at the dendrite tips.

Then, from this equation $t_s \to 0$ as $GV \to \infty$ and $\lambda_o \to 0$ as $GV \to \infty$. Thus, $\lambda_o \to 0$, as $t \to 0$. However, in the experiments carried out in the present work, the appropriate parameter is not the local solidification time, but the time available for coarsening. Hence, the equivalent relationship in this case is

$$\lambda = \lambda_o + 7.5\, t^{0.39}$$

since $\lambda_o \neq 0$ as $t \to 0$.

Difficulties arise in measuring λ_o at the tips, because the initial spacings are of the same order of size as the quenched structure. Figure 78 shows the tip of a dendrite surrounded by quenched liquid. There is then the possibility that tip spacings are smaller than the scale of the quenched microstructure and can therefore not be seen. However, the curve on figure 65 which runs through the points corresponding to spacings in Al - 10% Cu alloys is that plotted from the equation

$$\lambda = \lambda_o + 7.5t^{0.39}$$

where λ_o is 7.5 μm

The curve seems to fit the data very well in these high concentration alloys and it suggests that the operable mechanism is different from that which produces coarsening in branched cells. The significance of the index 0.39 is not understood but it seems likely that this is related to the laws of diffusion controlled spherical particle coarsening. Wagner (1961) has shown theoretically that the equation for coarsening is

$$\bar{r}^3 - \bar{r}_o^3 \propto Dt$$

where $\bar{r}$ is the mean dimension of the particles at time t and $\bar{r}o$ is the initial mean dimension of the particles.

Thus, when $\bar{r}^3 \gg \bar{r}_o^3$, the equation can be approximately written as

$$r \propto (Dt)^{0.33}$$

In practical terms the ripening mechanism involves a redistribution of solid from some parts of the arms to others. This leads either to a gradual shrinkage of the secondary arms or a narrowing and severance of their necks at the point where they join the primary stalk. Both of these processes can be observed on microstructures and in transparent organic analogues (Jackson et al 1966).

VI SUMMARY OF CONCLUSIONS

The main conclusions of this work can be summarised as follows:

1. Cells and dendrites, grown within the range of conditions used in these experiments, have solute enrichment peaks in front of their tips. The solute enrichment is as high as possible, consistent with the condition that the average concentration gradient in the liquid in the growth direction is equal to G/m.

2. Growth of cells and dendrites ~~does~~ may not take place, in the range of conditions employed, at minimum possible tip undercooling. The contribution to undercooling from the curvature term is negligible compared to that from the solute term in the range of conditions investigated.

3. The radii of curvature of the tips of cells decrease with increase of alloy concentration, growth velocity and imposed temperature gradient.

4. In the case of stirred melts which exhibit steady convection, there is a boundary layer in front of the interface, inside which there is no effective convection. Outside the boundary layer, the liquid is fully mixed.

5. The thickness of the boundary layer depends on the magnitude of the temperature gradient and the concentration of the alloy, but not on the growth rate.

6. If the boundary layer is sufficiently thick, then the interface has no means of knowing that the melt is stirred and the amount of lateral segregation is unaffected.

7. In melts where the temperature gradient is such as to favour no convection and solute gradient promotes convection, 'salt-fingering' is found to occur. In these cases the boundary layer is not well defined and a more complex convection pattern gives rise to a more complex solute distribution.

8. When a planar interface breaks down, there is an incubation period before cells appear. The first cells observed do not therefore grow under steady-state conditions.

9. The size of simple cells measured at the interface does not depend on composition or growth rate but appears to be dependent on the average concentration gradient in the liquid in front of the cell tips.

10. When cells branch, their size increases markedly and then decreases with further increase of growth rate. Radii of curvatures fall steadily with increasing growth rate, alloy concentration or temperature gradient.

11. Extensive rearrangement of intercellular liquid occurs behind cellular growth fronts. This is orientation dependent and is caused by reduction of solid-liquid interface area. A secondary cell array is formed whose spacing is a function of growth rate.

12. Coarsening of branched cell arms occurs by the same mechanism as intercellular liquid rearrangement. The spacing of arms can be given by the formula

$$\lambda = \lambda_o + {}^{At}/_{L^2}$$

where λ_o is the initial spacing and L is the primary arm spacing. This applies for alloys containing 4% copper or less.

13. Coarsening of higher concentration alloys takes place by mechanisms which involve shrinkage of arms or their thinning and severance at the point where they join the primary stalk. The secondary arm spacing can be given by the formula

$$\lambda = \lambda_o + 7.5\ t^{0.39}$$

VII REFERENCES

B P Bardes, M C Flemings. Mod Castings 74 (1966) 100

W Bardsley, J M Callan, H A Chedzey, D T J Hurle. Solid State Electron 3 (1961) 142

J A E Bell, W C Winegard. J Inst Met 92 (1963/4) 357

H Biloni, G F Bolling, G S Cole. TAIMME 236 (1966) 930

G F Bolling, J W Rutter, W A Tiller. Can J Phys 34 (1956) 234

G F Bolling, W A Tiller. J Appl Phys 31 (1960) 2040

G F Bolling, W A Tiller. J Appl Phys 32 (1961) 2587

T Bowers, H D Brody, M C Flemings. TAIMME 236 (1966) 624

H D Brody, M C Flemings. TAIMME 236 (1966) 615

M H Burden. Communication (1971)

J A Burton, R C Primm, W P Slichter. J Chem Phys 21 (1953a) 1987

J A Burton, E D Kolb, W P Slichter, W P Struthers. J Chem Phys 21 (1953b) 1991

J R Carruthers. J Cryst Growth 2 (1968) 1

R Castaing. Thesis: University of Paris and WAL (1951)

R Castaing. 3rd Int Symp on X-ray Optics and Microanalysis (1963) 263

B Chalmers. 'Principles of Solidification' Wiley (1964)

G S Cole, W C Winegard. Can Met Q 1 (1962) 29

G S Cole, W C Winegard. J Inst Met 93 (1964/5) 153

J O Coulthard, R Elliott. J Inst Met 95 (1967) 21

J O Coulthard, R Elliott.'The Solidification of Metals' I.S.I. Publication 110 (1968) 93

G J Davies. 'The Solidification of Metals' I.S.I. Publication 110 (1968) 66

K G Davis, P Fryzuk. TAIMME 233 (1965) 1796

F V Dean, J R Kerr, A Hellawell. J Inst Met 90 (1961/2) 234

R T Delves. Phys Status Solidi 16 (1966a) 621

R T Delves. Phys Status Solidi 17 (1966b) 119

R T Delves. J Cryst Growth 3,4 (1968) 562

R Doherty, A Feest. Unpublished Work (1971)

R Doherty, D A Melford. J.I.S.I. 204 (1966) 1131

L F Donaghey, W A Tiller. 'The Solidification of Metals' I.S.I. Publication 110 (1968) 87

P Duncumb, D A Melford. 2nd Int Symp on X-ray Optics and Microanalysis (1959) 358

J B Edwards, E E Hucke, J J Martin. Met Revs 13 (1968) 1

J Forstén, H M Miekk-oja. J Inst Met 95 (1967) 143

M E Glicksman, R J Schaefer. 'The Solidification of Metals' I.S.I. Publication 110 (1968) 43

M Hansen. 'The Constitution of Binary Alloys' McGraw-Hill (1958)

A Hellawell. TAIMME 233 (1965) 1516

E L Holmes, J W Rutter, W C Winegard. Can J Phys 35 (1957) 1223

J A Horwath, L F Mondolfo. Acta Met 10 (1962) 1037

G Horvay, J W Cahn. Acta Met 9 (1961) 695

M D Hunt, J A Spittle, R W Smith. 'The Solidification of Metals' I.S.I. Publication 110 (1968a) 57

M D Hunt, J A Spittle, R W Smith. J Cryst Growth 3,4 (1968b) 656

D T J Hurle. Solid State Electron 3 (1961) 37

D T J Hurle. J Cryst Growth 5 (1969) 162

G P Ivantsov. Doklady A.N.SSR. 58(4) (1947) 567

K A Jackson, J D Hunt, D R Uhlmann, T P Seward III TAIMME 236 (1966) 149

D J James. TAIMME 236 (1966) 936

R E Jesse, H F J I Giller. J Cryst Growth 7 (1970) 348

W C Johnston, W A Tiller. TAIMME 221 (1961) 331

T Z Kattamis, J C Coughlin, M C Flemings. TAIMME 239 (1967a) 1504

T Z Kattamis, U T Holmberg, M C Flemings. J Inst Met 95 (1967b) 343

J S Kirkaldy. Can J Phys 37 (1959) 739

A Kohn, J Philibert. Mem Sci Rev Met LVII No 4 (1960) 291

G R Kotler, L A Tarshis. J Cryst Growth 3,4 (1968) 603

J J Kramer, G F Bolling, W A Tiller. TAIMME 227 (1963) 374

C S Lindenmeyer. Thesis: Harvard (1959)

J K Mackenzie, A J W Moore, J F Nicholas. J Phys Chem Solids 23 (1962) 185

A B Michael, M B Bever. TAIMME 200 (1954) 47

L R Morris, W C Winegard. J Cryst Growth 5 (1969) 361

L R Morris, W C Winegard. J Cryst Growth 6 (1969) 61

W W Mullins, R F Sekerka. J Appl Phys 35 (1964) 444

W Oldfield 'The Solidification of Metals' I.S.I. Publication 110 (1968) 70

W G Pfamm. TAIMME 194 (1952) 747

J Philibert. 3rd Int Symp on X-ray Optics and Microanalysis (1963) 379

T S Plaskett, W C Winegard. Can J Phys 37 (1959) 1555

D M Poole, A E R E Report R5555 (1967)

J W Rutter, B Chalmers. Can J Phys 31 (1963) 15

R M Sharp. Part II Thesis, Oxford University (1968)

R M Sharp, A Hellawell. J Cryst Growth 5 (1969) 155

V G Smith, W A Tiller, J W Rutter. Can J Phys 33 (1955) 723

C J Smithells. 'Metal Reference Book' Butterworths (1962)

J A Spittle, M D Hunt, R W Smith. J Inst Met 93 (1965) 234

M E Stern, J S Turner. Deep Sea Research 16 (1969) 497

S V Subramanian, C W Haworth, D H Kirkwood. Communication (1968)

B E Sundquist. Acta Met 12 (1964) 67

D E Temkin. Doklady A.N. SSR 132(6) (1960) 1307

P Thomas. A E R E Report R4593 (1964)

W A Tiller, K A Jackson, J W Rutter, B Chalmers. Acta Met 1 (1953) 428

W A Tiller, J W Rutter. Can J Phys 34 (1956) 96

W A Tiller. Can J Phys 37 (1959) 1204

W A Tiller. 'The Art and Science of Growing Crystals' Ed Gilman Wiley (1963)

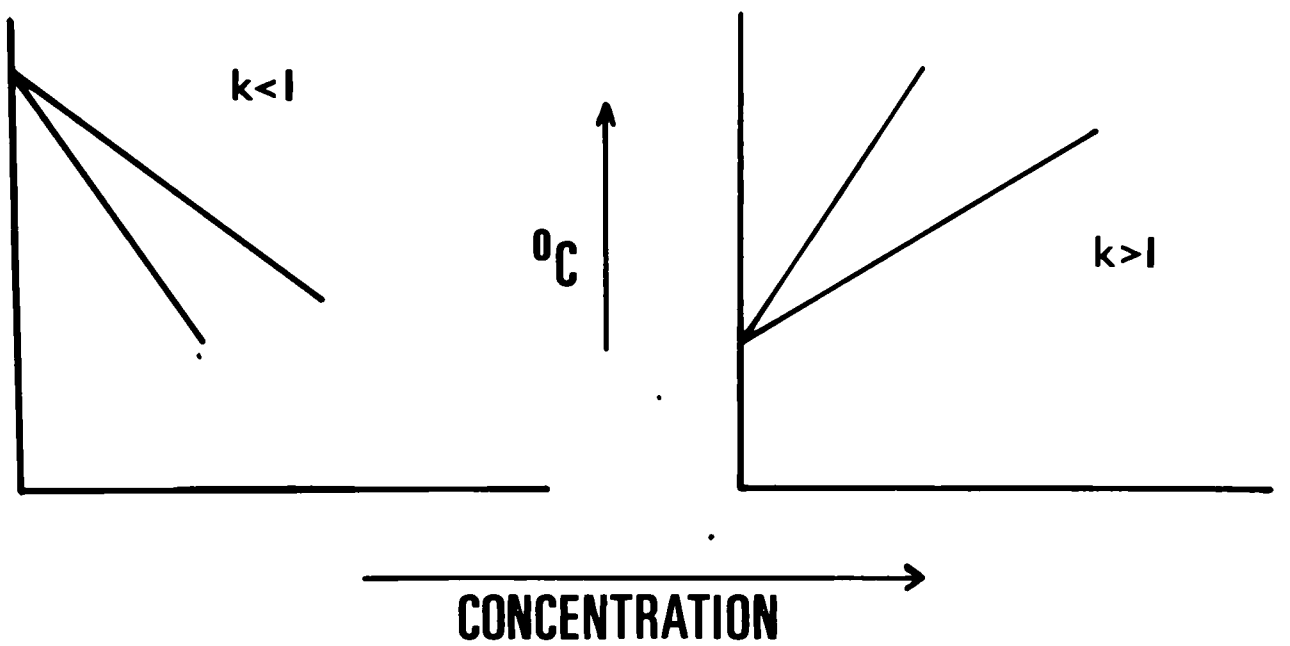
C Wagner. Z Electrochem 65 (1961) 581

D Walton, W A Tiller, J W Rutter, W C Winegard. J Metals N Y 7 (1955) 1023

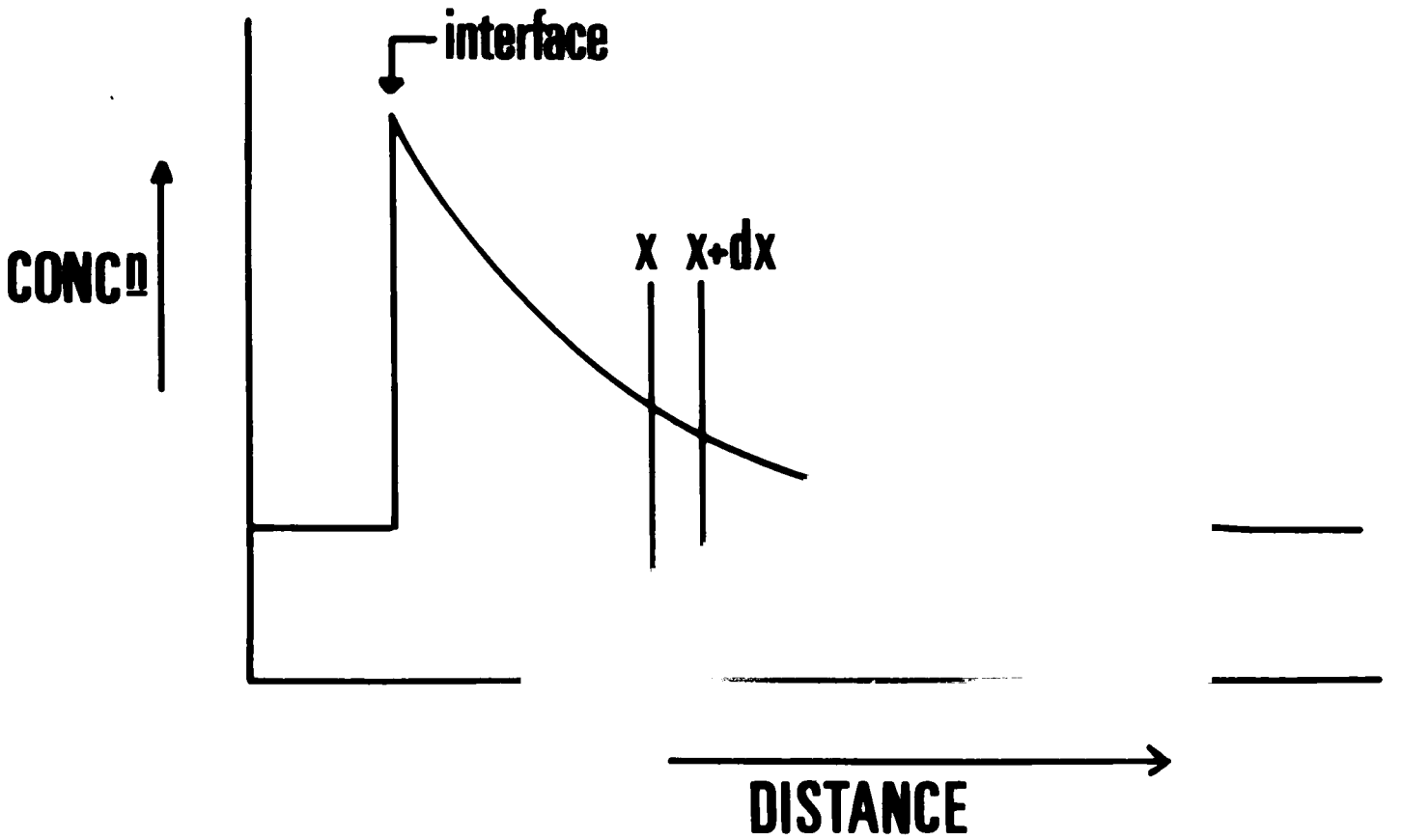
D Walton, B Chalmers. TAIMME 215 (1959) 447

F Weinberg. TAIMME 227 (1963) 231

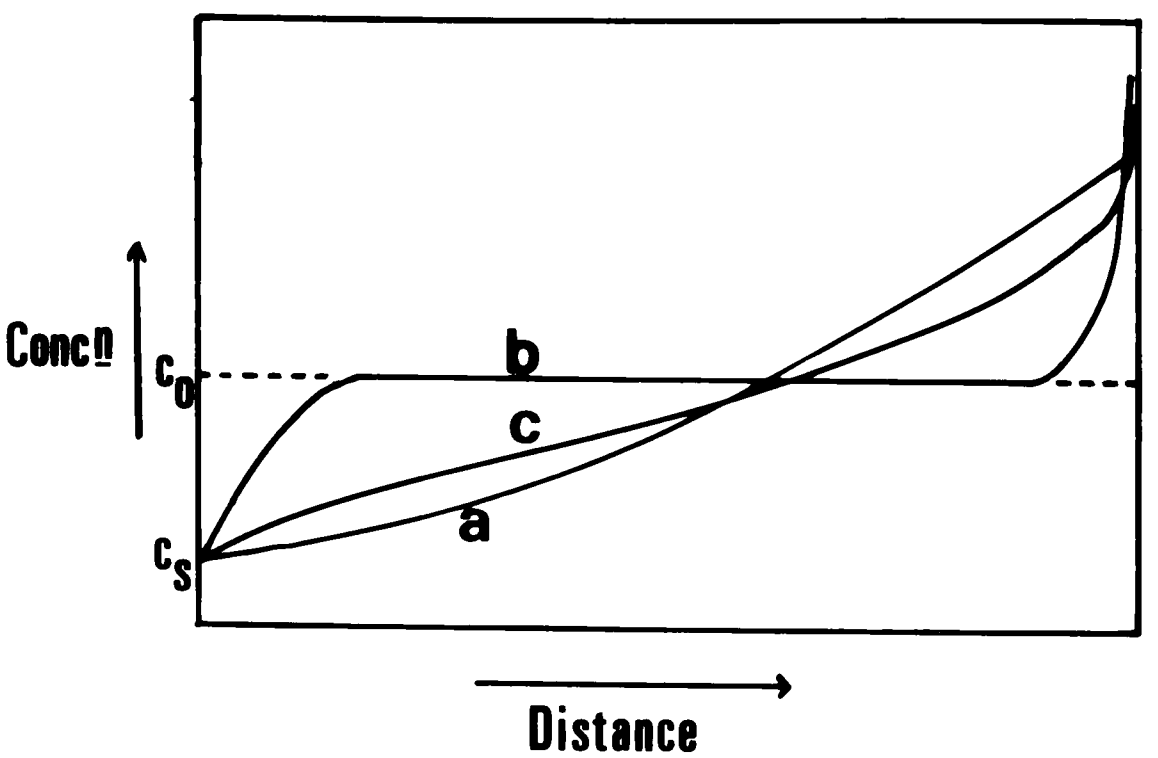
F Weinberg. Proc Int Conf on Cryst Growth, Boston (1966) 639



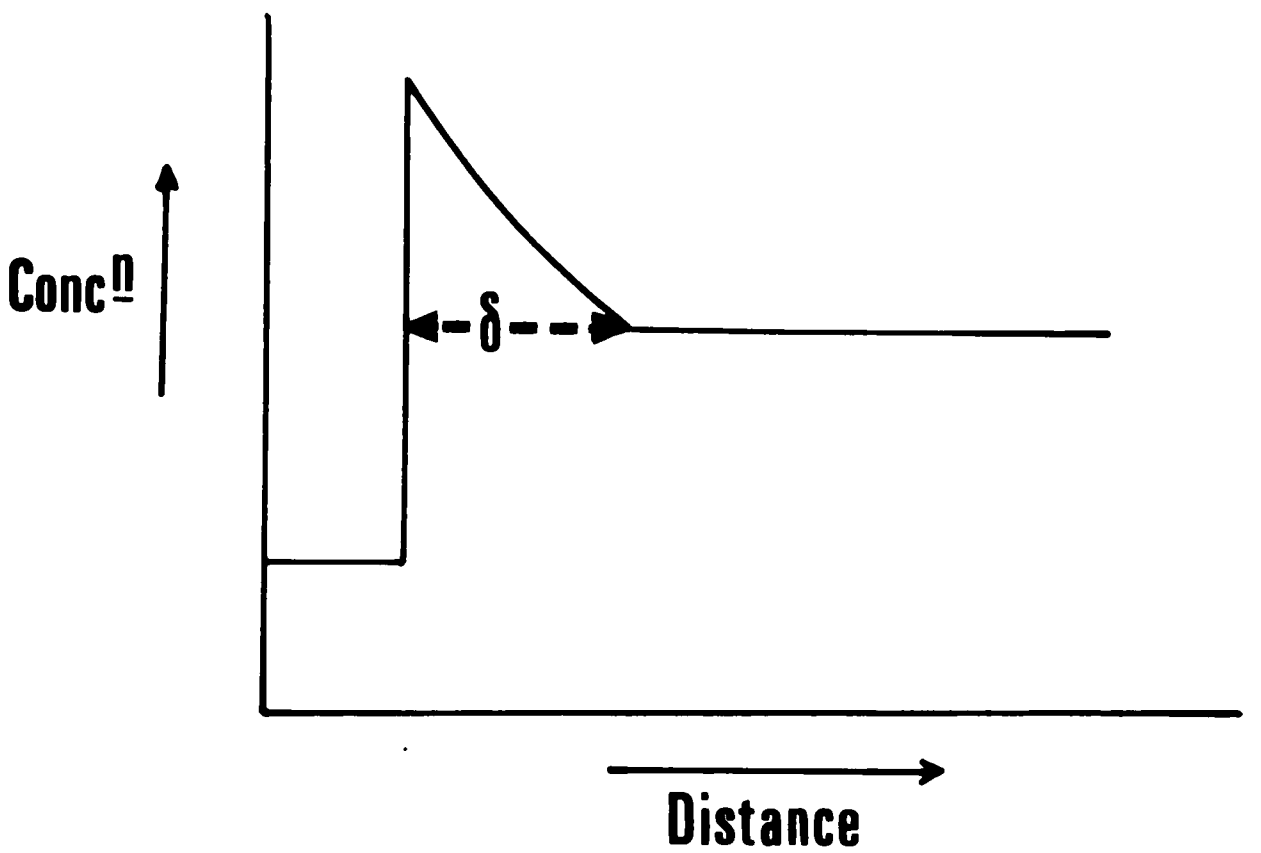
1. Portions of typical phase diagrams showing (a) k < 1 and (b) k > 1.



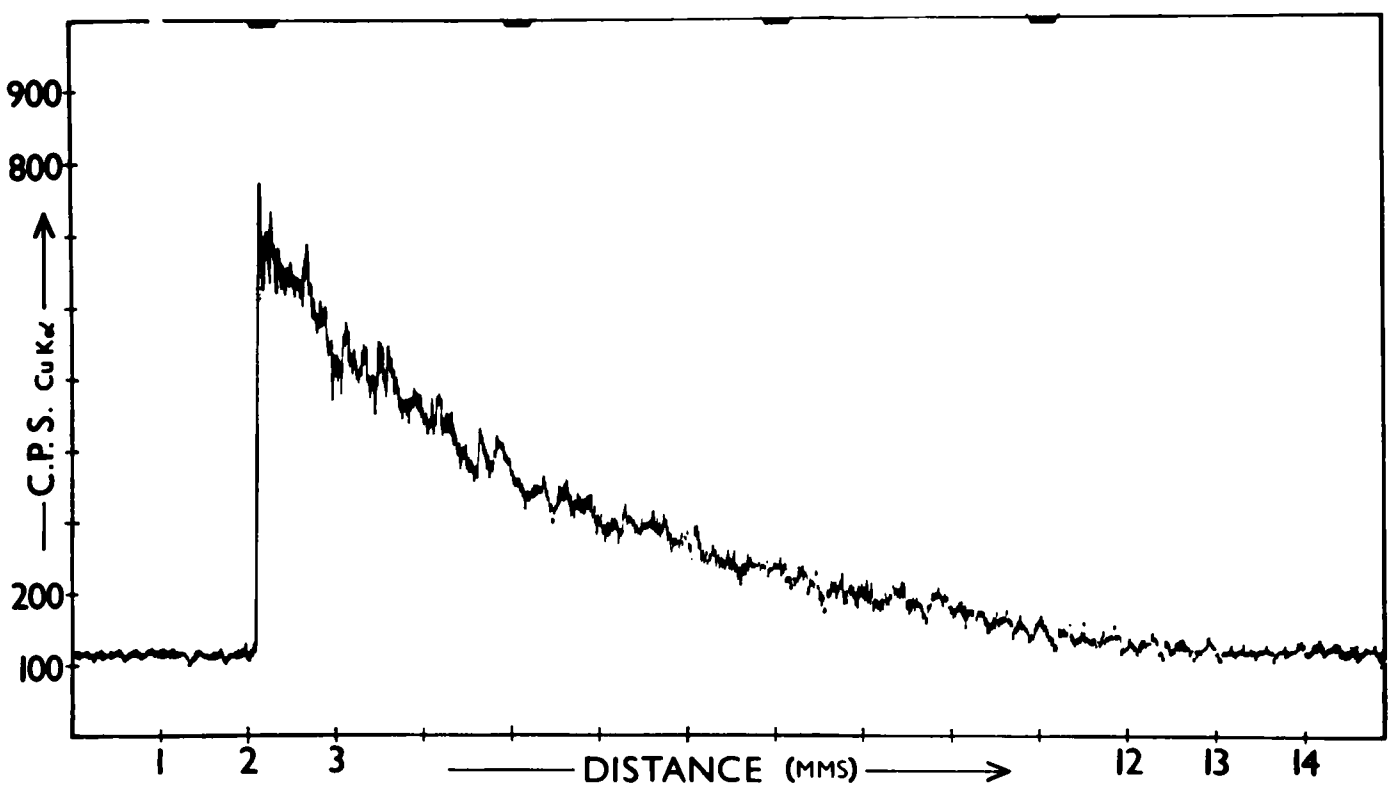
2. Concentration of solute in front of a moving planar interface. The lines at x and (x + dx) represent planes of unit area.



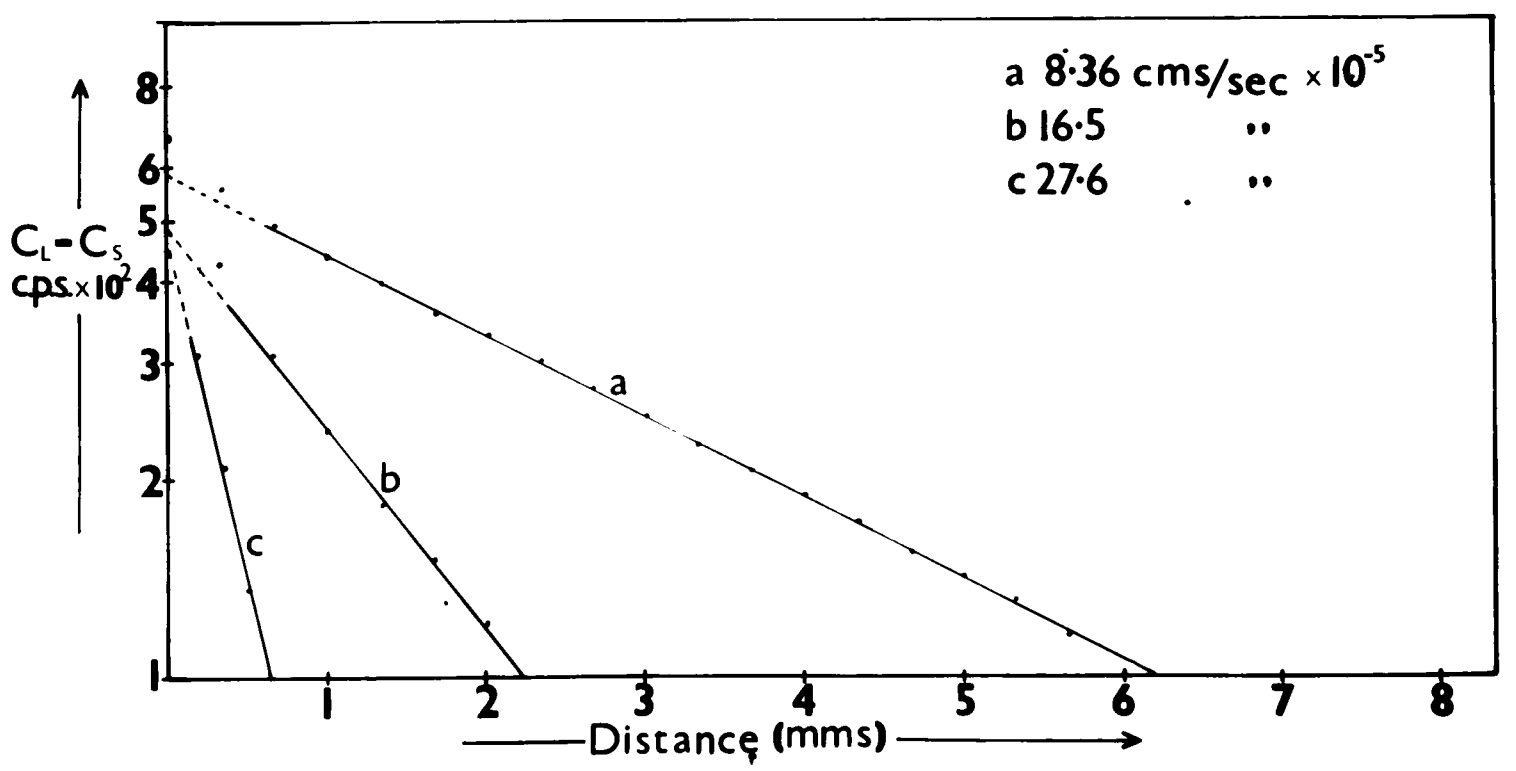
3. Solute distribution after solidification (a) with complete mixing, (b) no convection, (c) with partial mixing.



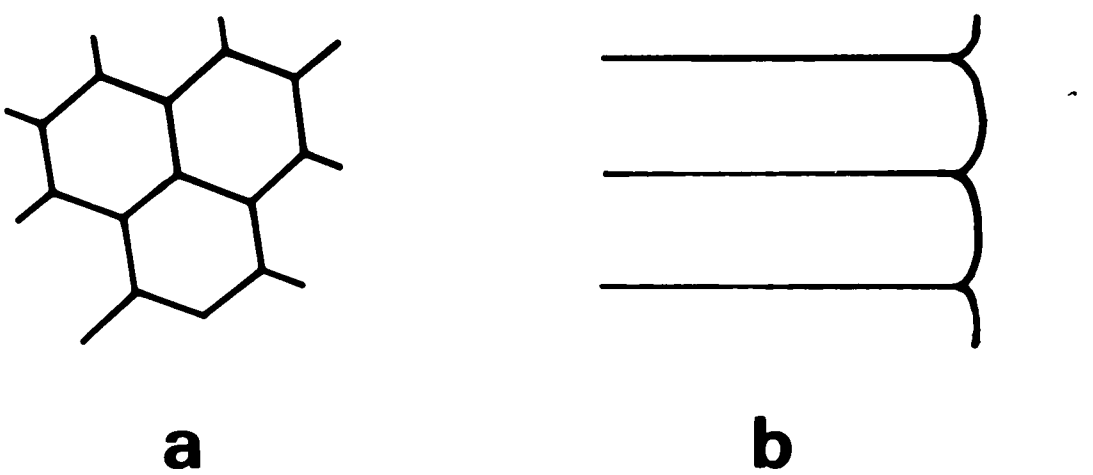
4. Diagram of the model used by Burton et al for calculation of effective distribution coefficient.



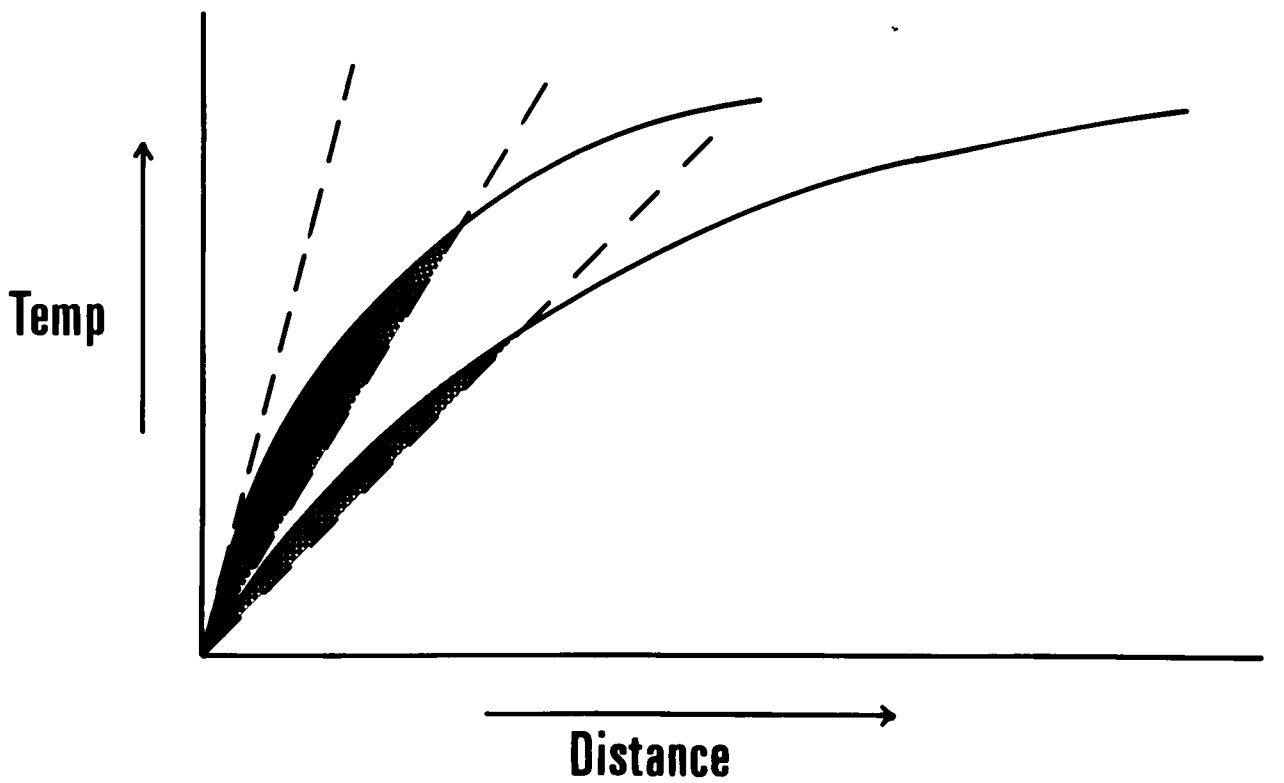
5. Electron microprobe trace showing the concentration of copper in front of a planar interface moving at 0.84 μm/sec (from Sharp and Hellawell).



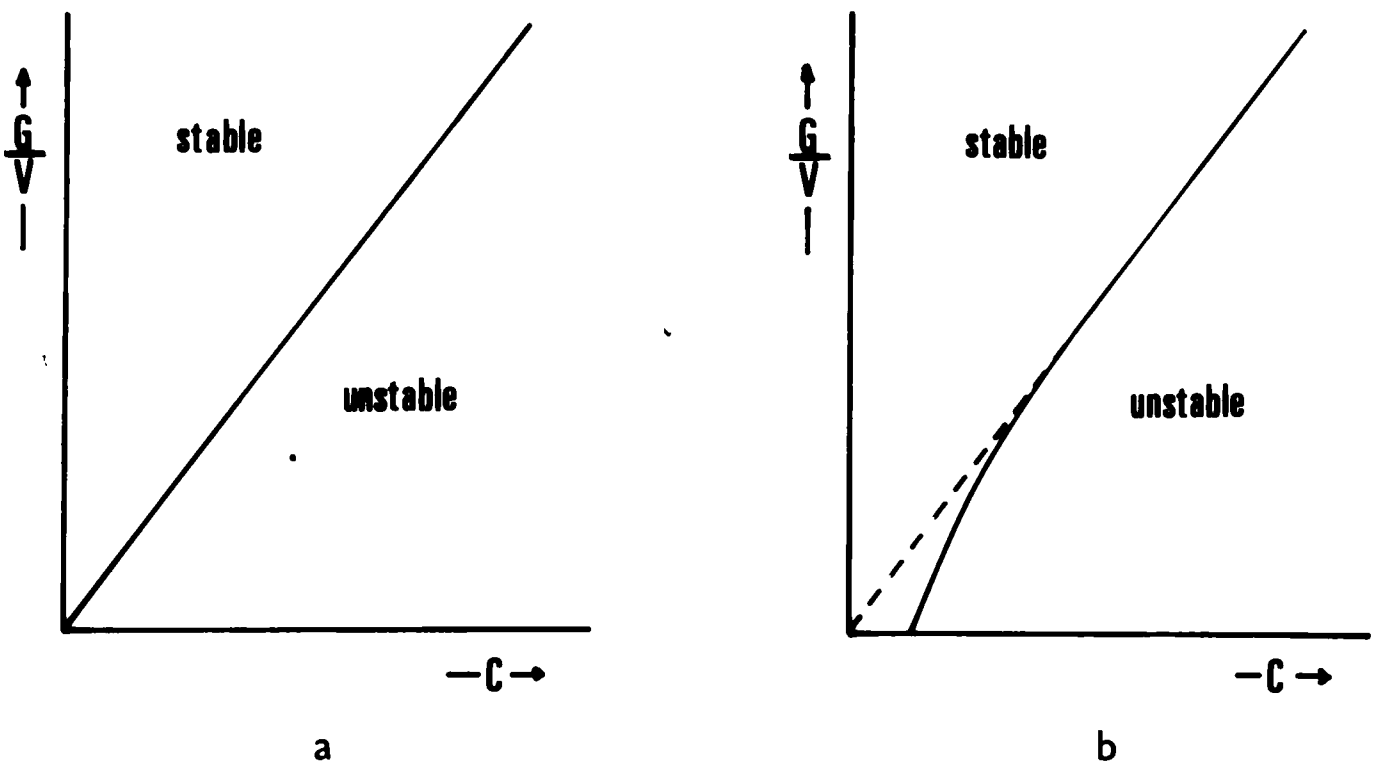
6. Logarithmic plots of concentration and distance for three diffusion profiles (from Sharp and Hellawell).



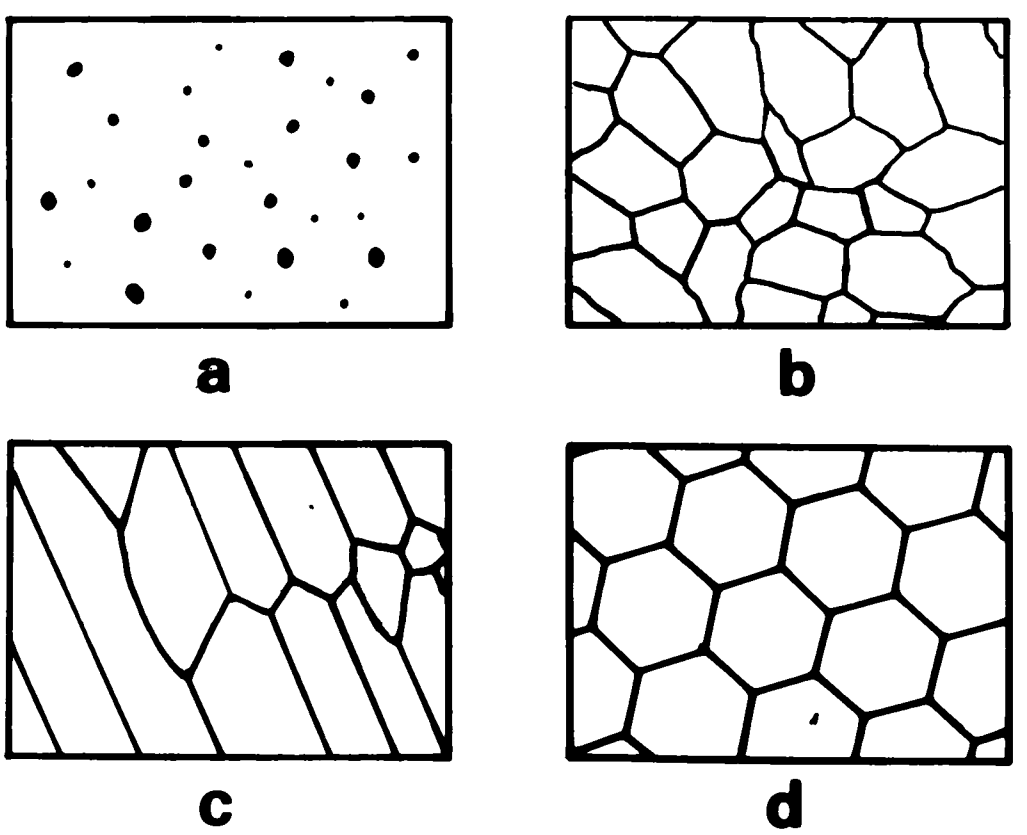
7. (a) Transverse and (b) Longitudinal diagrammatic sections of a cellular substructure.



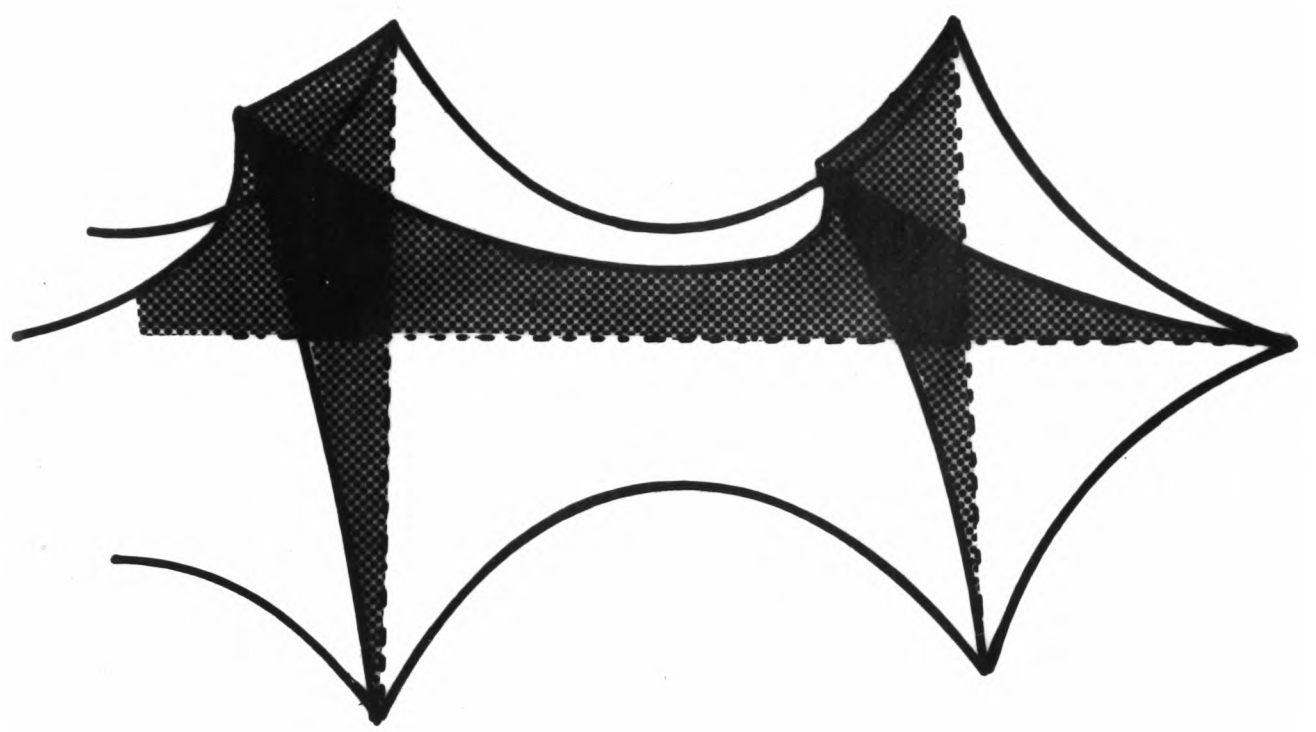
8. Equilibrium liquidus temperatures (full lines) and actual temperatures (dotted lines) ahead of the interface. Shaded areas represent zones of constitutional supercooling.



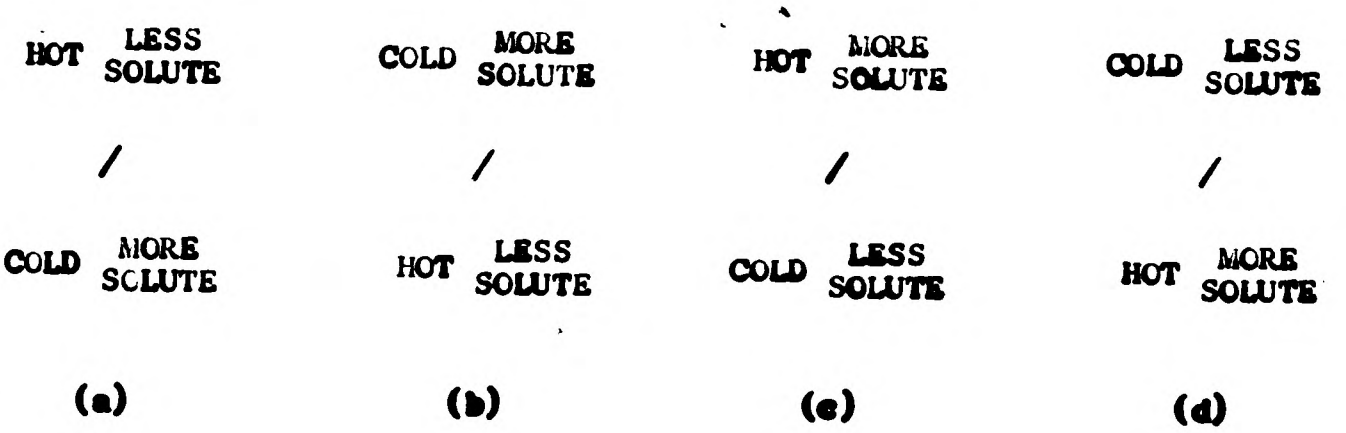
9. Comparison between the constitutional supercooling theory and perturbation analysis predictions.



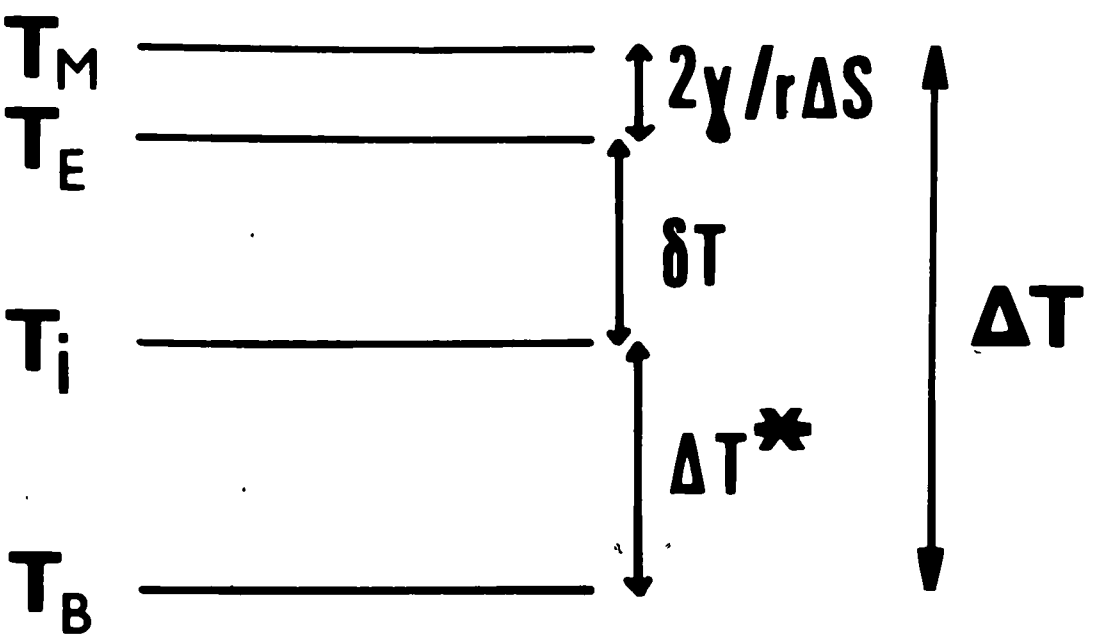
10. Diagrammatic transverse sections of various interface morphologies (a) pox, (b) irregular cells, (c) elongated cells, (d) hexagonal cells.



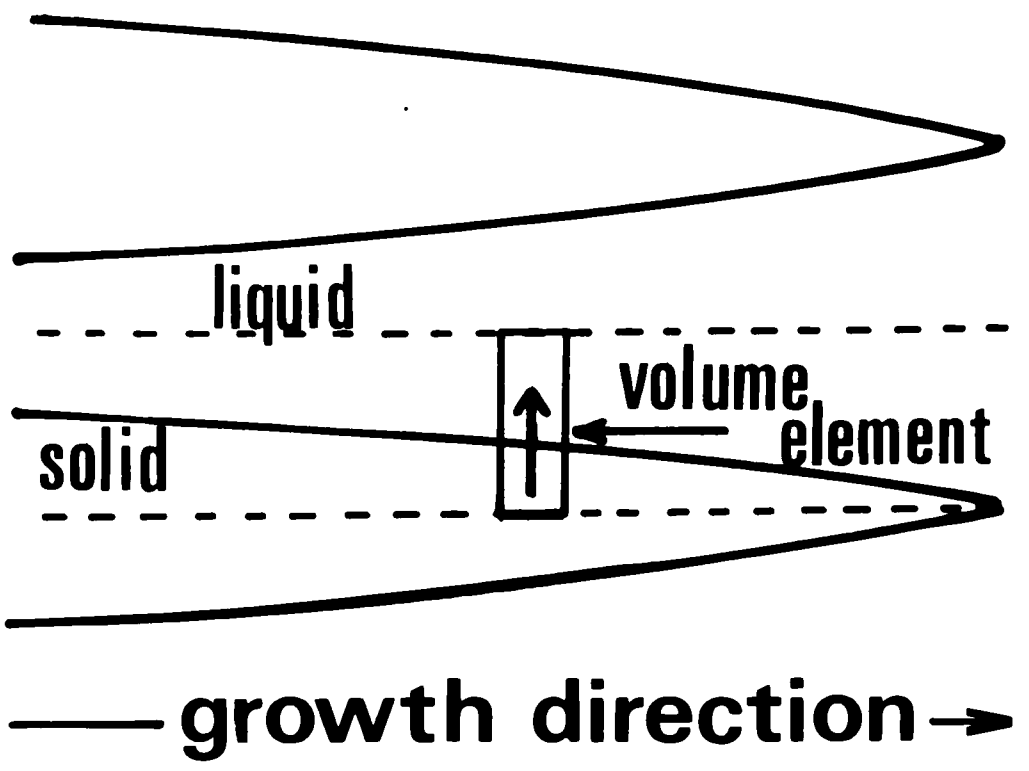
11. Plate-like dendrite morphology.



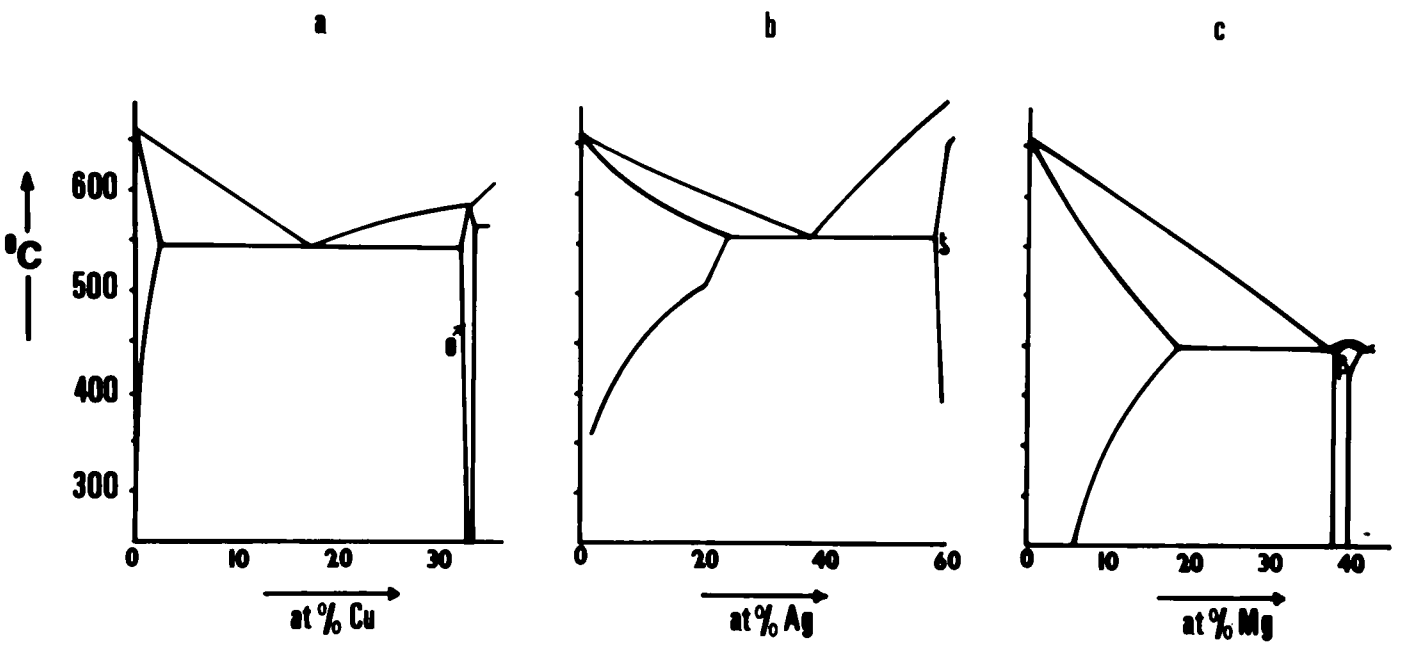
12. Possible combinations of temperature and solute giving rise to different convection characteristics. (a) No convection, (b) Steady convection, (c) Salt-fingering, (d) Temperature oscillations.



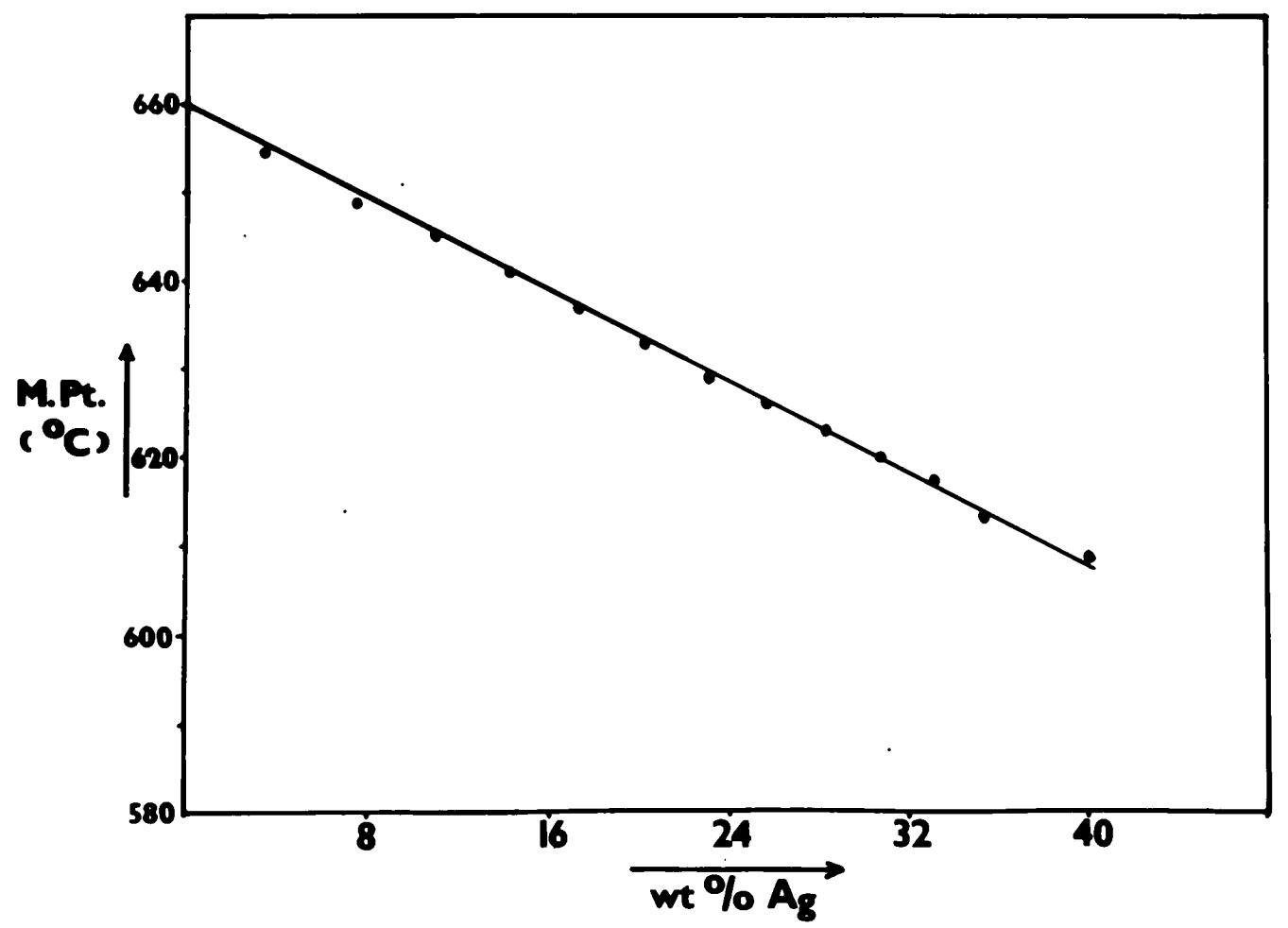
13. Temperatures involved in dendrite growth.



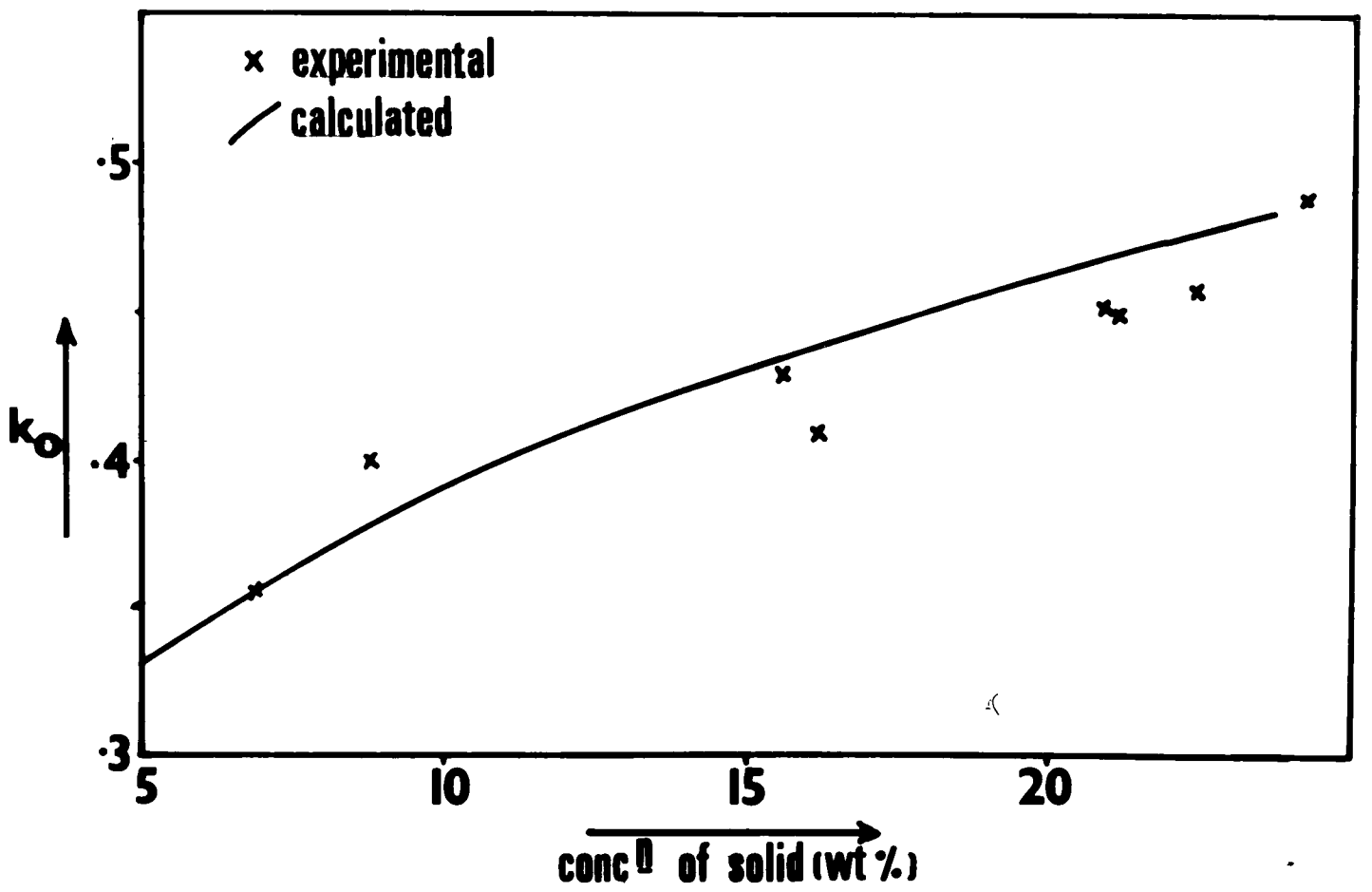
14. Diagrammatic representation of the thickening of dendrite arms.



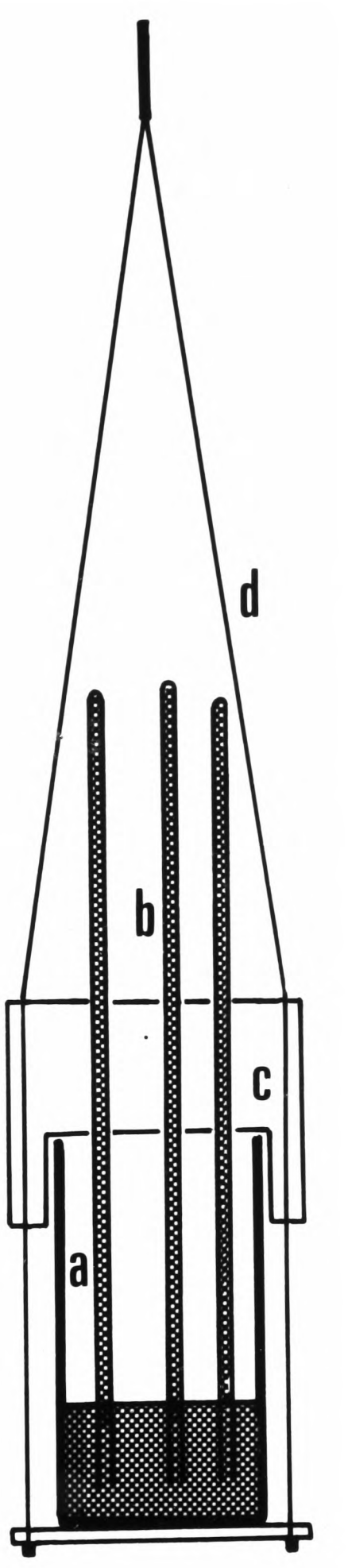
15. Portions of phase diagrams corresponding to alloys used in this work (a) Al-Cu, (b) Al-Ag, (c) Al-Mg.



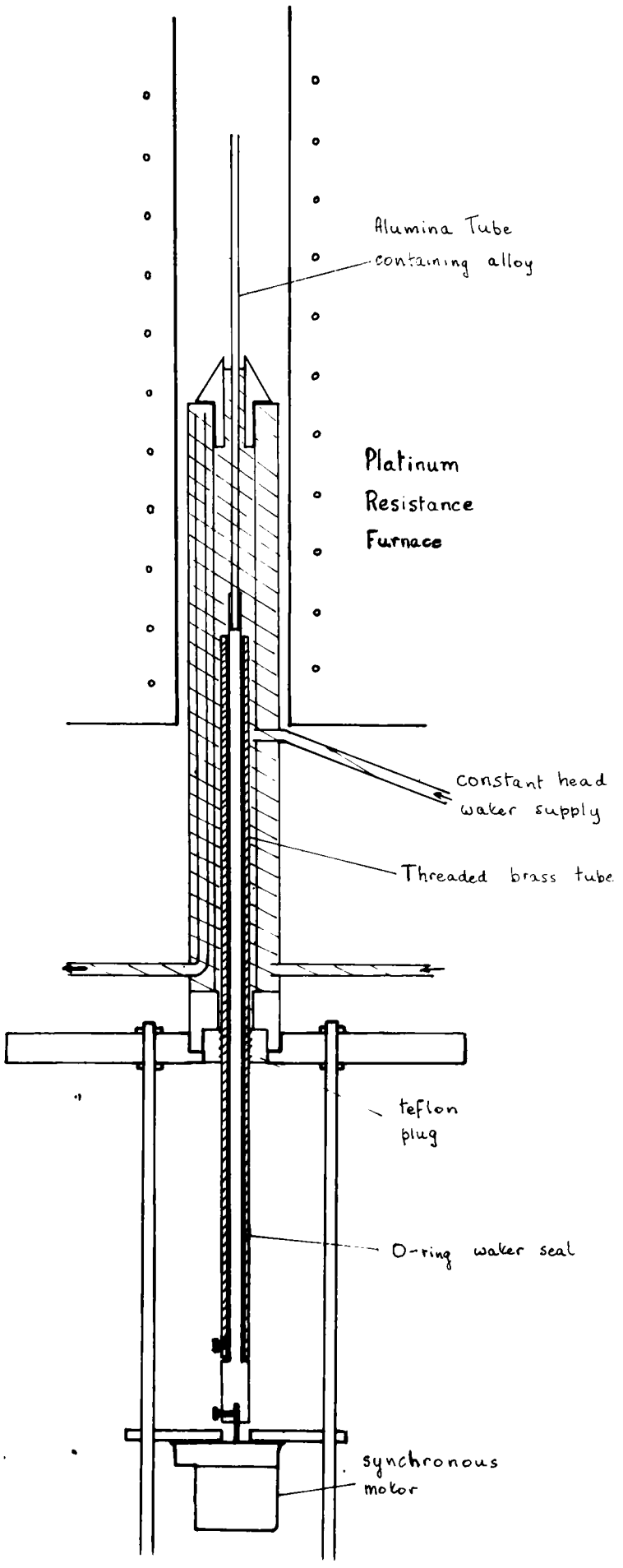
16. The aluminium silver phase diagram plotted in terms of weight percentage.



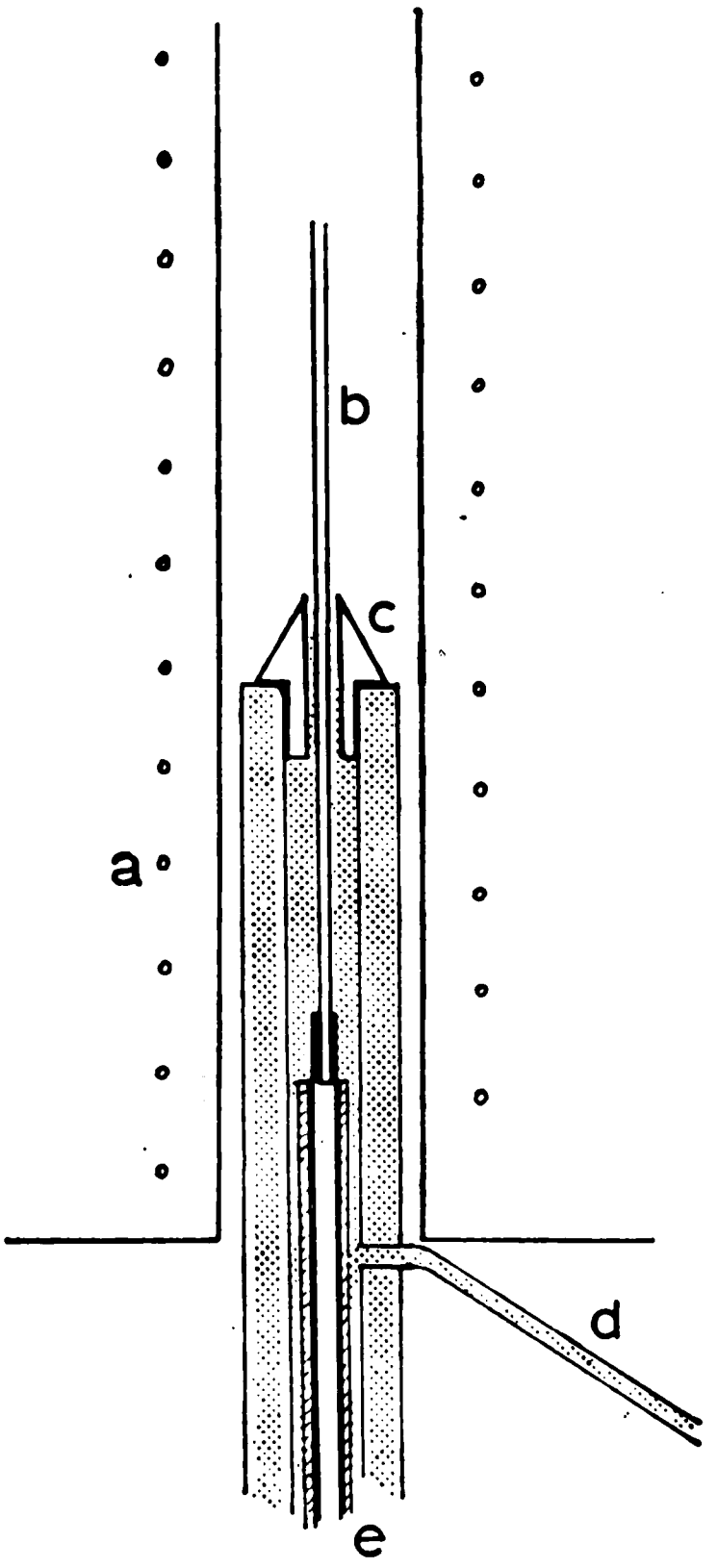
17. Calculated and experimental values for ko in the Al-Ag system.



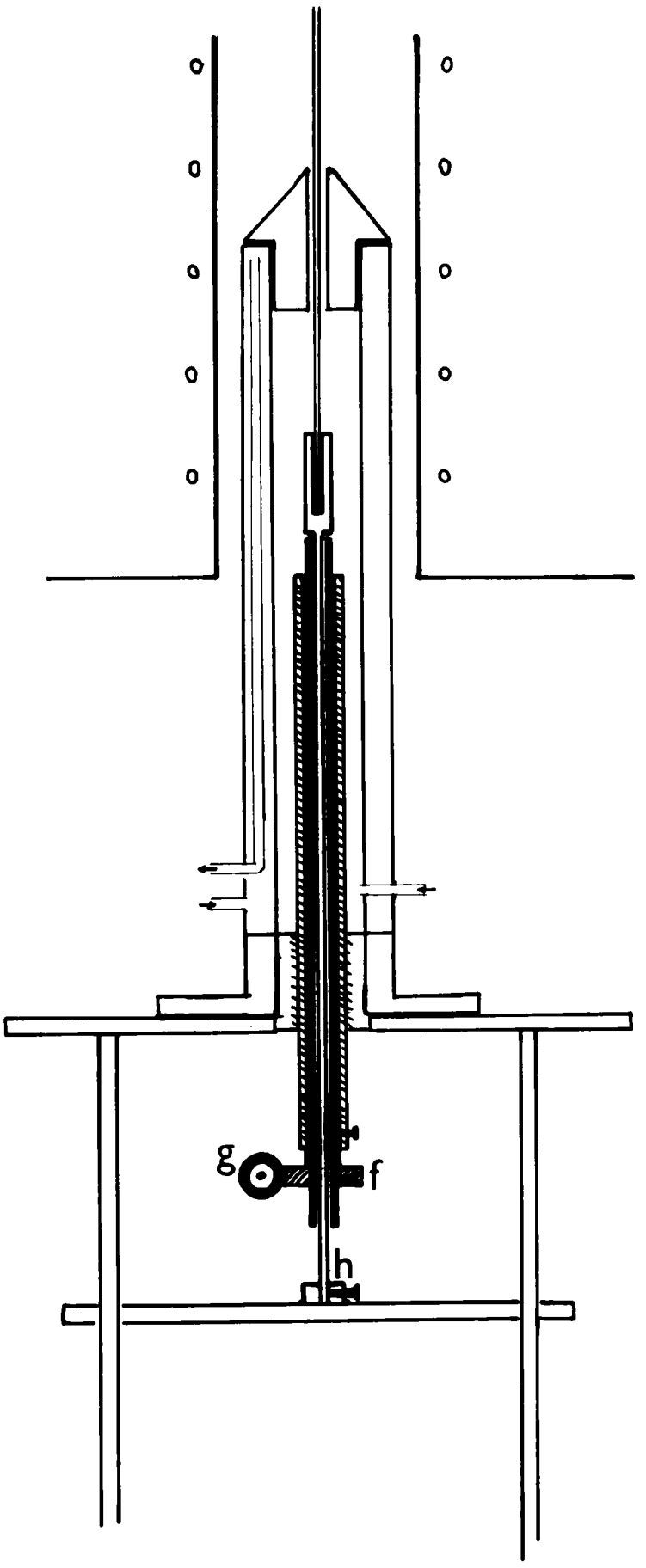
18. Apparatus used for the filling of alumina tubes with alloy. (a) Alumina crucible containing metal, (b) Alumina tubes, (c) Steel block, (d) wire supports.



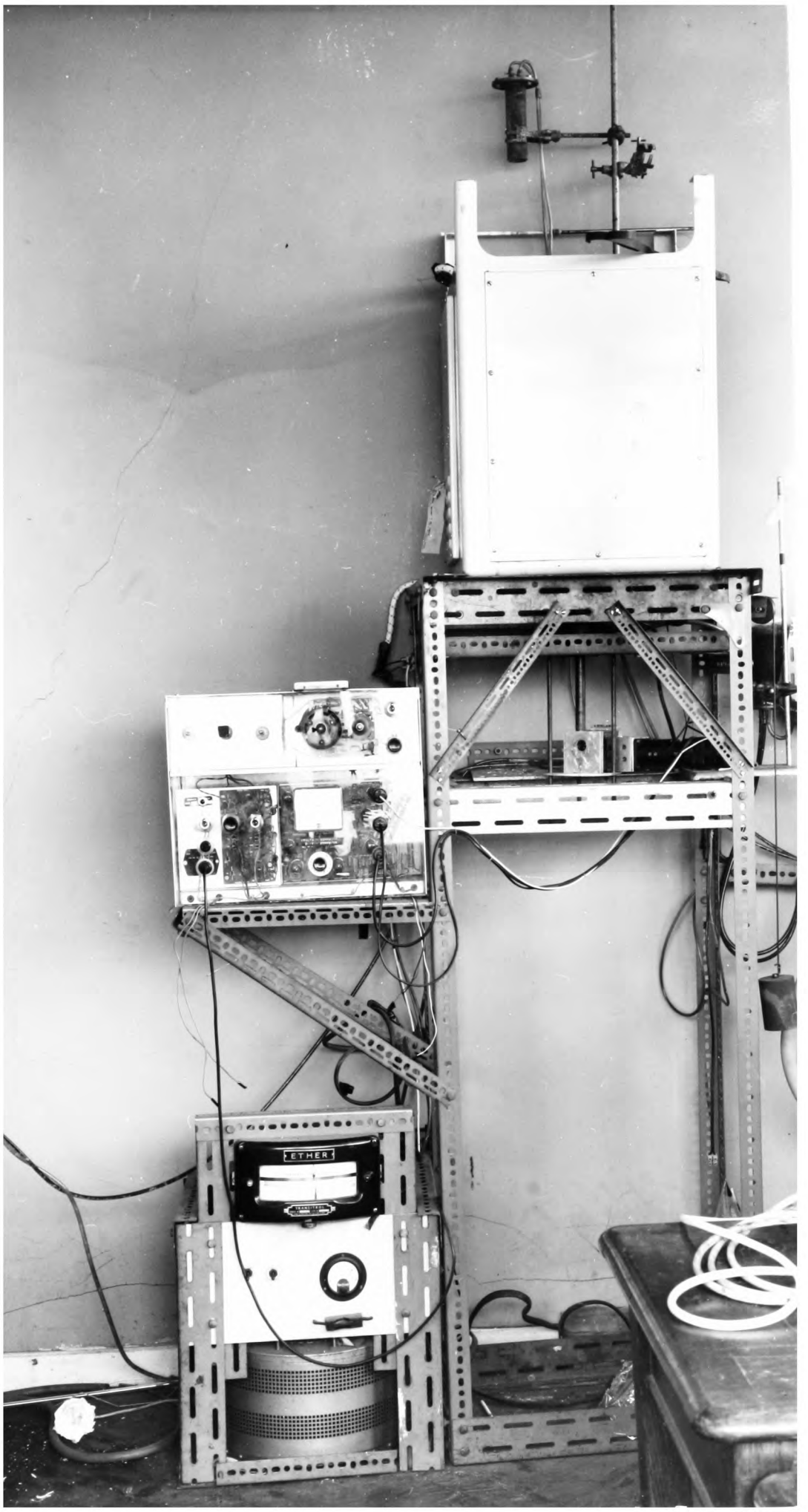
19. Apparatus used for growing specimens.



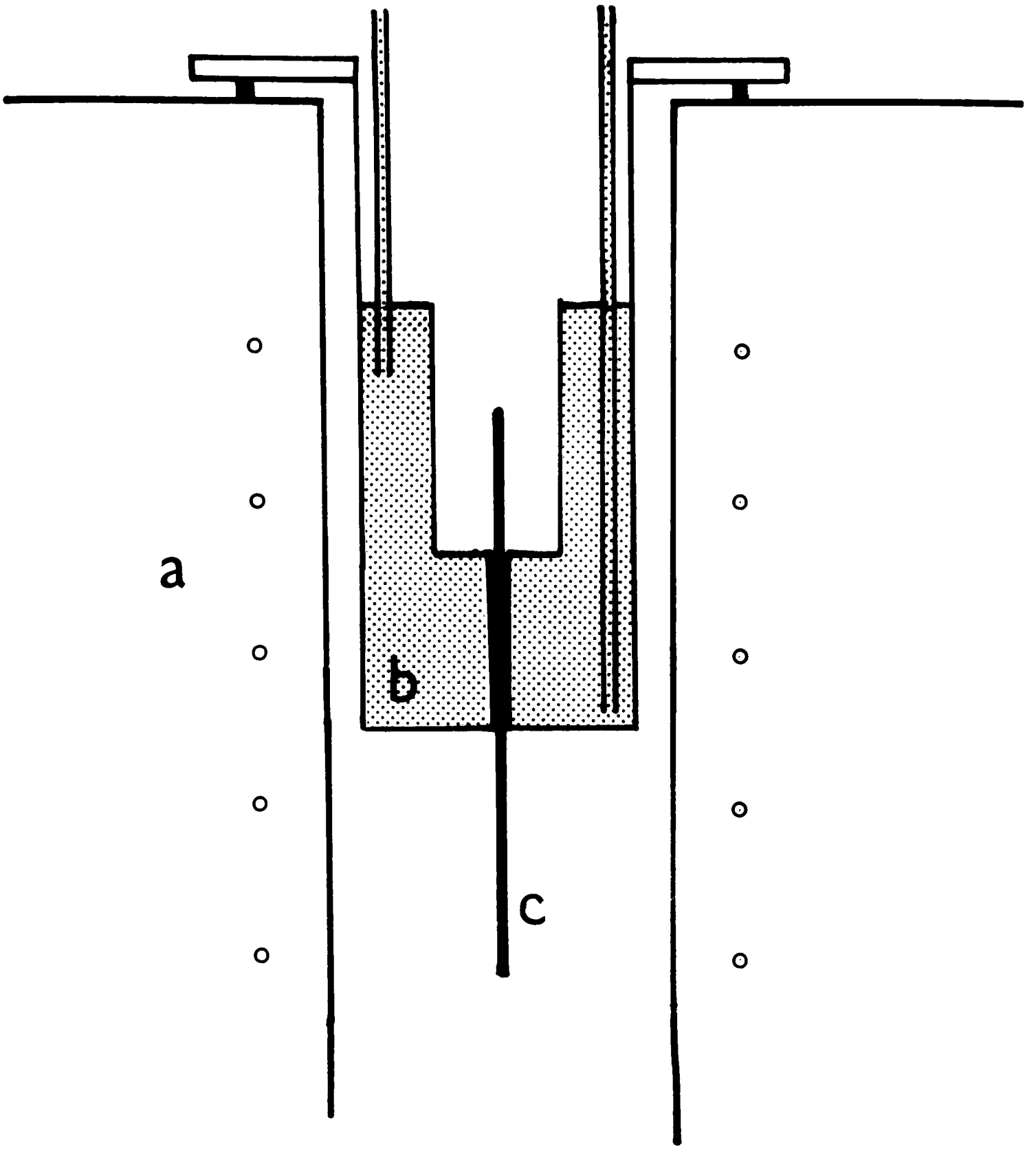
20. Detail of the top part of the directional freezing apparatus (a) Platinum resistance furnace, (b) Specimen in alumina tube, (c) brass cone, (d) inlet for constant head water supply, (e) threaded brass tube.



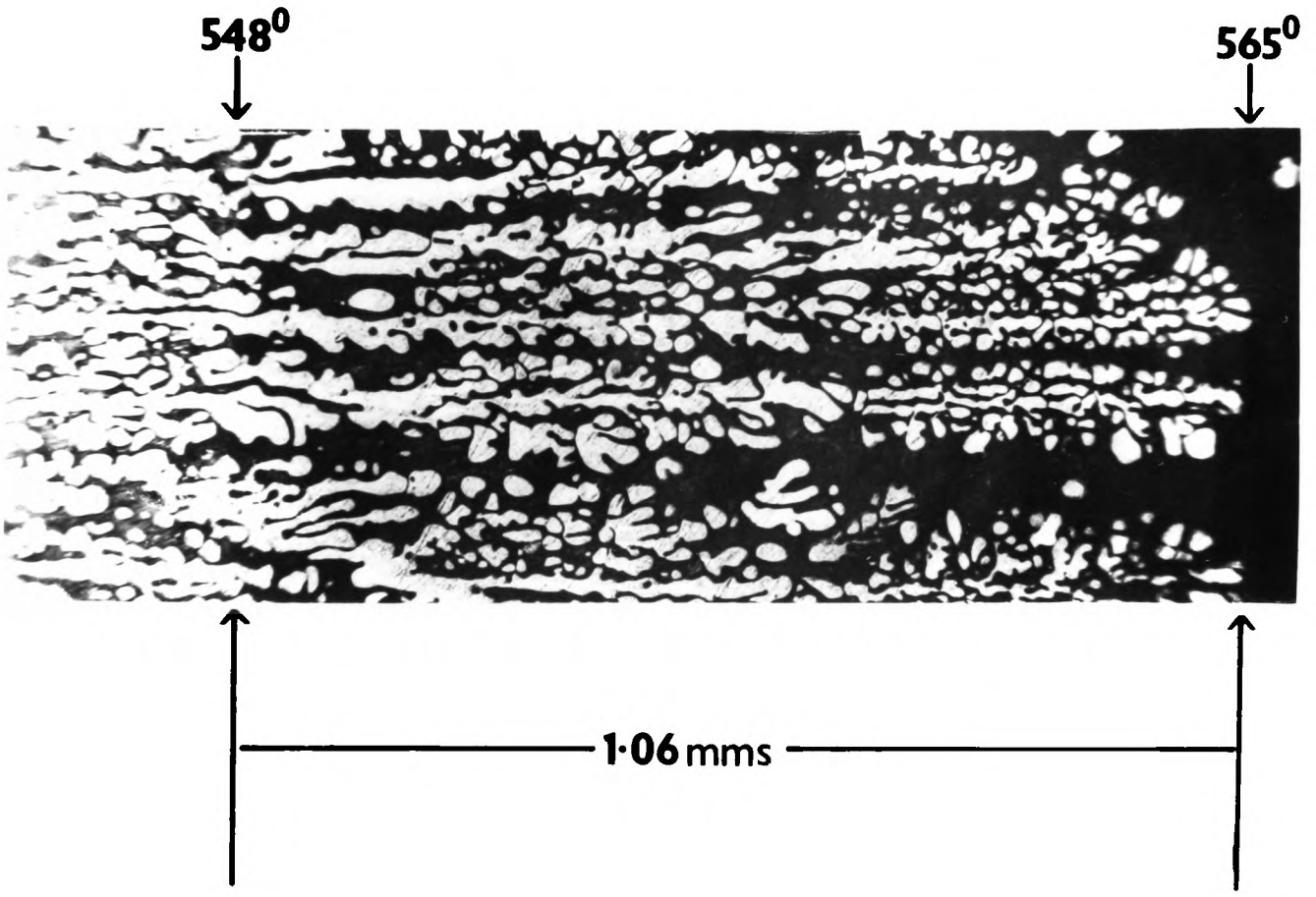
21. Modified directional freezing apparatus. Arrangement as figure 20 plus (f) gear wheel driven by motor driven worm (g), (h) rod clamped to base-plate.



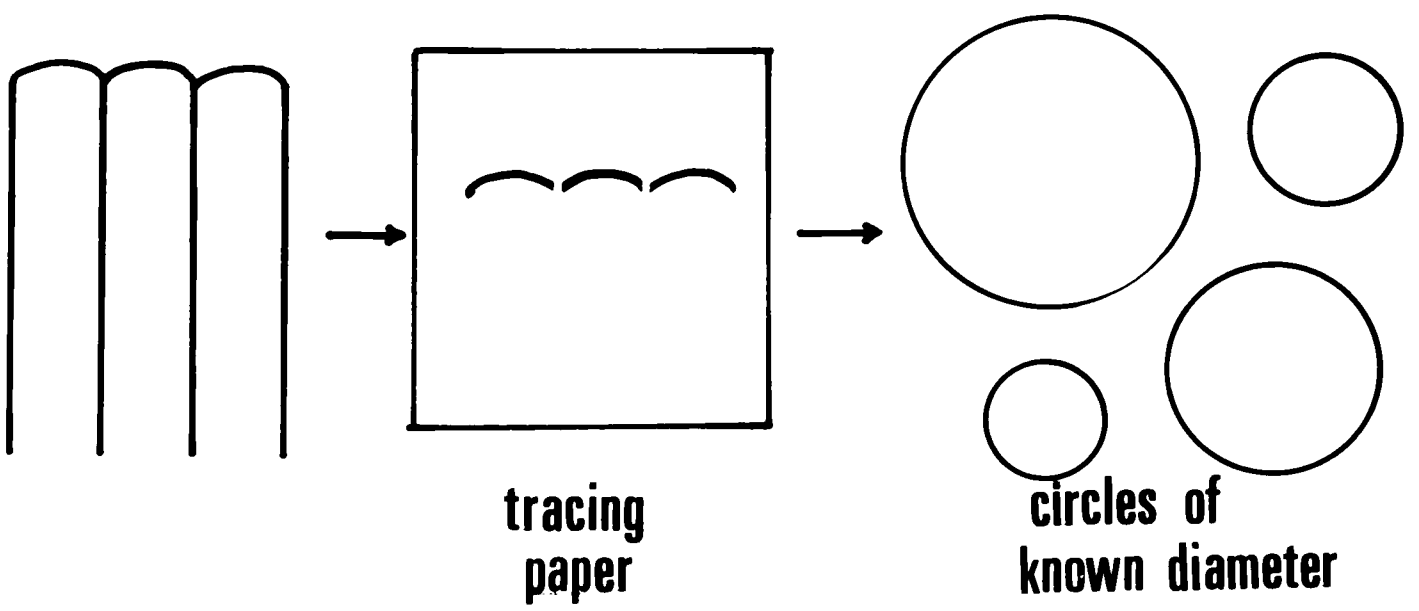
22. General view of the apparatus used for directional freezing experiments in this work.



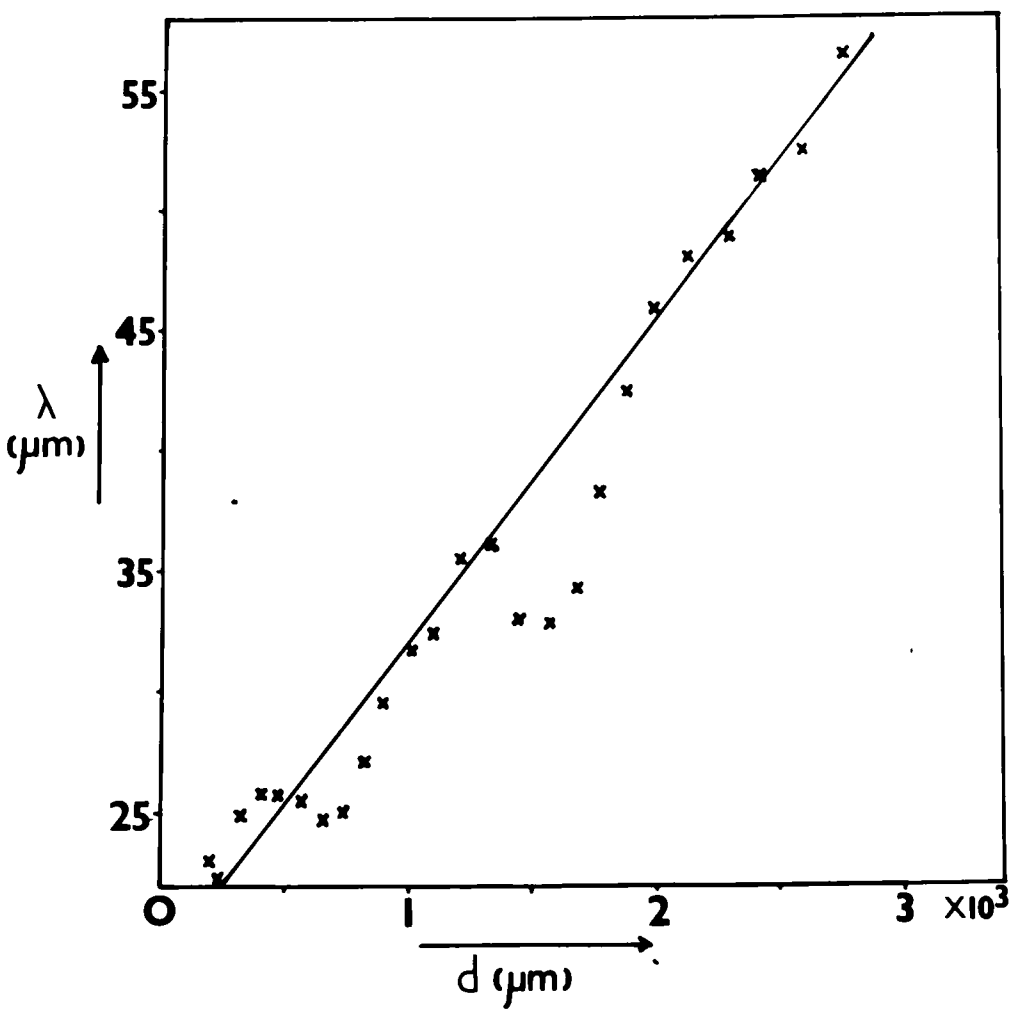
23. Apparatus used for directional freezing with convective mixing (a) platinum resistance furnace (b) water jacket (c) alumina tube containing specimen.



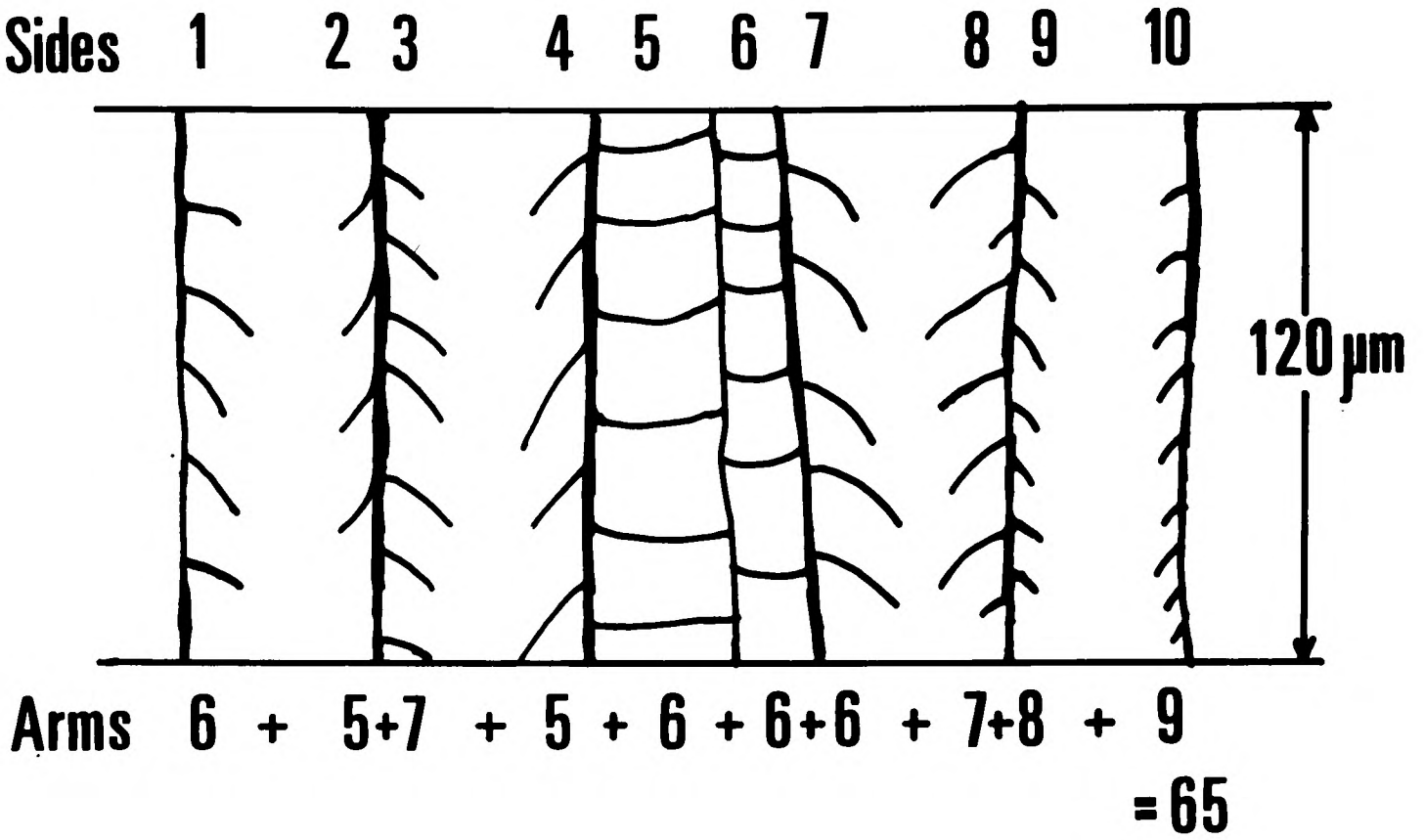
24. Diagram showing method of estimating temperature gradients.



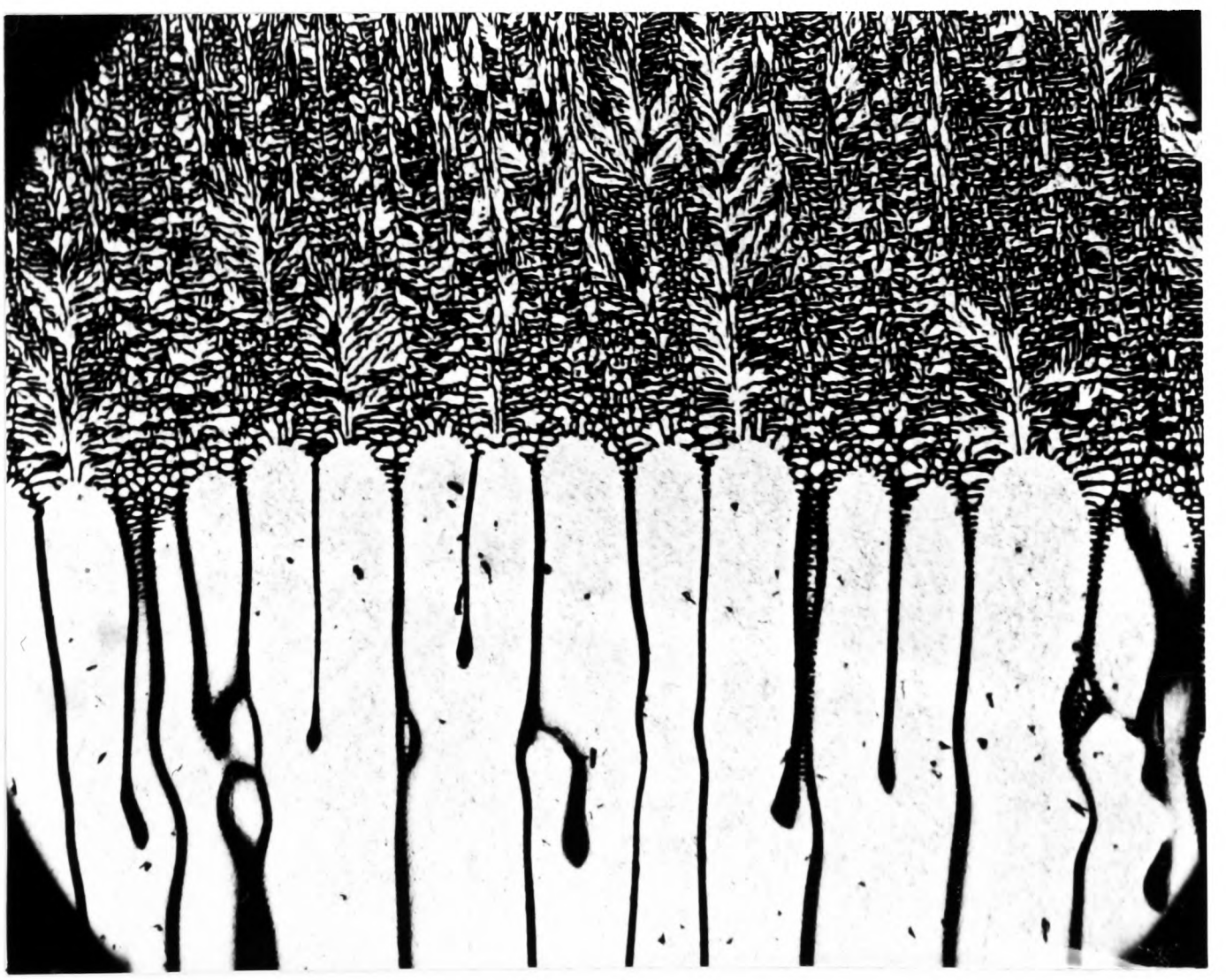
25. Method of measuring cell curvatures. Traces of the tips were made and these were fitted to a range of circles in order to estimate the curvatures.



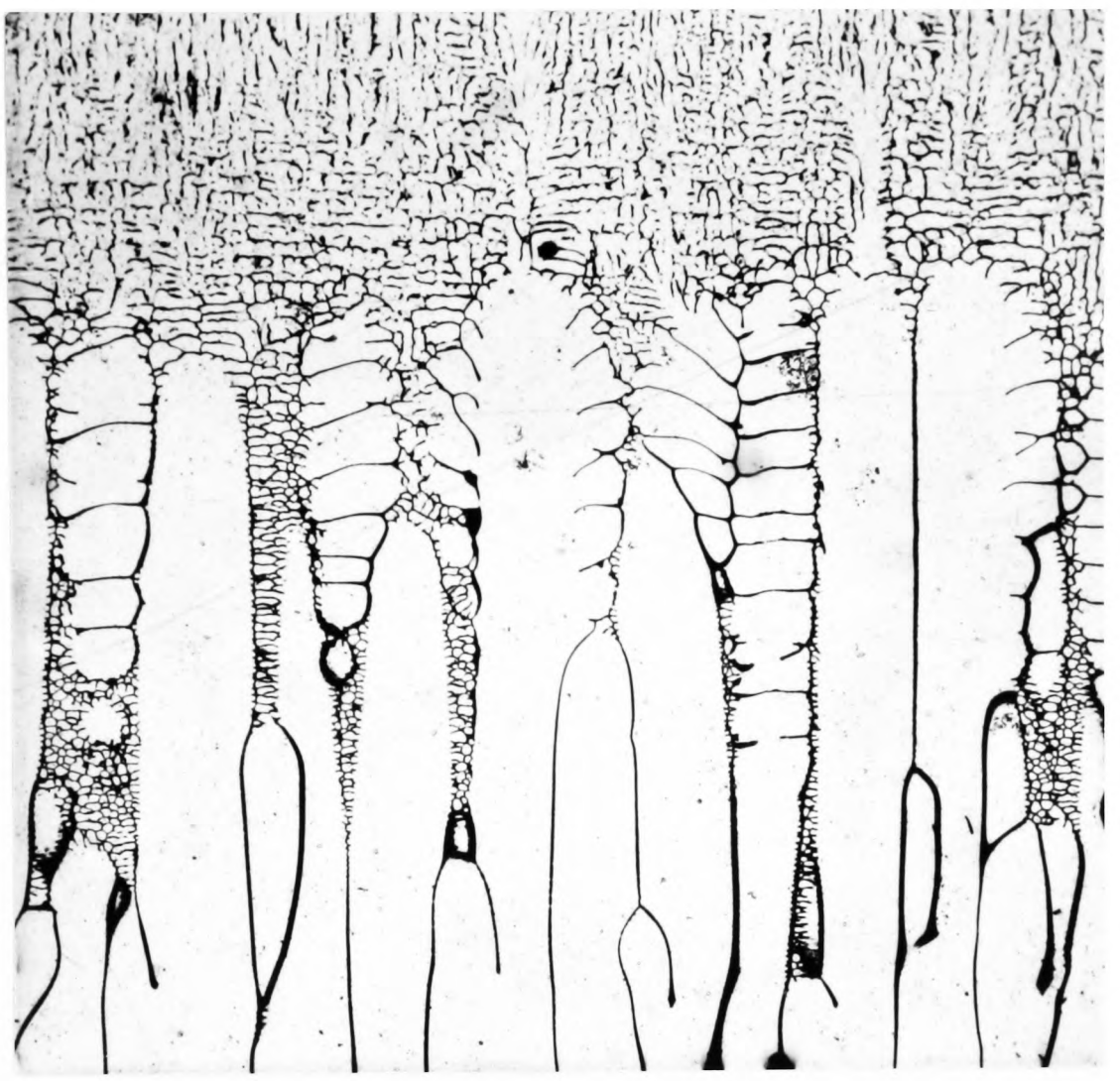
26. Secondary dendrite arm spacing plotted against the distance from the dendrite tips. V = 111μm/sec. C = 2 wt%. G = 7.5°C/mm.



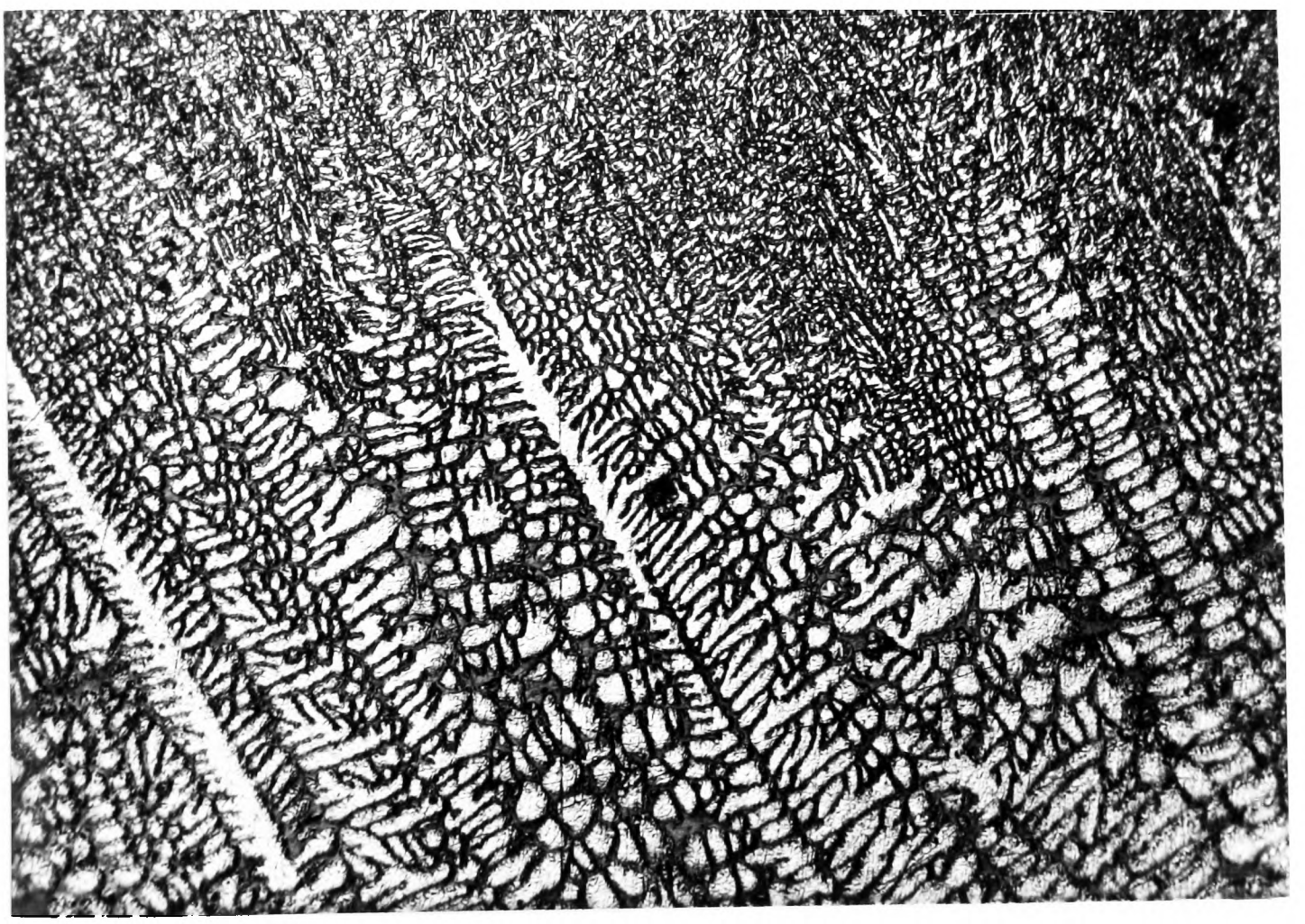
27. Method of measuring dendritic coarsening. The number of arms per side is given by $\frac{65}{10}$ = 6.5 and the width of an arm is therefore $\frac{120}{6.5}$ = 18.5µm.



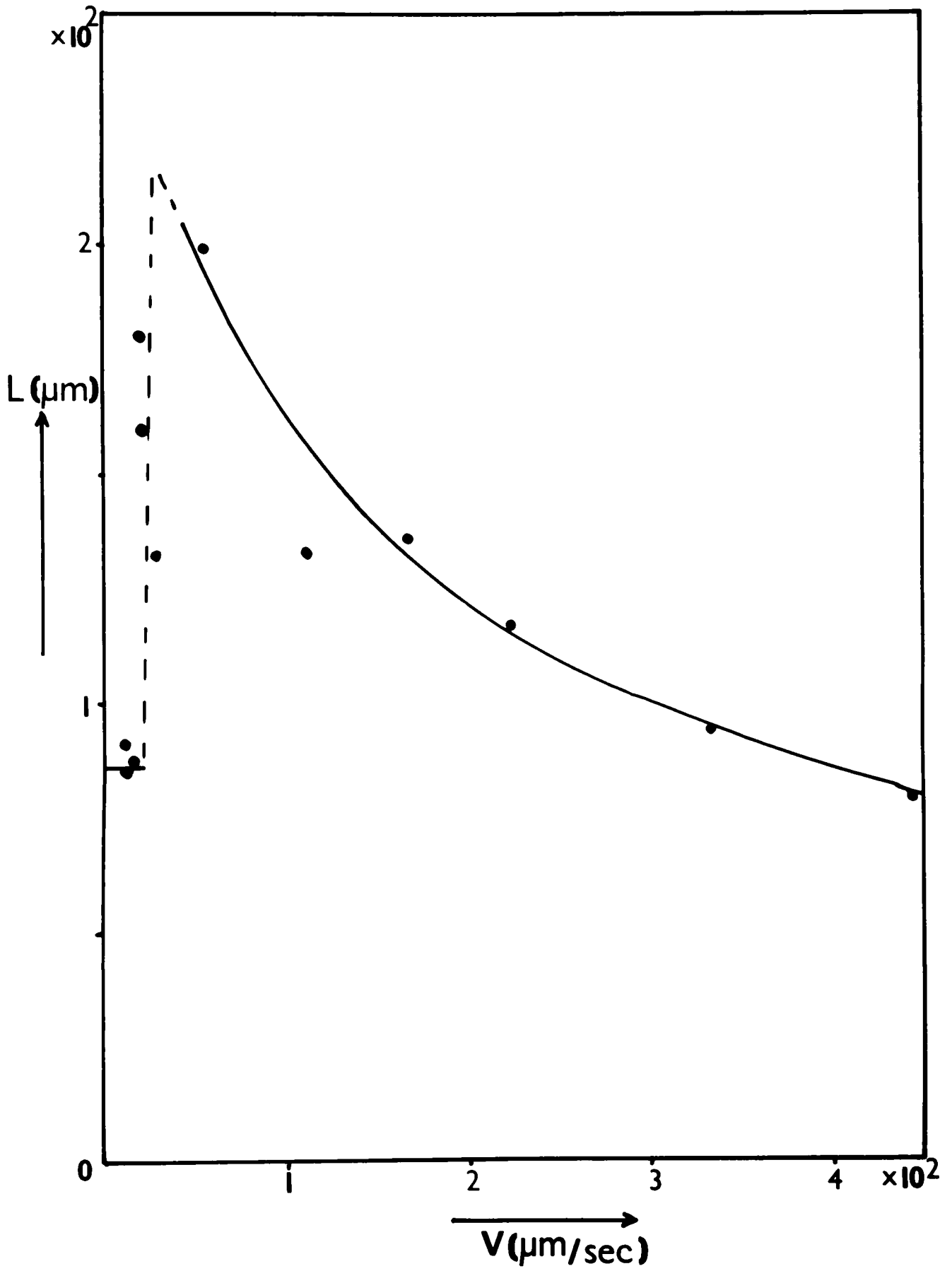
28. Simple cell morphology. V = 6.5µm/sec G = 16°C/mm C = 2 wt% x 150.



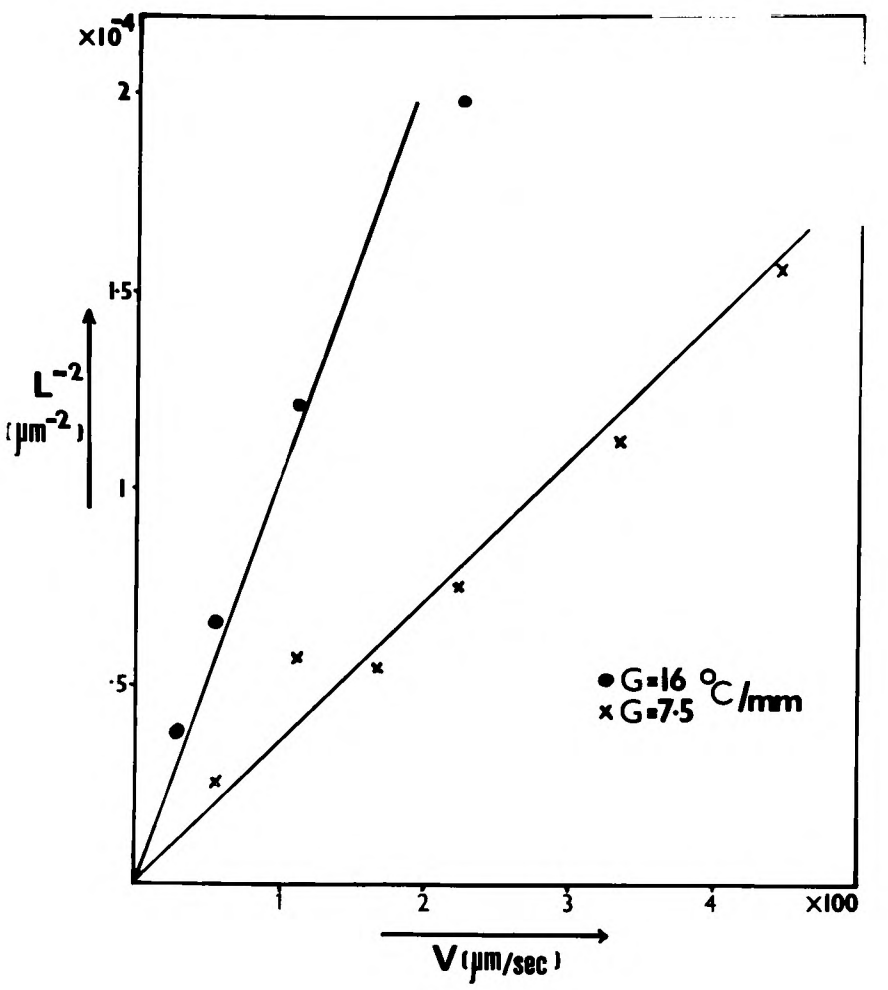
29. Branched cell morphology. V = 10μm/sec. G = 7.5°C/mm. C = 10 wt%. x 150



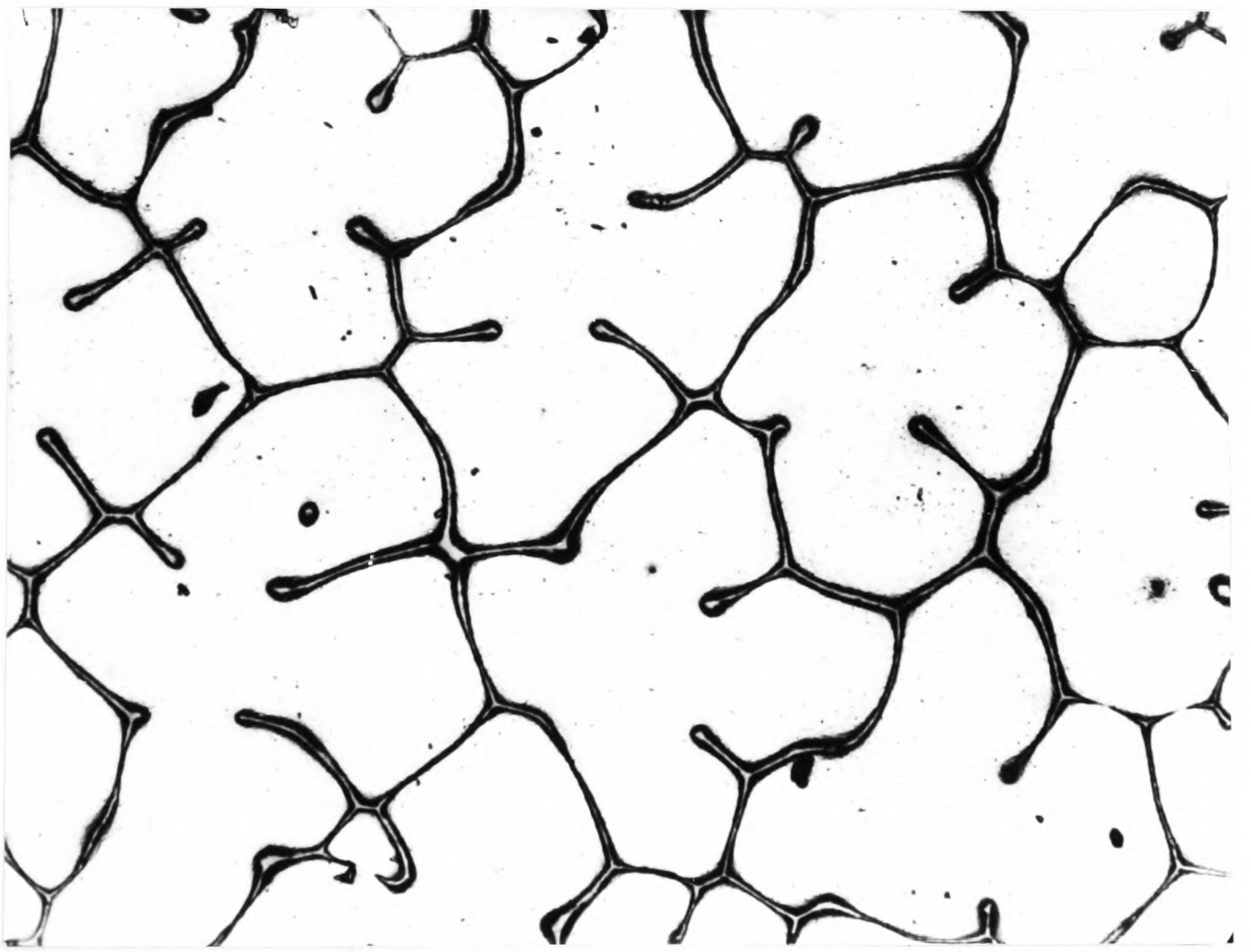
30. Dendrites. $V = 444\mu m/_{xc}$ G = 7.5°C/mm C = 10 wt%. x 600



31. Variation of cell size (L) with velocity of growth.

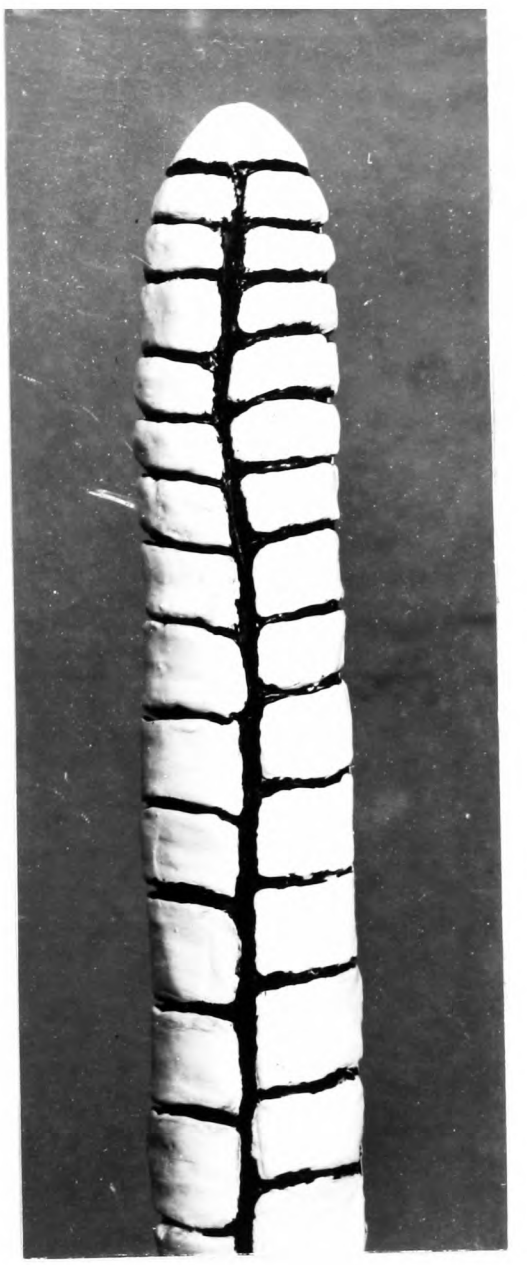


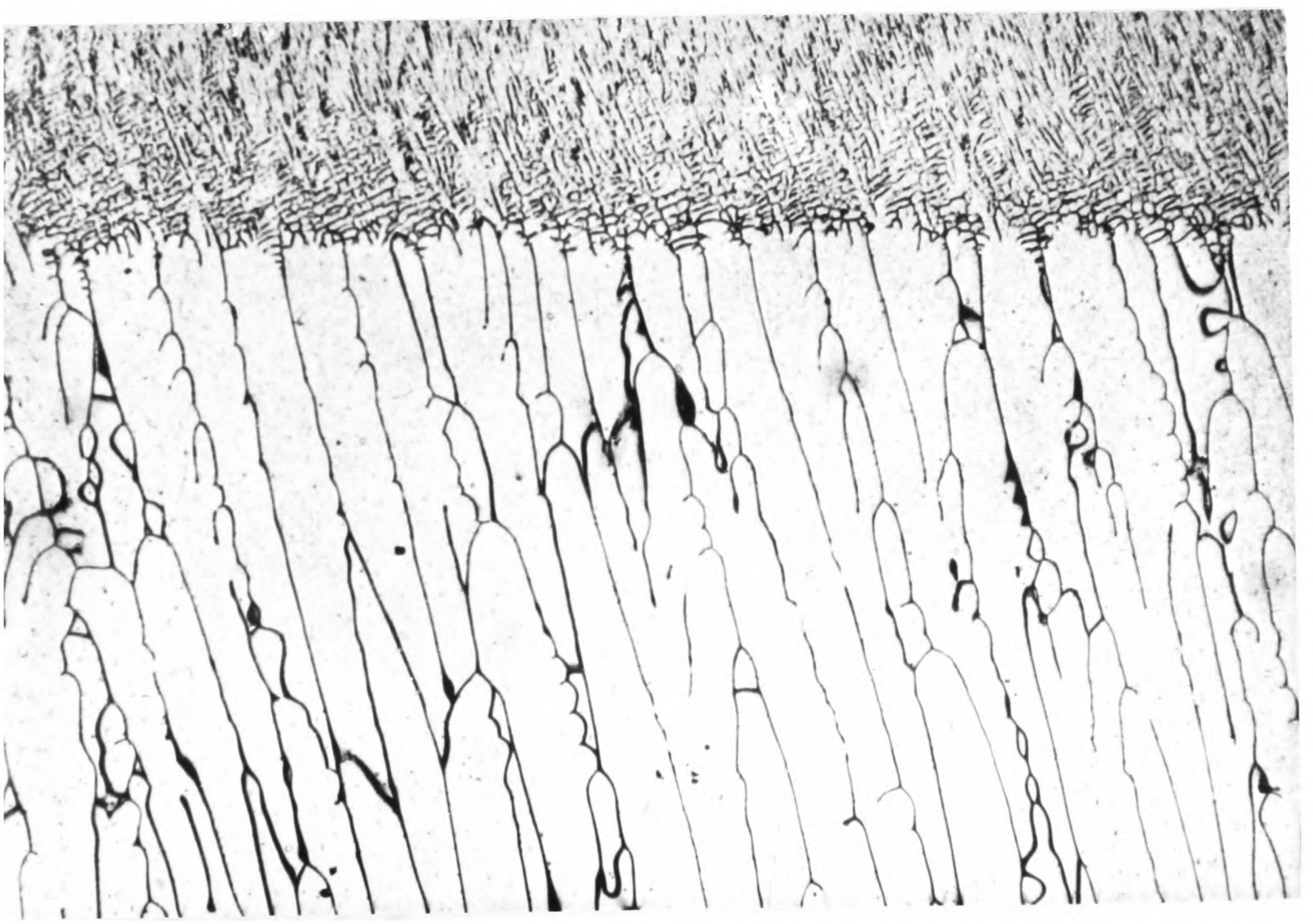
32. Showing the relation between the size of branched cells (L) and the velocity of growth.



33. Transverse section through branched cells. ×500

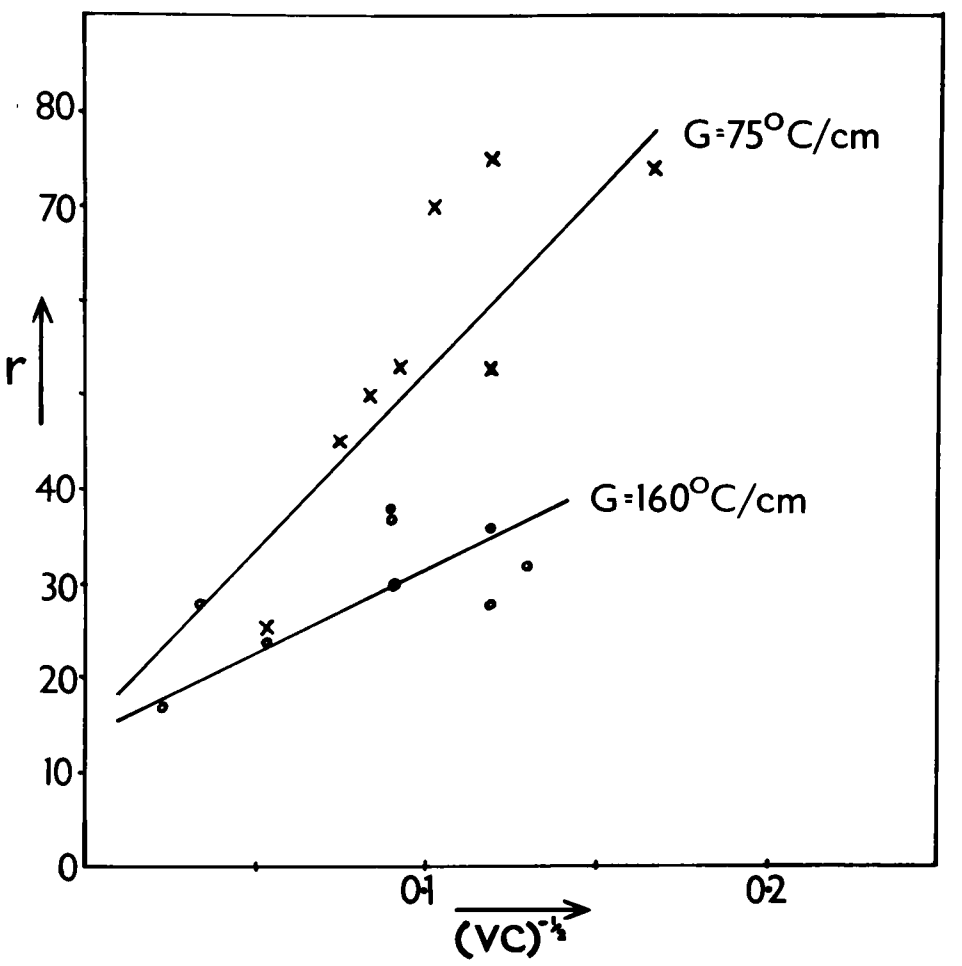
34. Model of a branched cell based on transverse and longitudinal sections.



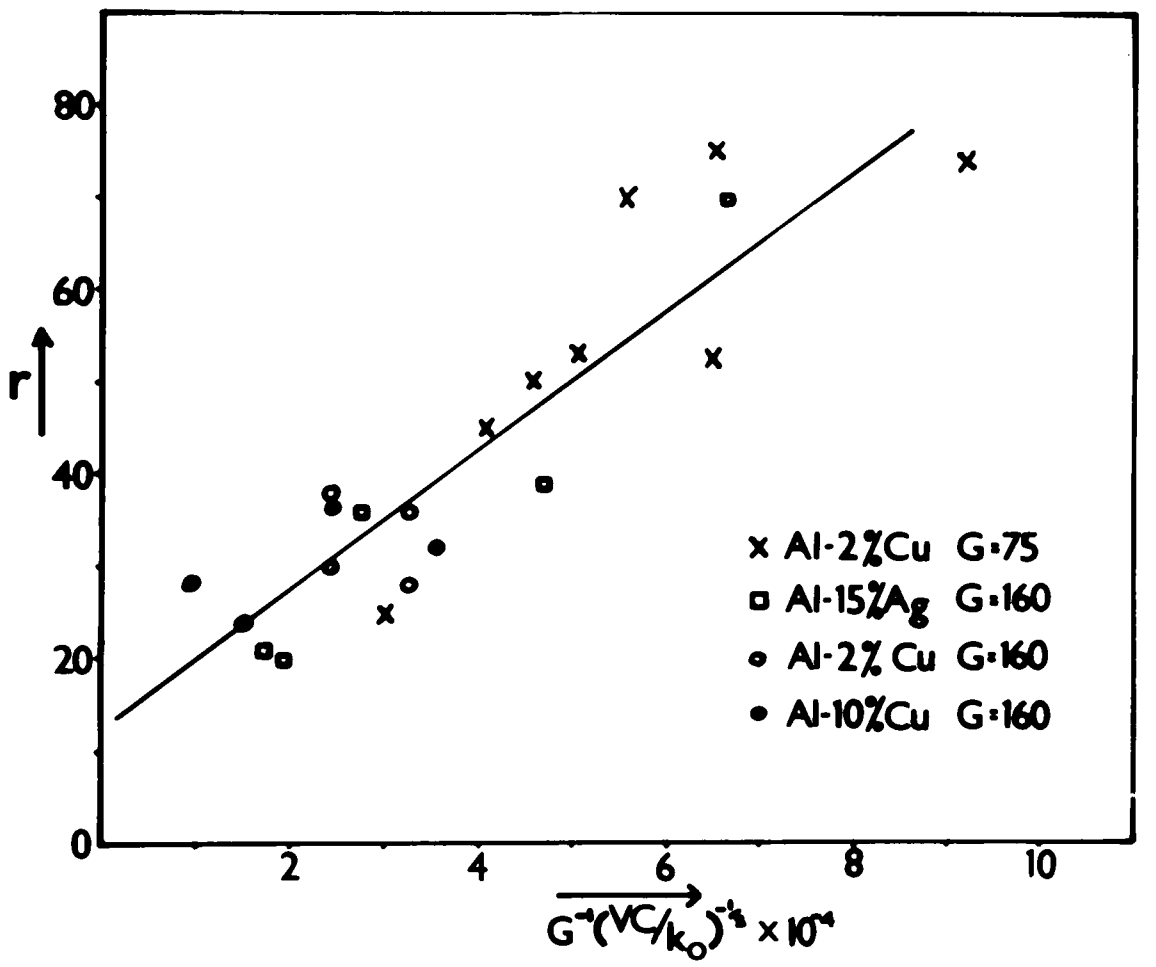


35. Quenched branched cell interface showing the orientation with respect to the growth direction of branched cells and fine dendrites. X 100

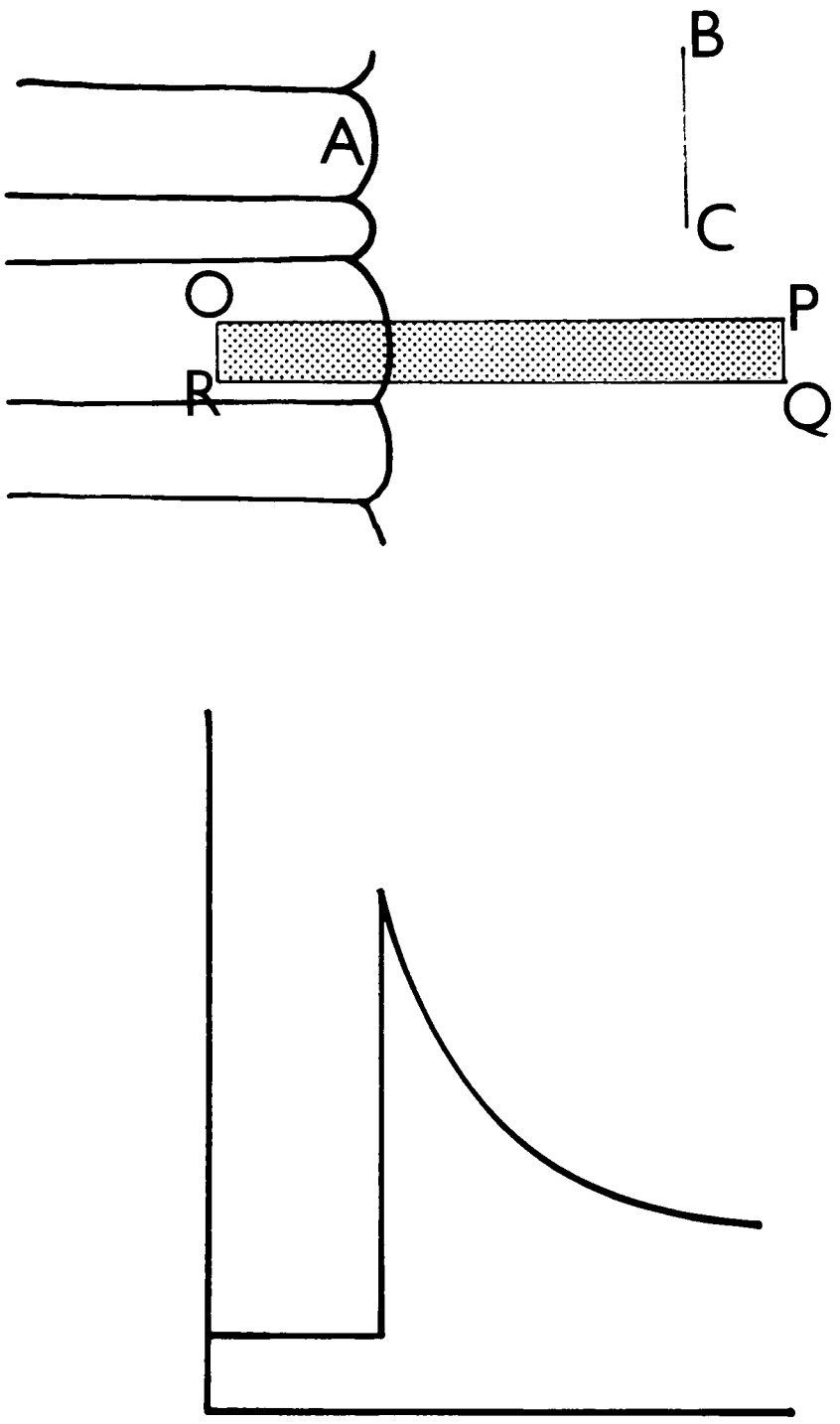
V($\mu m/_s$)	C_o(%)	G($^oC/_{mm}$)	r (μm)	k_e
Al-Cu alloys				
10	2	16	36	.38
16.7	2	7.5	53	.23
3.3	2	7.5	60	.39
16.7	2	16	38	.33
13.3	20	16	28	.22
5.0	2	7.5	74	.37
10.0	2	7.5	75	.31
10.0	2	7.5	53	.30
13.3	2	7.5	70	.26
20.0	2	7.5	50	.28
16.7	2	7.5	53	.23
3.3	2	7.5	60	.39
25	2	7.5	45	.20
50	2	16	24	.21
16.7	2	16	31	.26
10	2	16	28	.27
1.67	10	16	32	.38
3.3	10	16	37	.29
50	10	16	17	.23



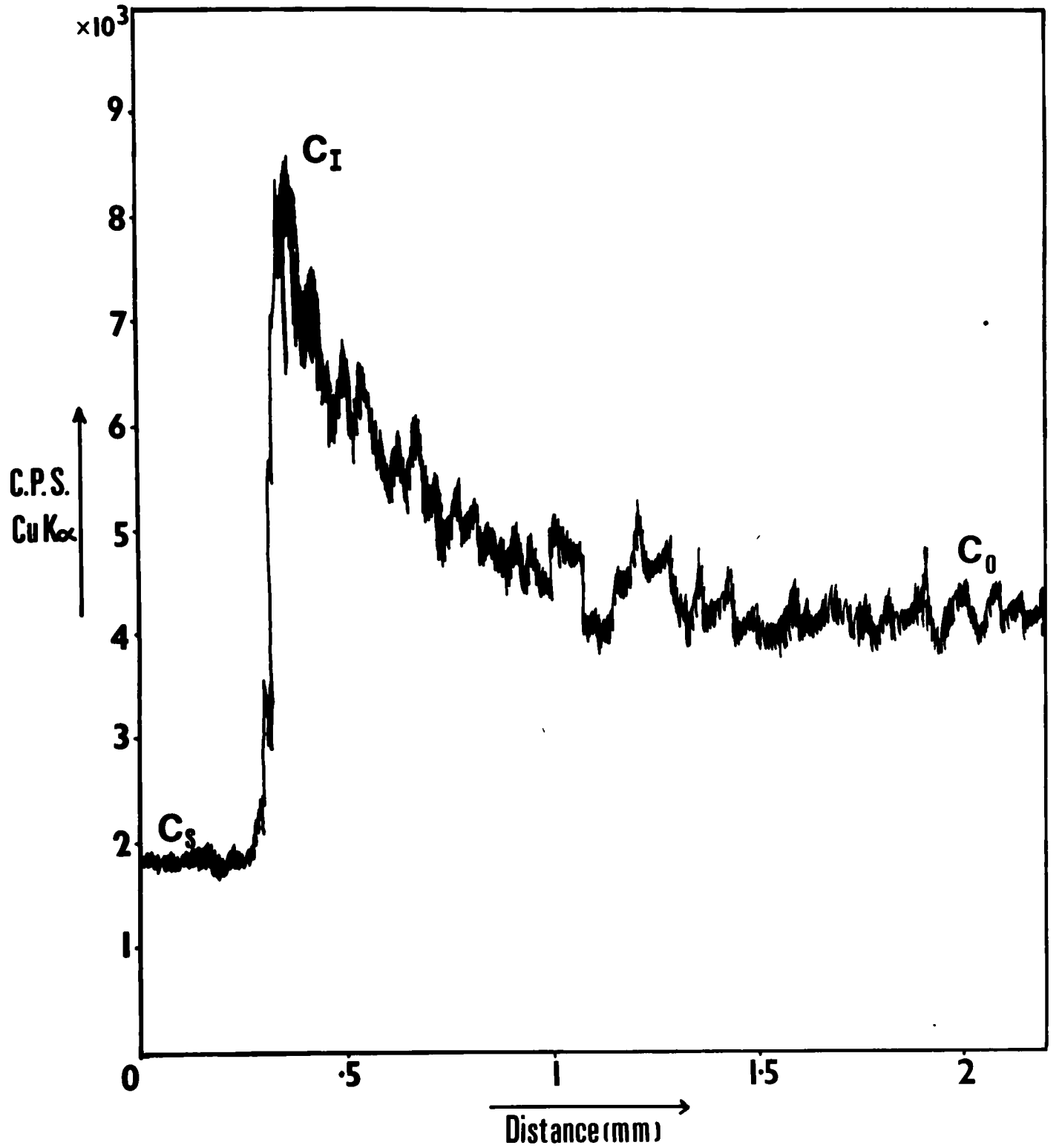
36. Radii of curvature at cell tips (r) expressed as a function of the parameter $(vc)^{\frac{1}{2}}$ for two different temperature gradients.



37. Radii of curvature plotted as function of the parameter $G^{-1} \left(^{vc}/ko\right)^{-\frac{1}{2}}$

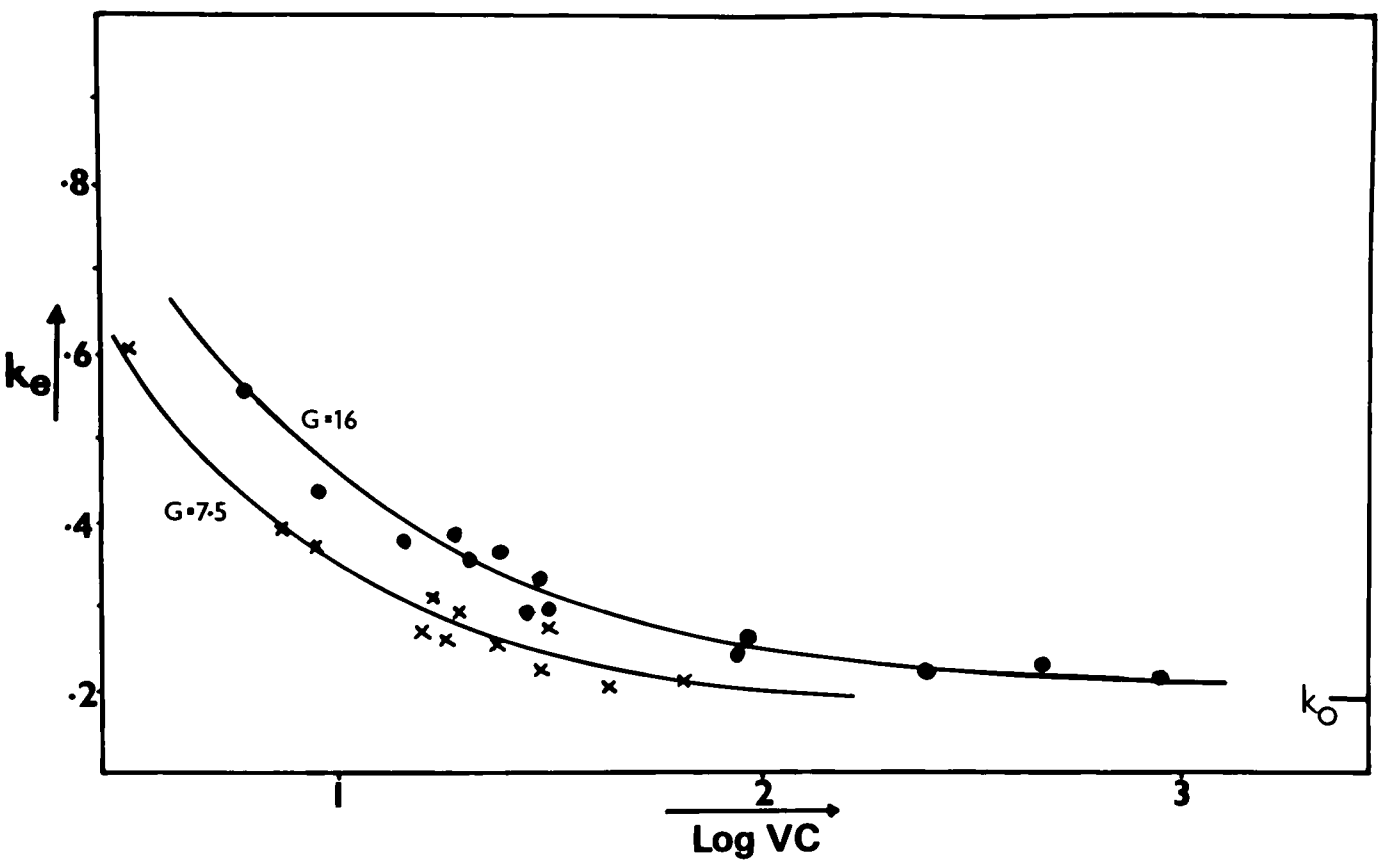


38. (a) Showing the method of making microanalysis measurements. Point counts were taken at A, line counts at B and scans over the region OPQR gave traces as in (b).

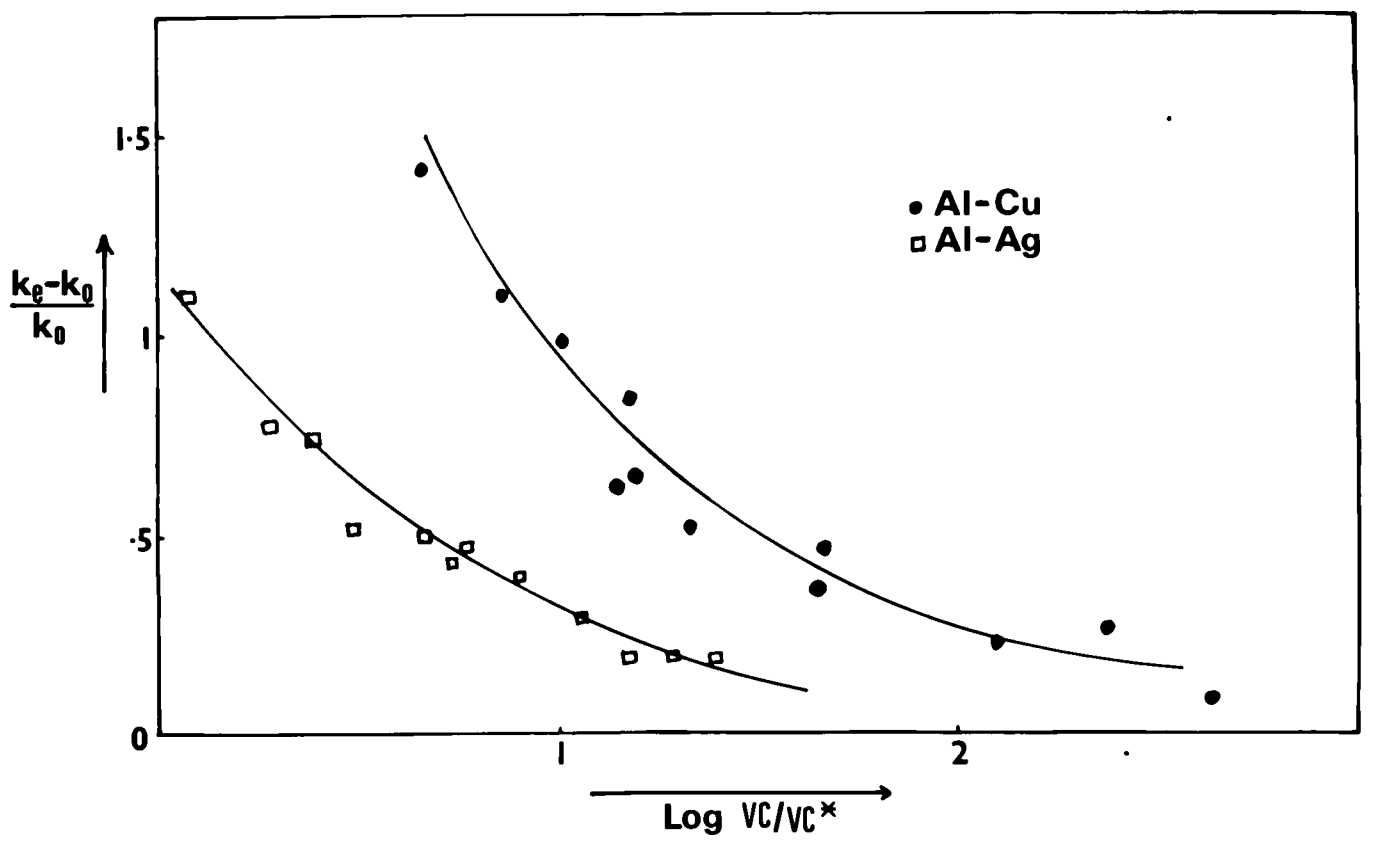


39. Electron microprobe trace over a cellular interface. Average composition in the solid $\bar{c}_s$ is equal to Co.

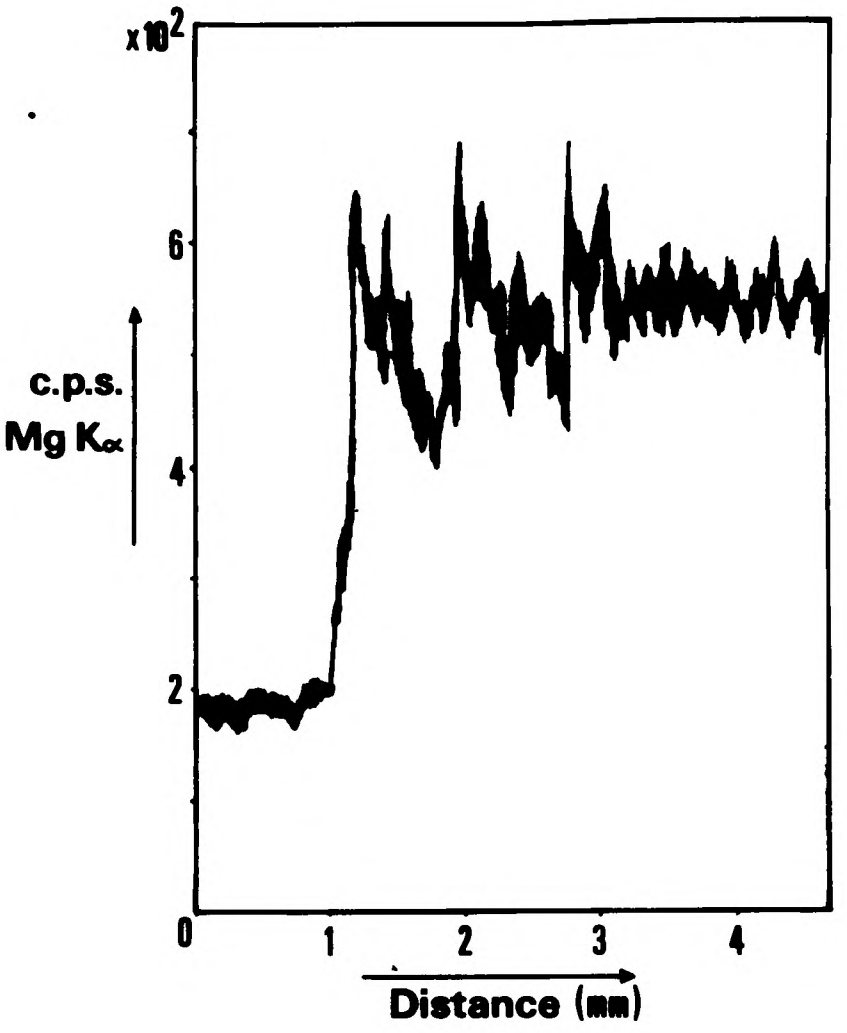
$V(\mu m/_s)$	$C_o(\%)$	$G(^oC/_{mm})$	$r(\mu m)$	k_e
Al-Ag alloys				
13.3	15	16	21	.43
10	15	16	20	.47
5	15	16	36	.52
3.3	15	16	39	.58
1.67	15	16	70	.71
13.3	25	16	39	.49
10	25	16	14	.49
5	25	16	-	.57
3.3	25	16	28	.63
1.67	25	16	23	.75



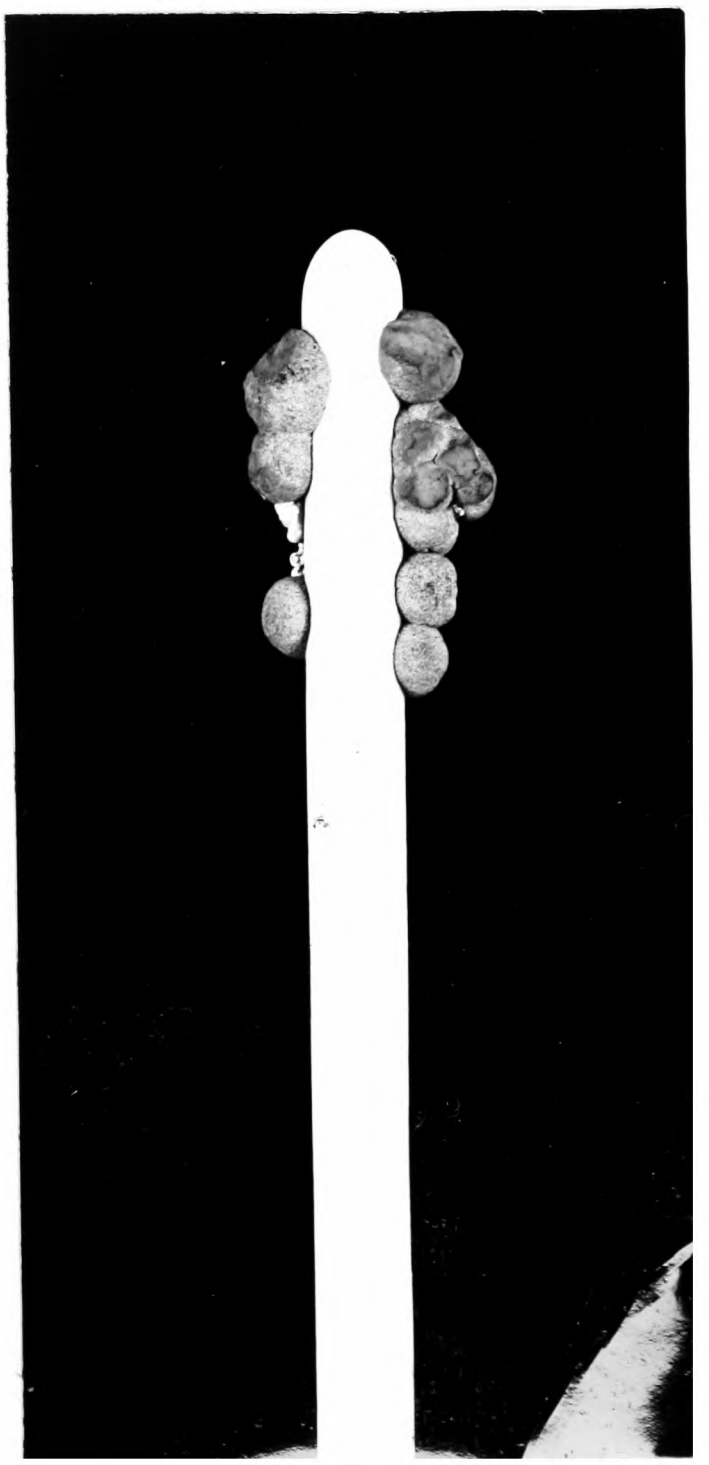
40. Variation of ke with VC for two different temperature gradients.



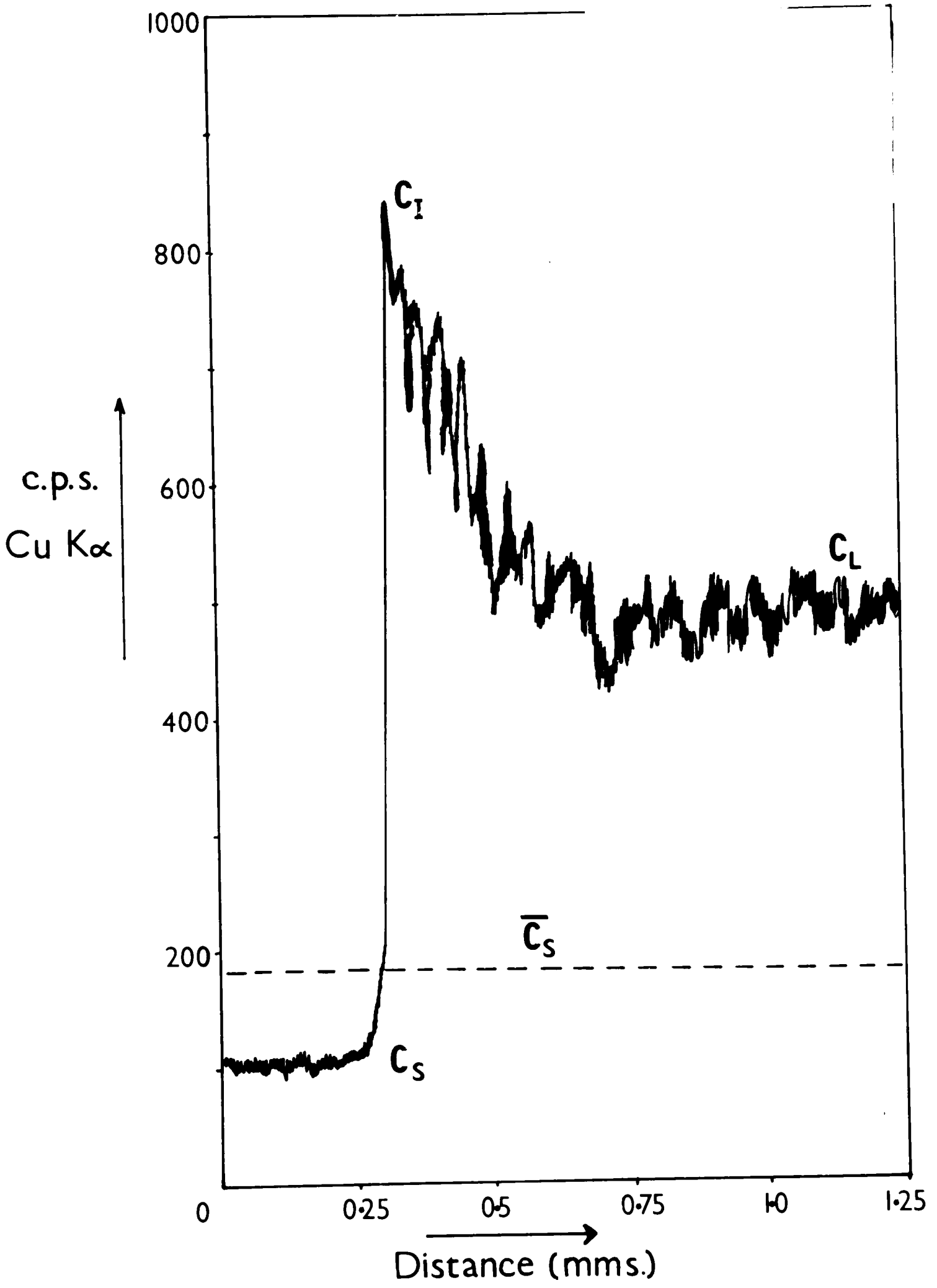
41. The function $^{(ke-ko)}/ko$ plotted against $^{(vc)}/(vc)^*$ for two different systems.



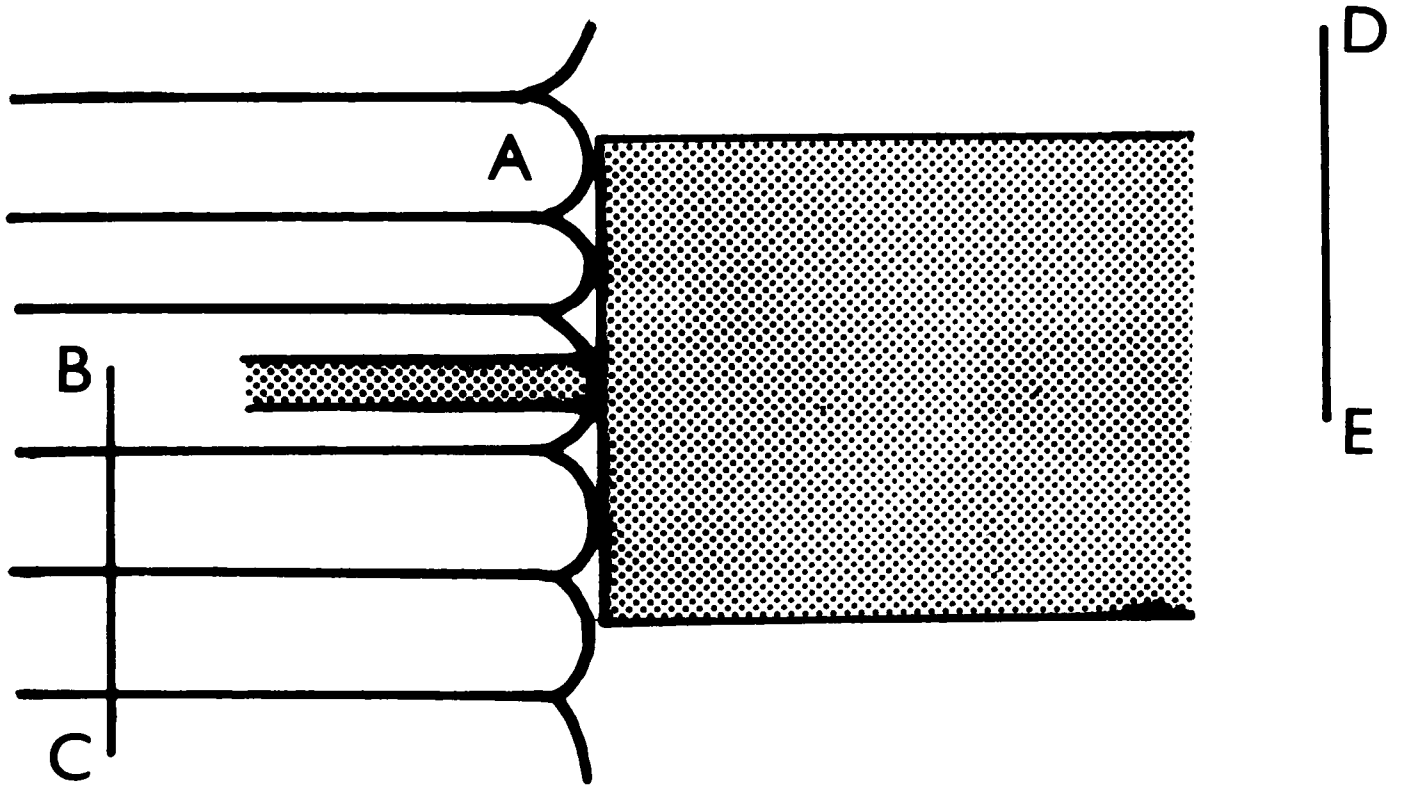
42. Typical electron microprobe trace over an interface in the Al-Mg system.



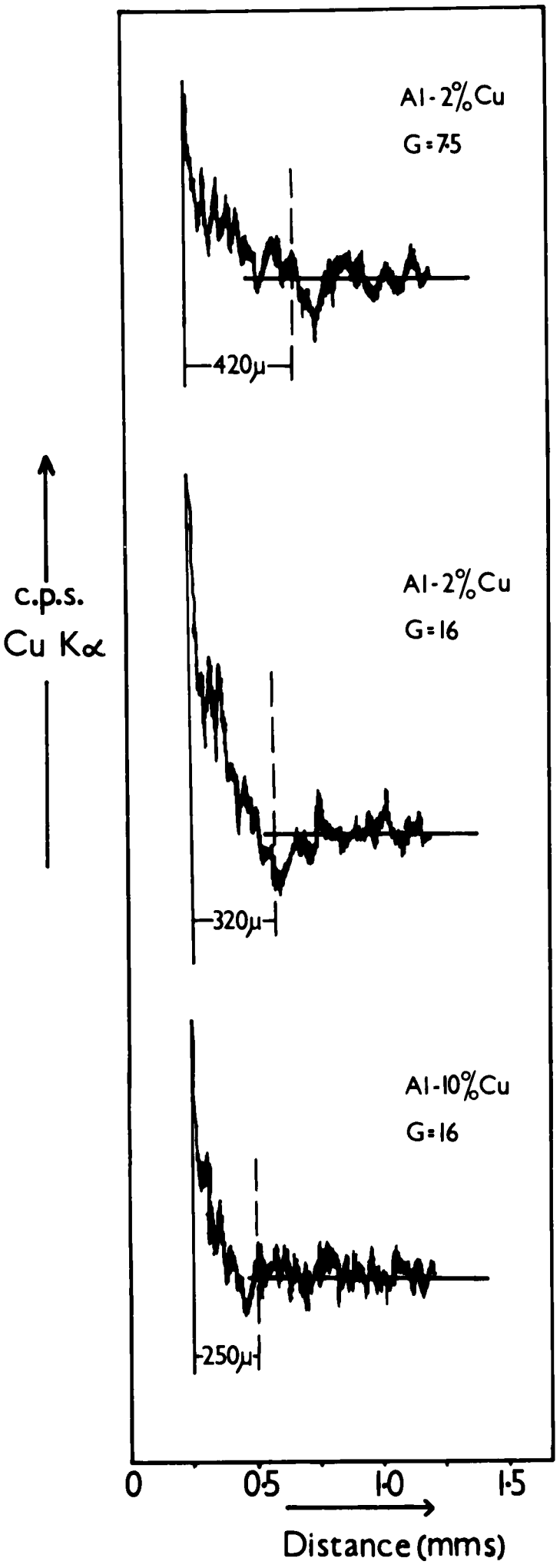
43. Tube containing Al-Mg alloy which has cracked and exuded liquid metal.



44. Typical diffusion profile over interface in a specimen of Al-Cu alloy in which there was liquid convection, showing the relevant concentrations.

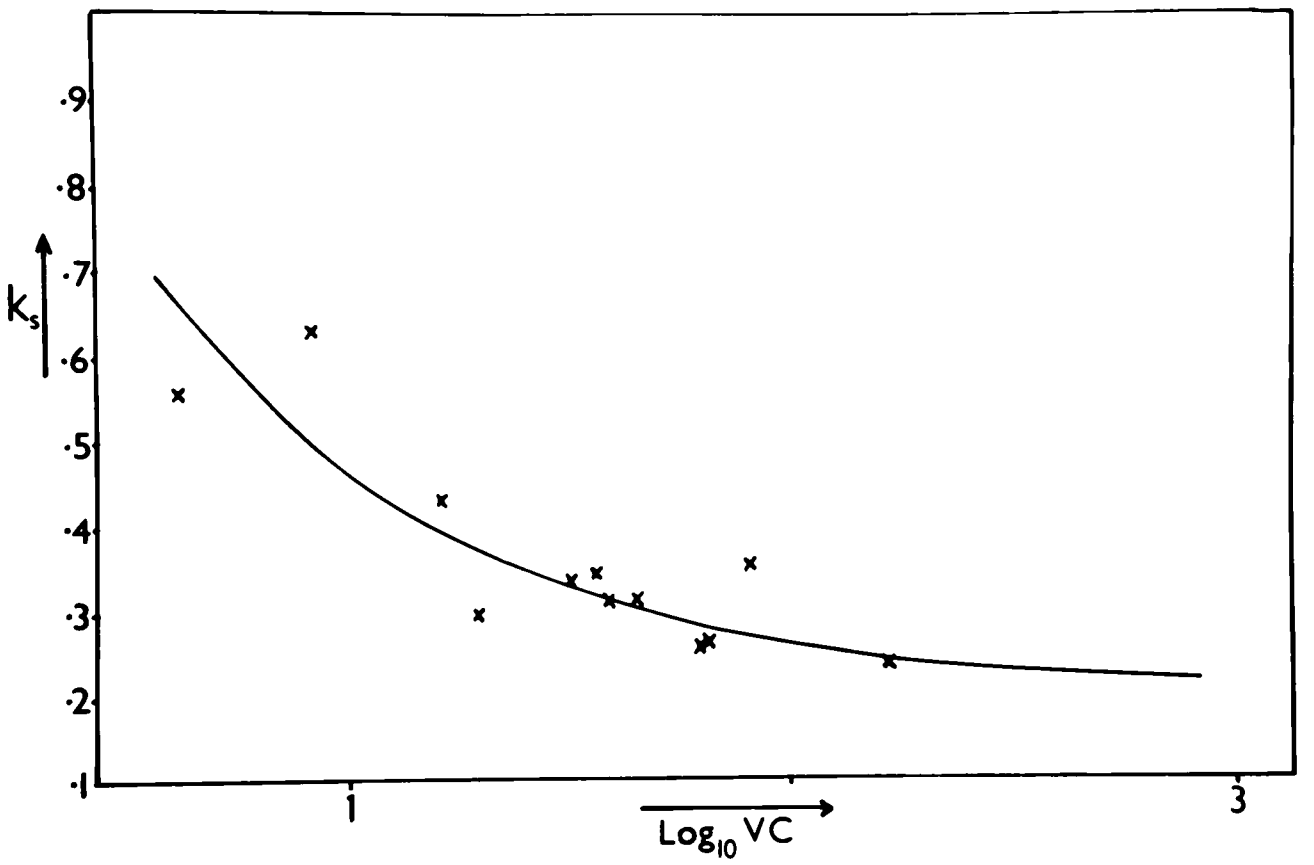


45. Diagrammatic representation of the method of making microanalysis measurements in specimens in which there was convective mixing. The shaded area shows the region over which solute profiles were obtained. Line counts were taken at DE and BC and point counts at A.



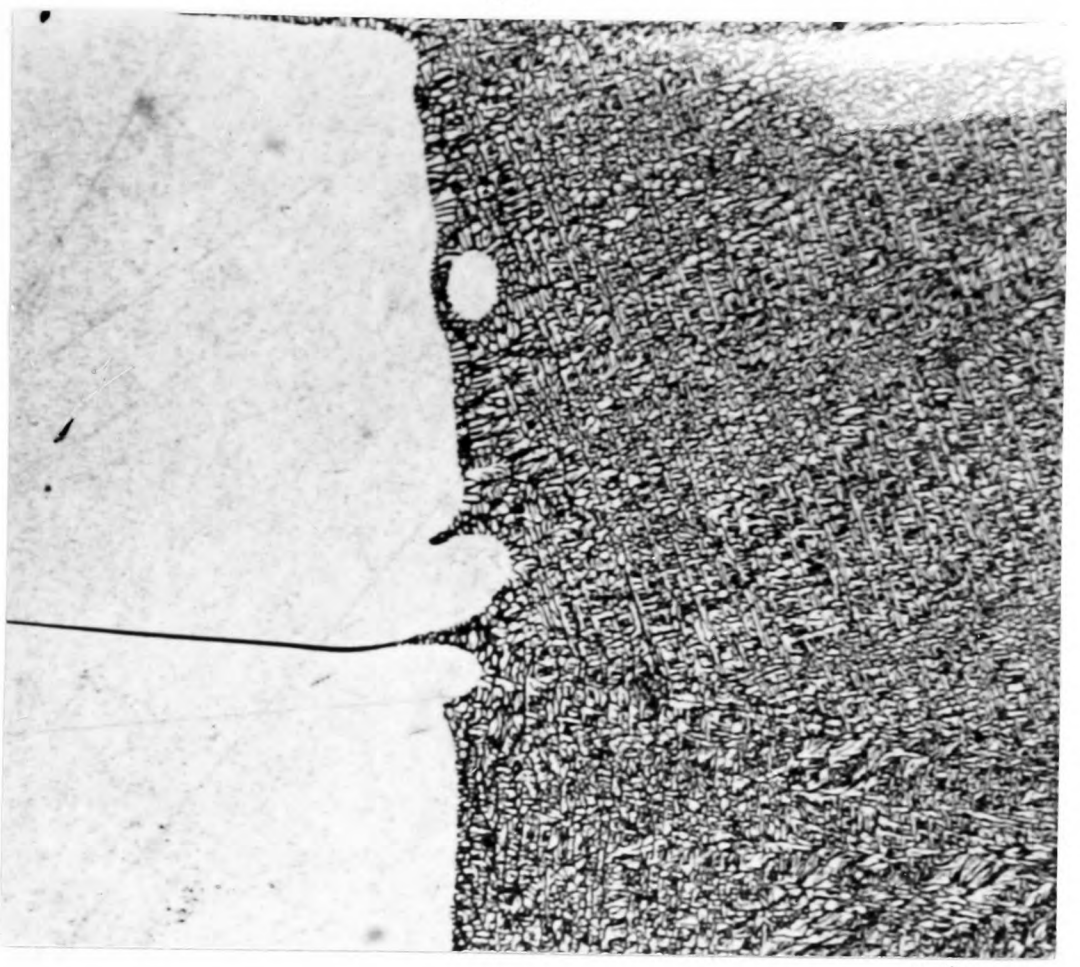
46. Superimposition of calculated values of δ on microprobe traces of the type shown in figure 44.

k_s	$\bar{C}_s$ (%)	V ($\mu m/_{sec}$)
.233	10	16.7
.34	6.39	5.55
.286	7.01	2.78
.245	1.83	33.3
.33	1.52	20.8
.63	0.67	12.5
.55	1.46	2.78
.45	1.95	8.33
.30	0.95	16.7
.35	1.63	50.0
.32	1.79	25.0



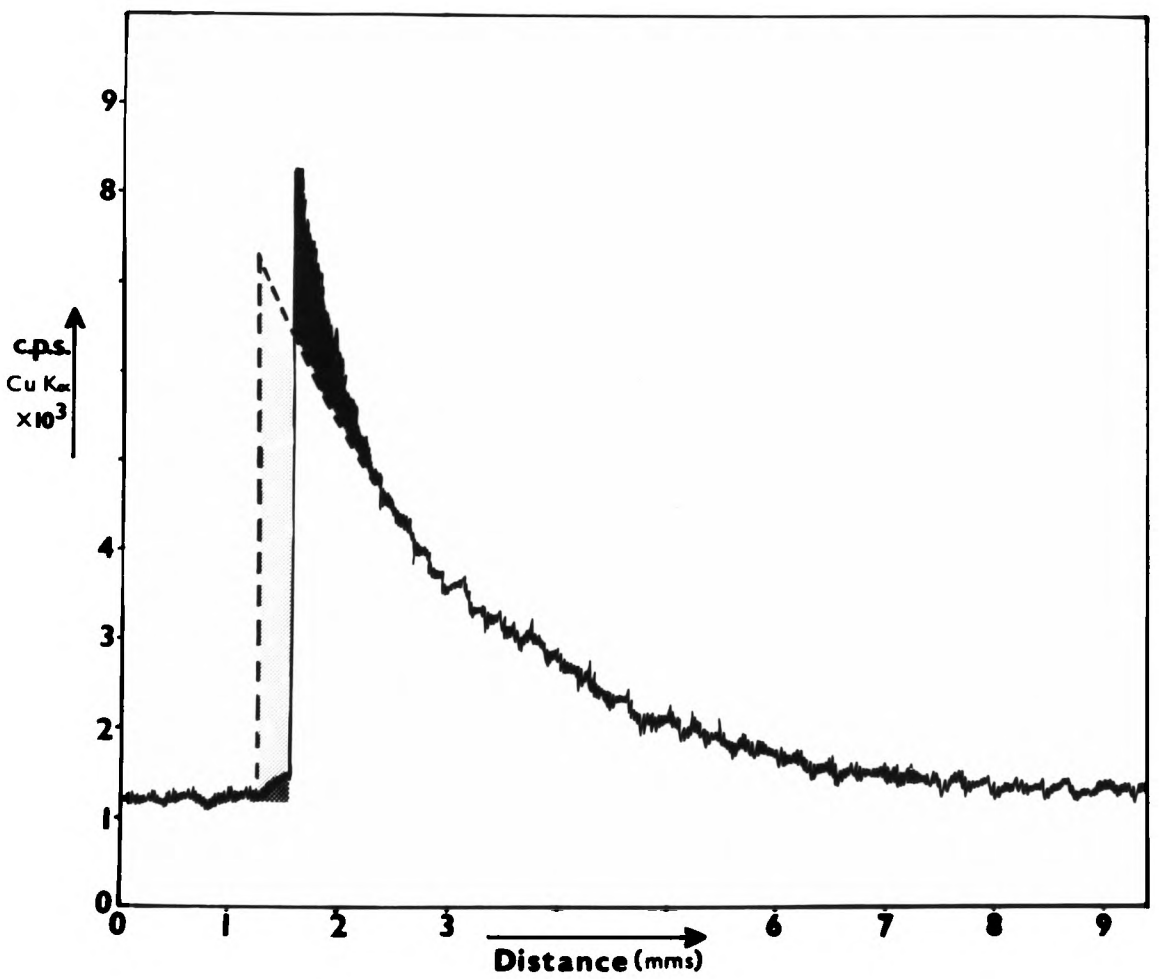
47. Values of solute segregation coefficient plotted against log VC. The full line corresponds to values of ke obtained from non-stirred melts.

(a)

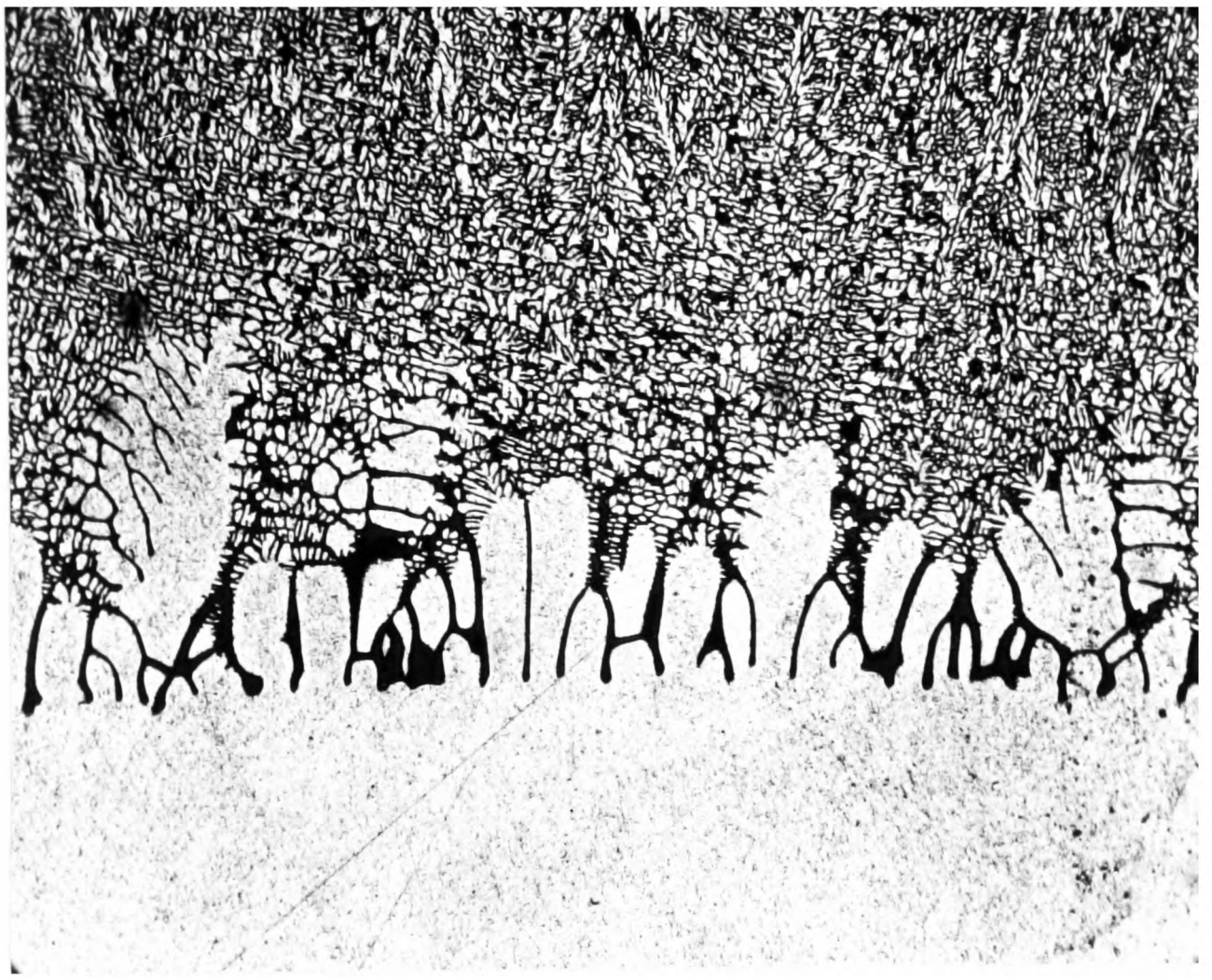


× 300

(b)

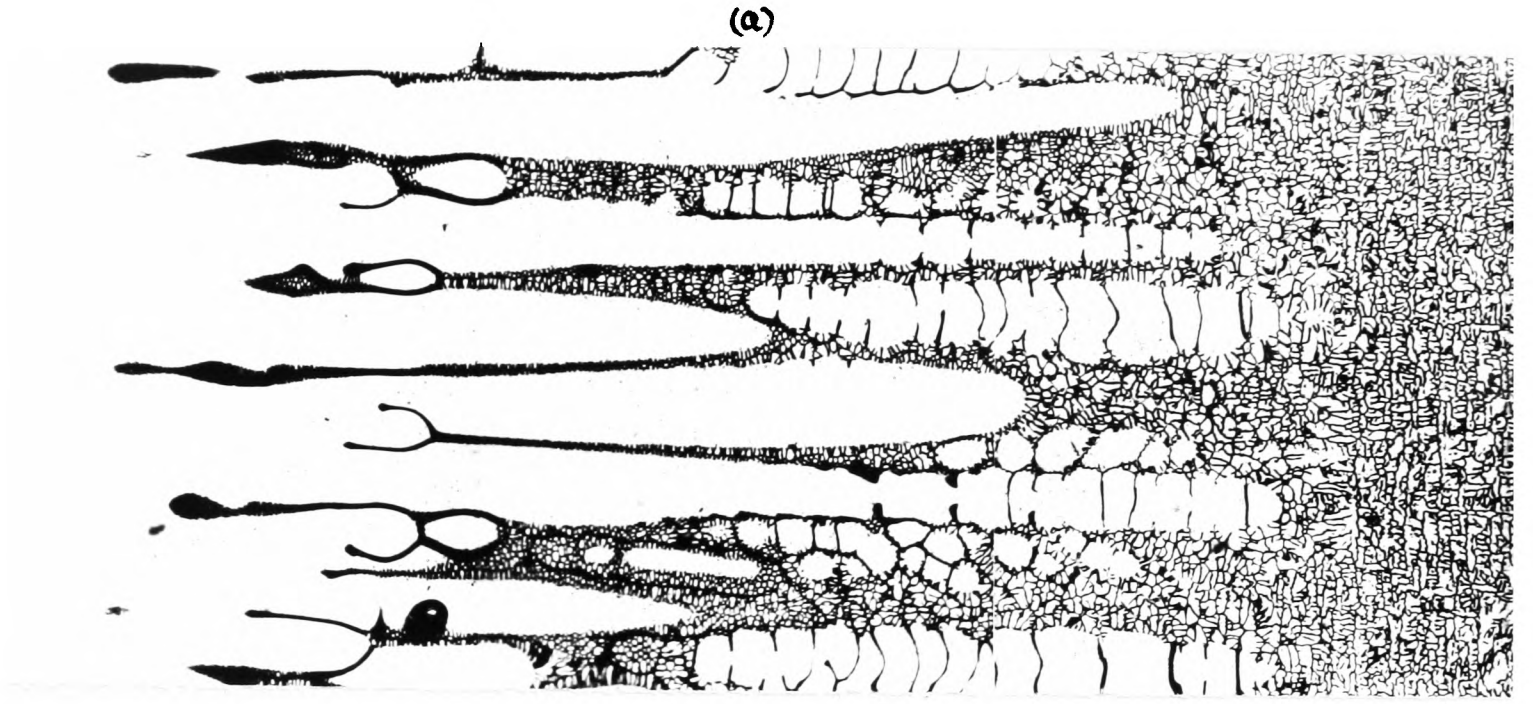


48. (a) Microstructure and (b) Solute profile corresponding to a specimen which has been accelerated for 30 seconds and then quenched.



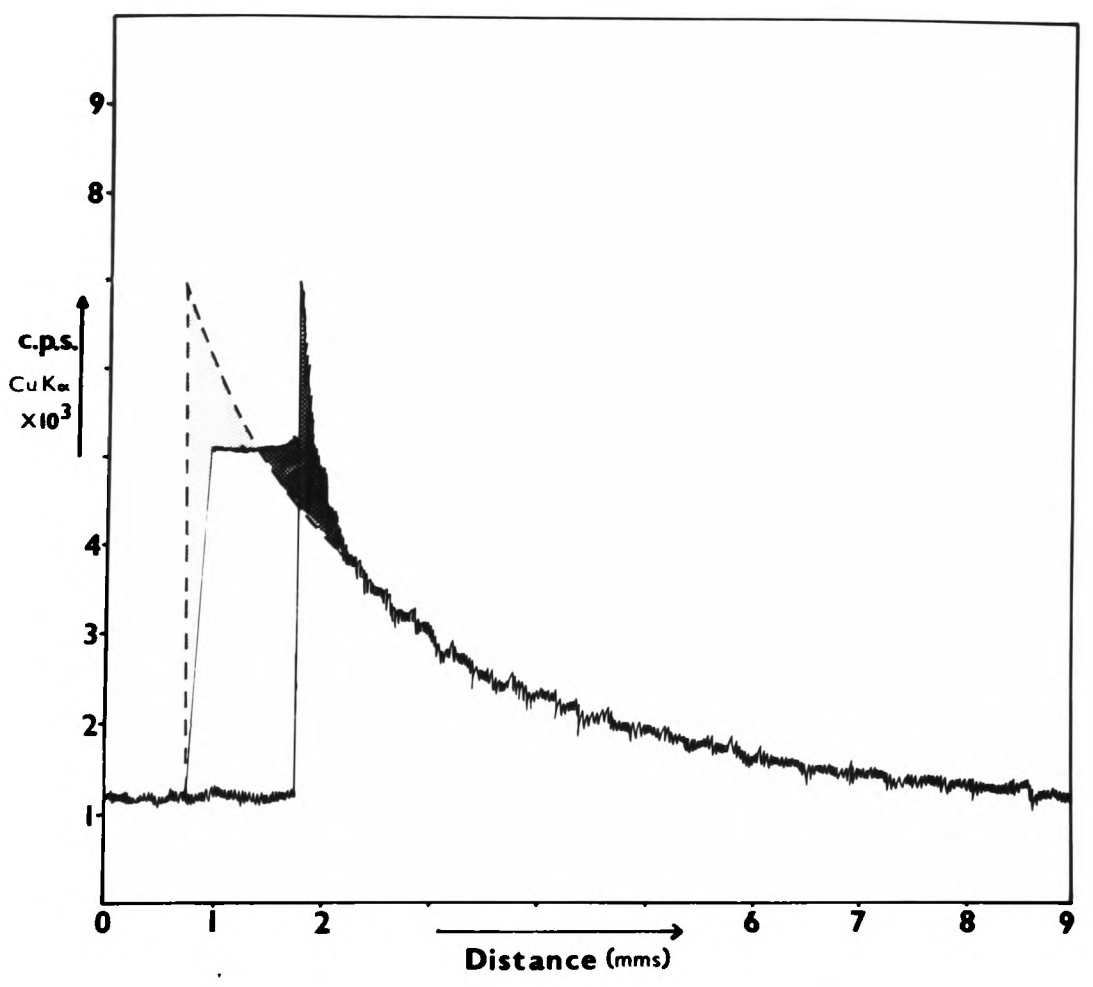
49. Microstructure corresponding to a specimen accelerated for 45 seconds and then quenched. x 250

(a)

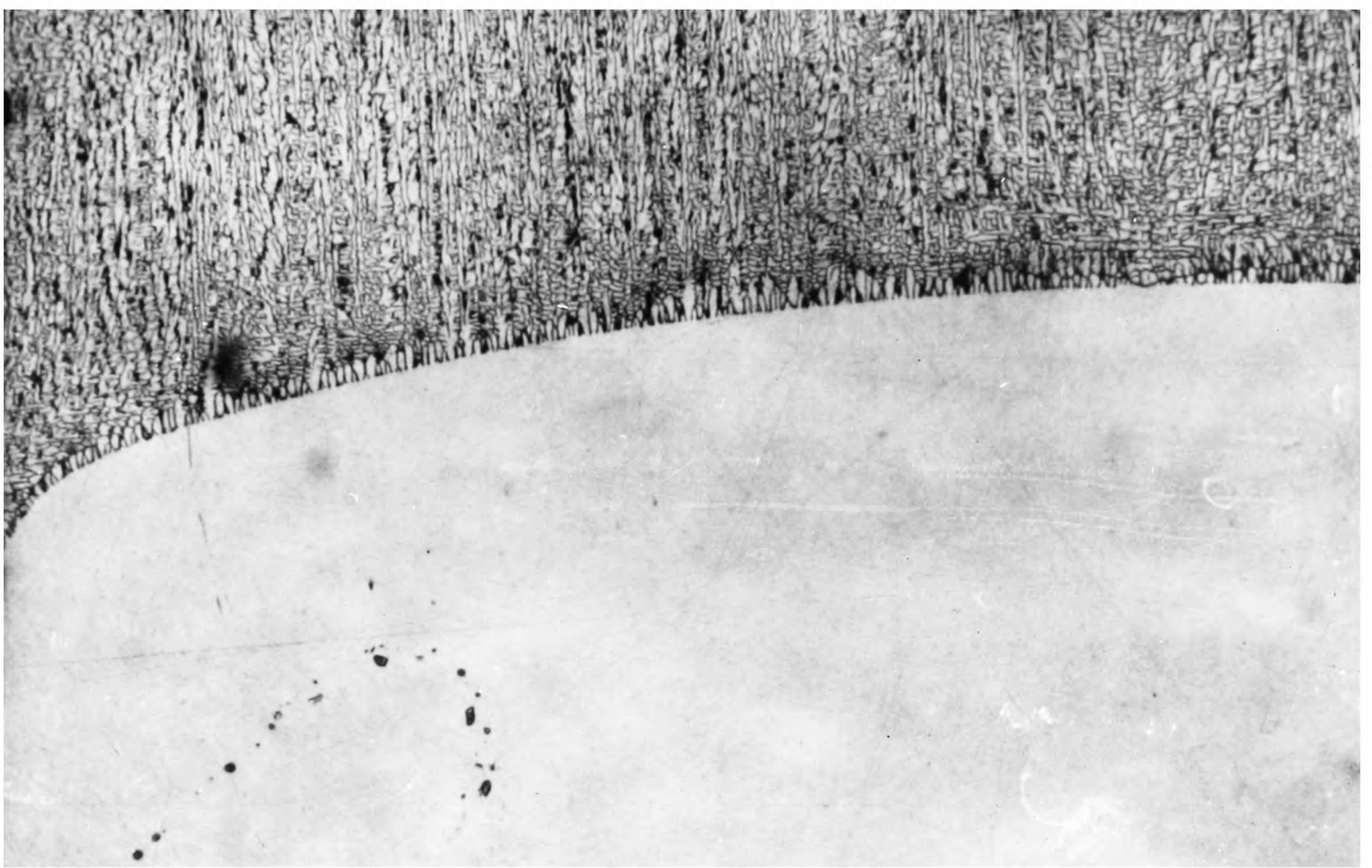


X 190

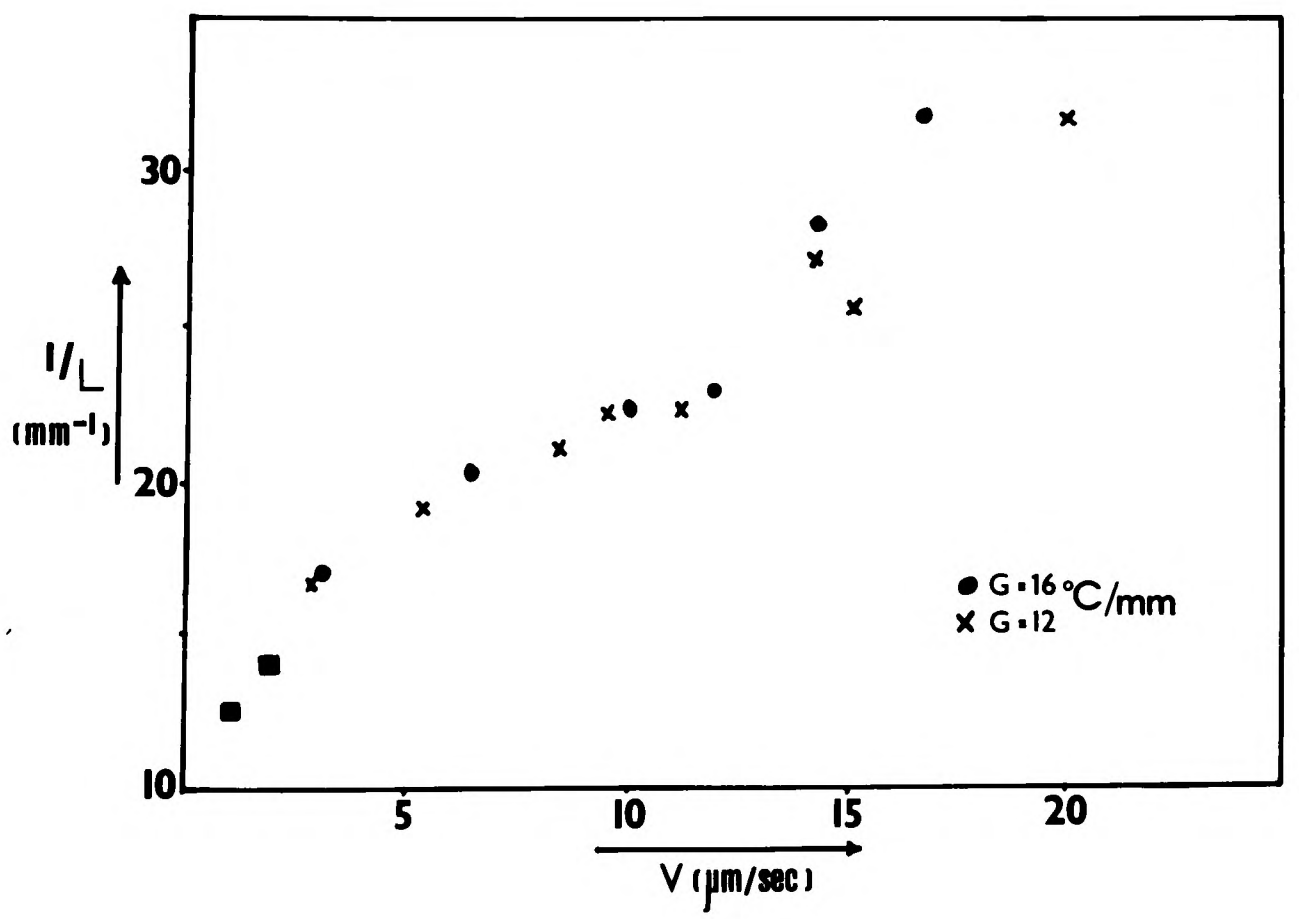
(b)



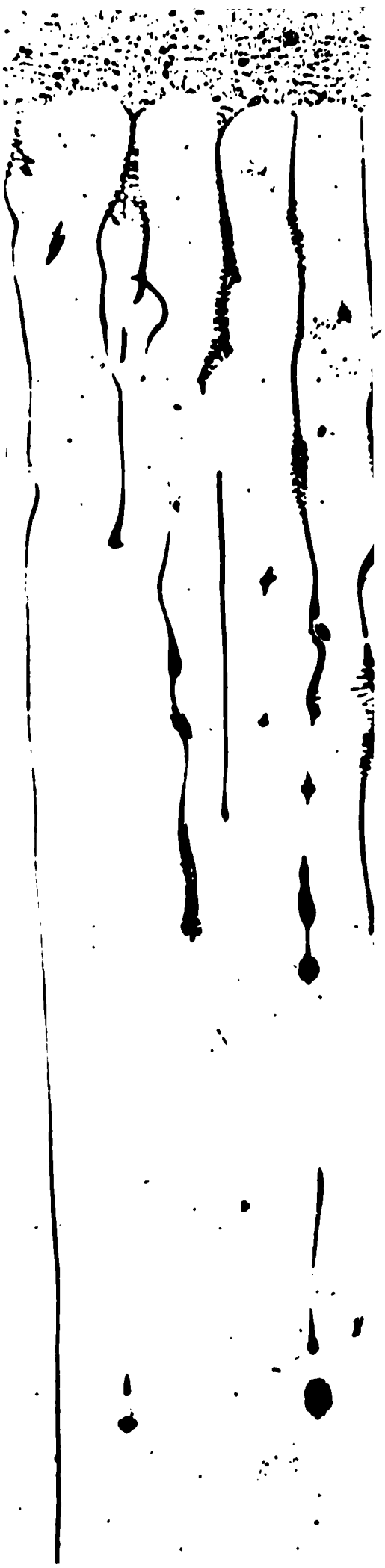
50. (a) Microstructure and (b) Solute profile corresponding to a specimen which has been accelerated for 60 seconds and then quenched.



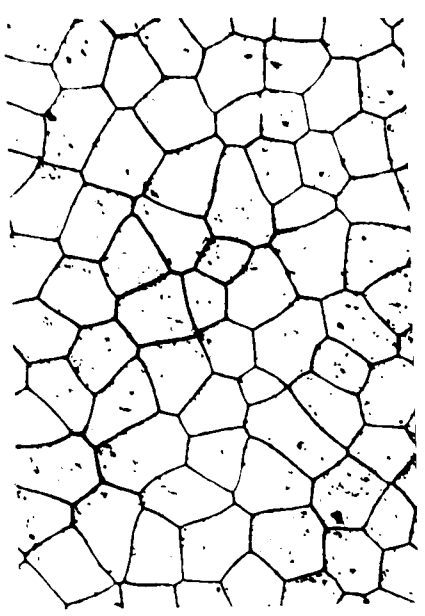
51. Showing how a planar front advances more at the centre of the specimen during acceleration. X 300



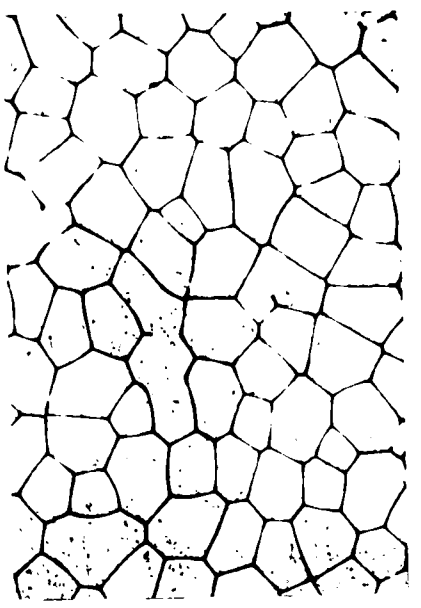
52. Initial spacings of cells (L) plotted as a function of the breakdown velocity. Equilibrium spacings are taken to have breakdown velocities given by constitutional supercooling theory.



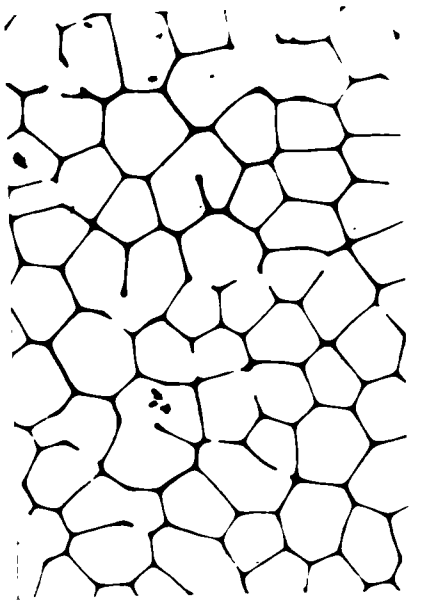
53. Longitudinal section of a specimen showing the effect of liquid movement behind the interface. Al-0.2% Cu alloy V = 50 μm/sec × 250



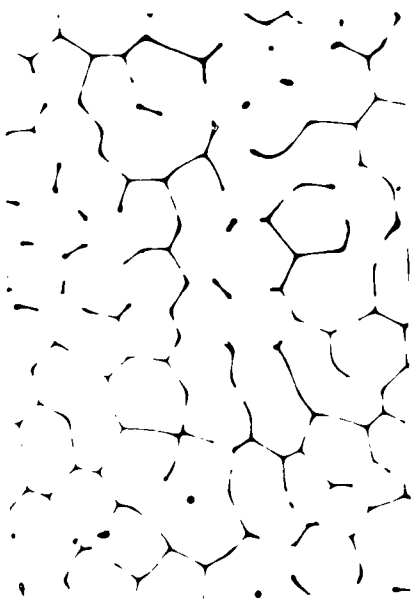
0 mm



·27 mm



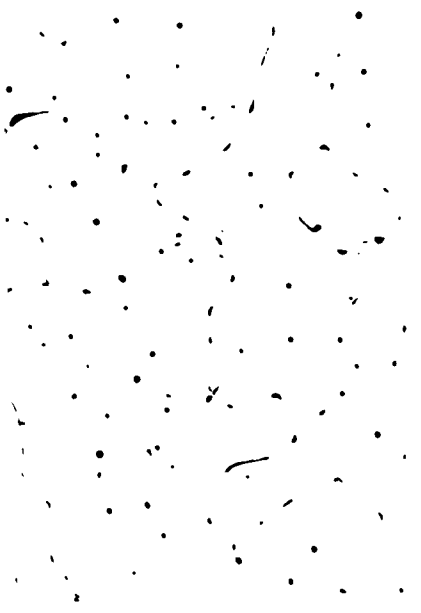
1·12 mm



1·58 mm



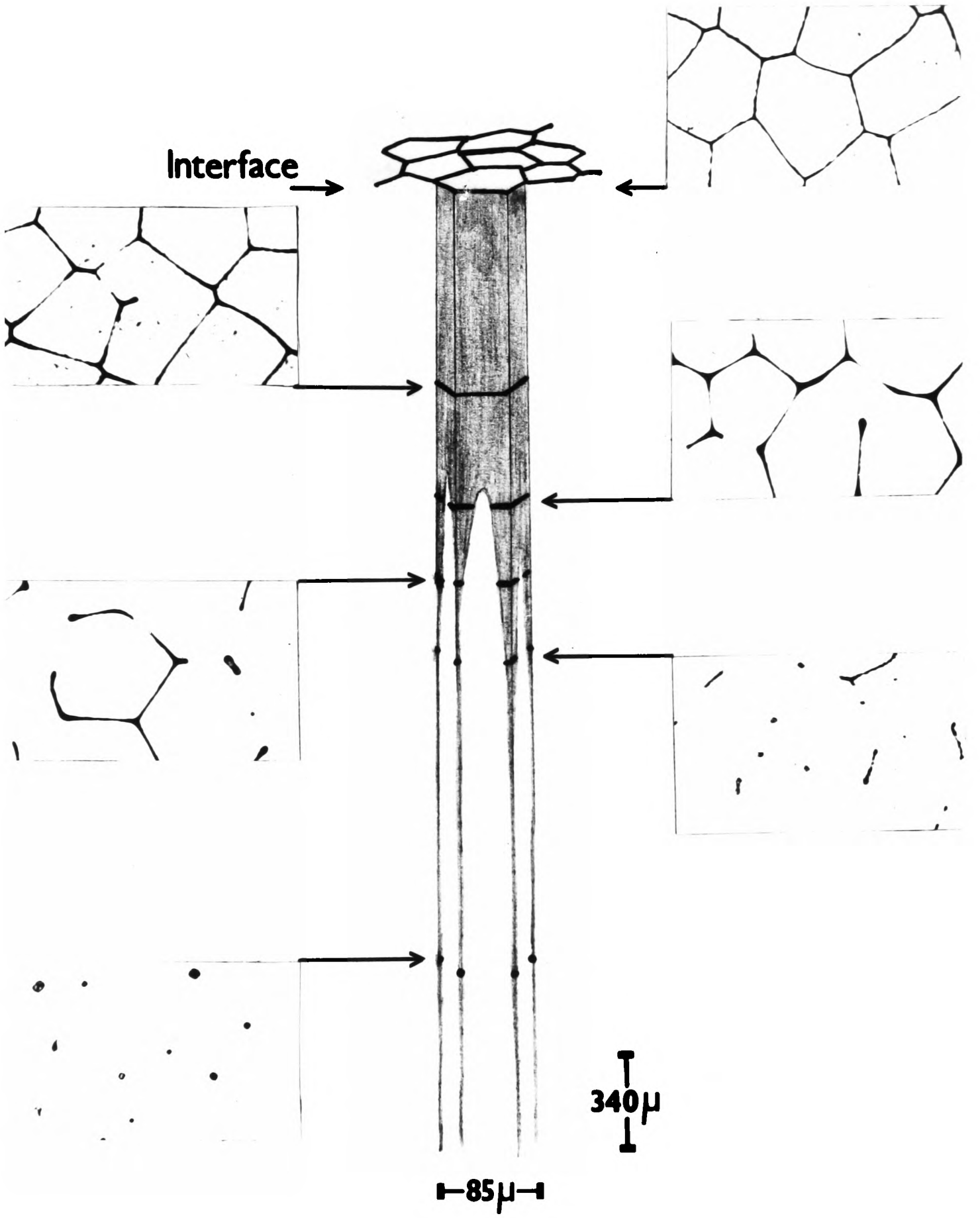
1·93 mm



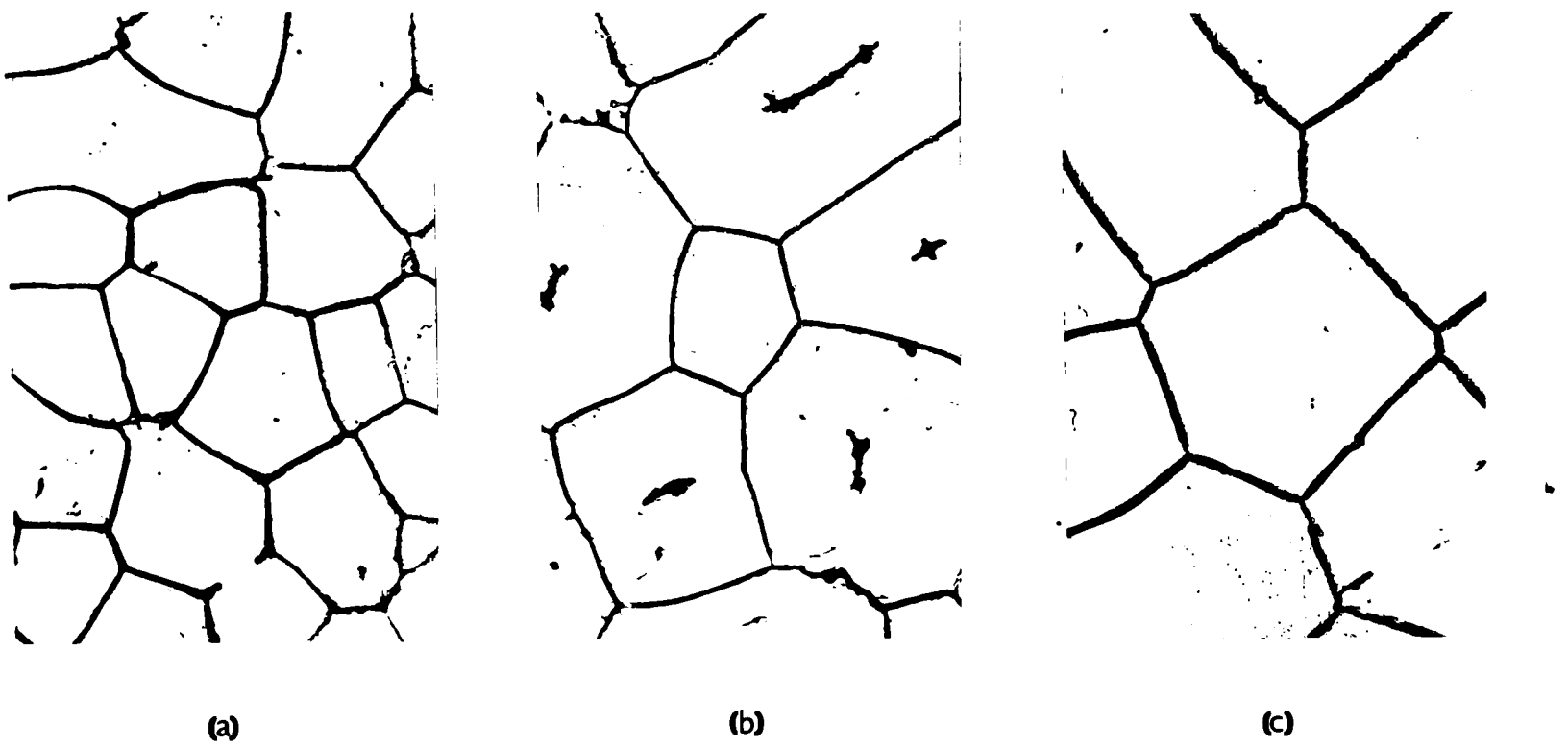
2·31 mm

54. Series of transverse sections from a specimen successively polished back from the interface Al-0.2% Cu. V = 50 μm/sec

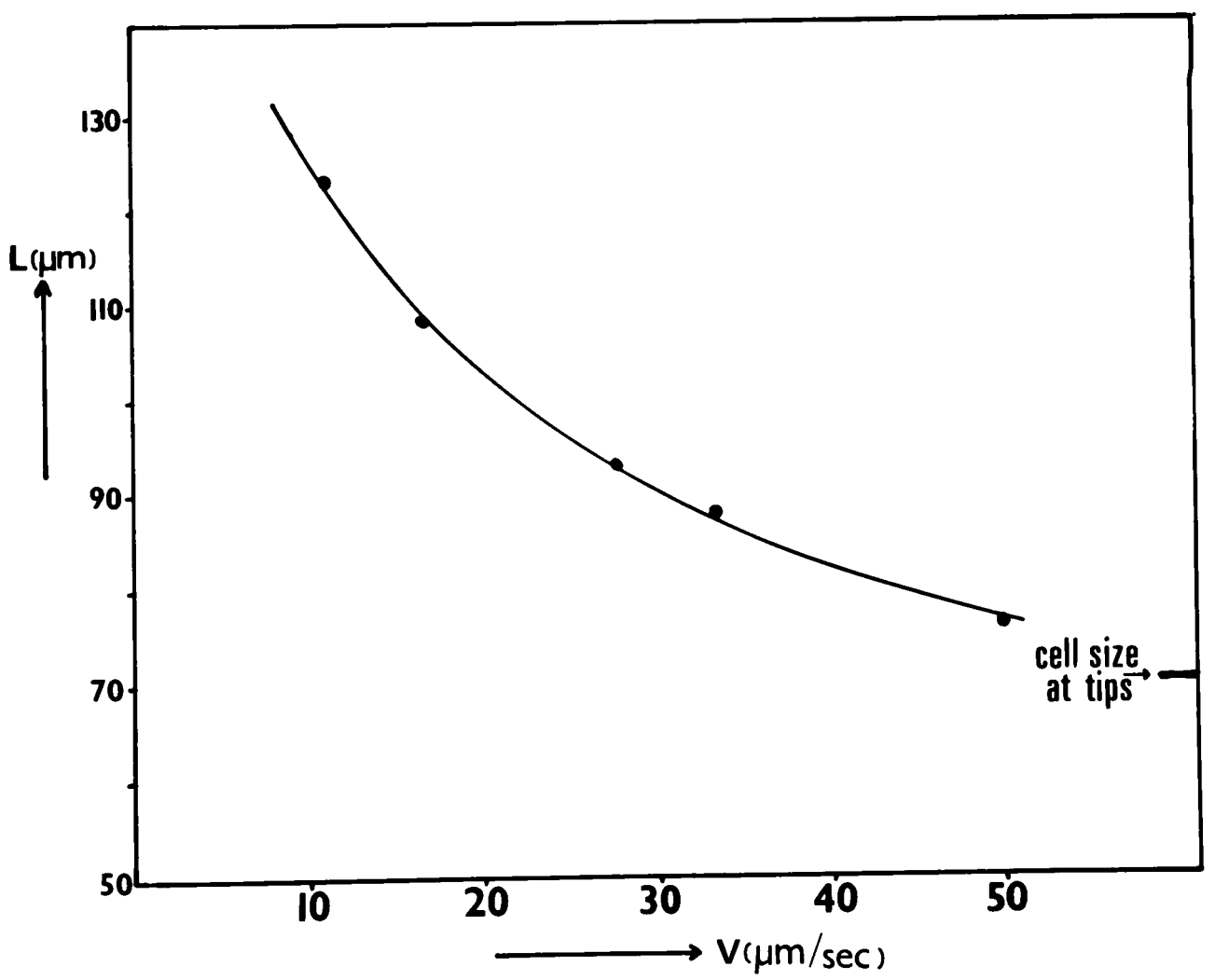
× 100



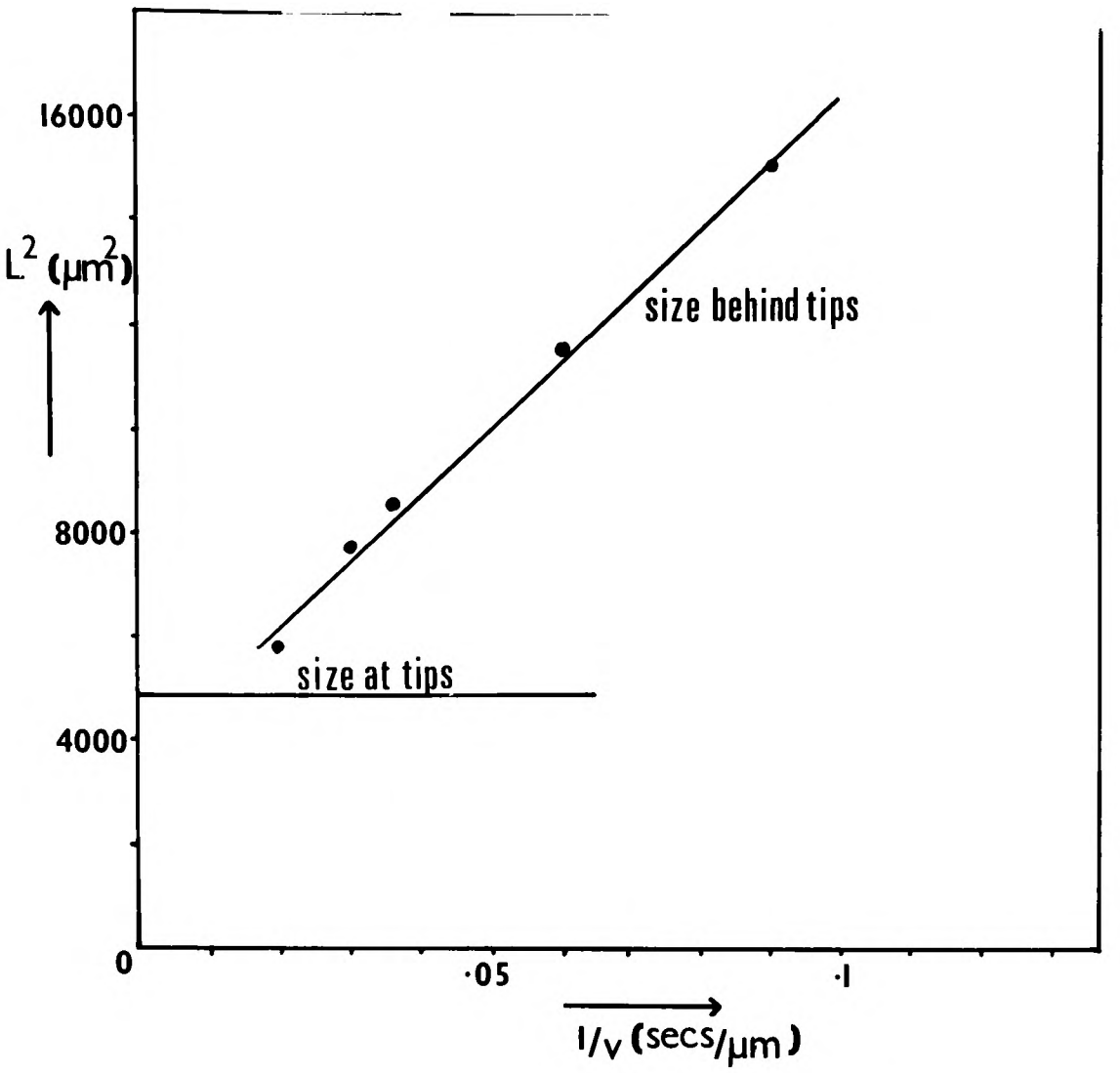
55. Diagrammatic representation of one cell of figure 53 showing transverse sections at appropriate points.



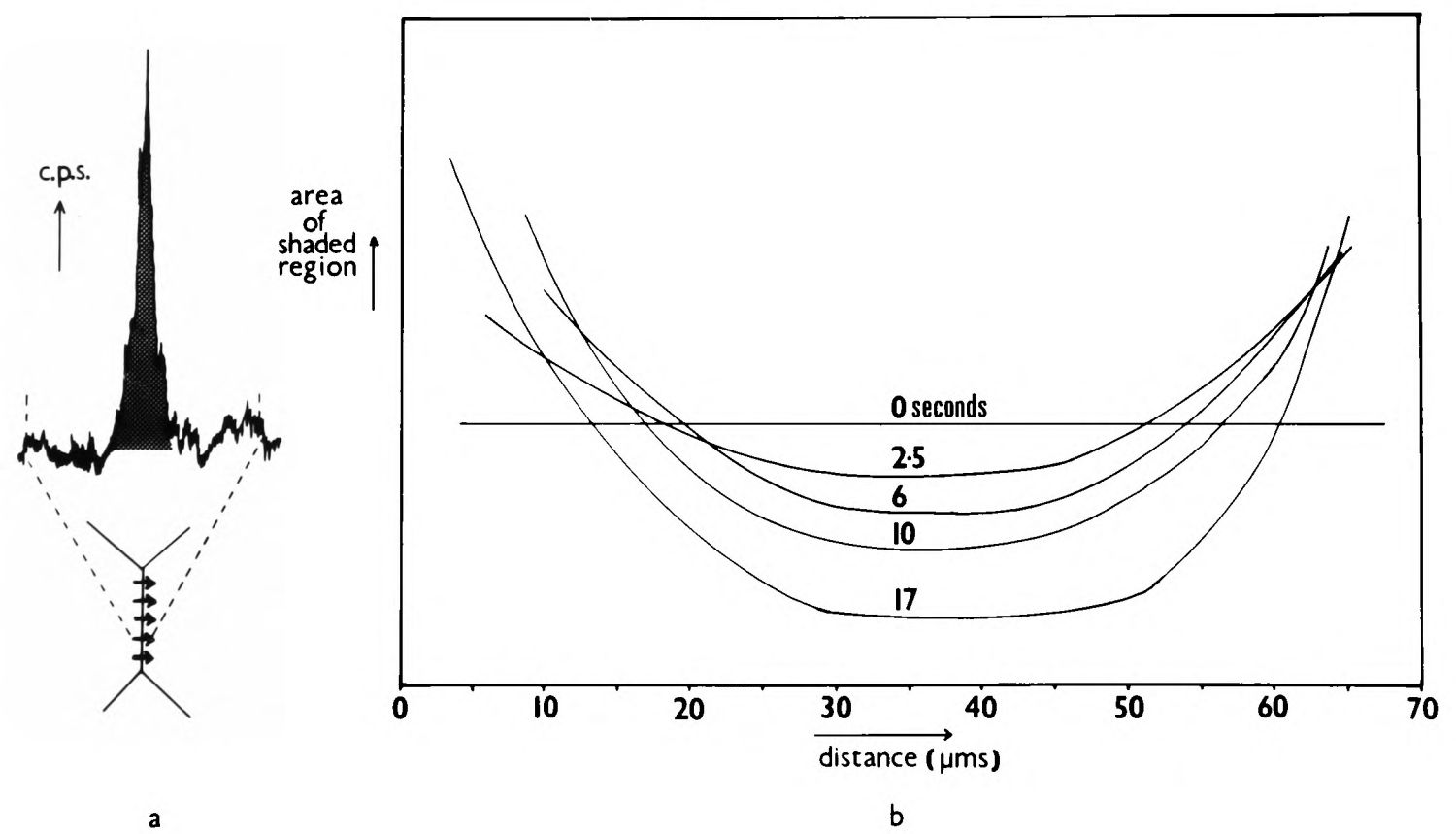
56. Morphology of cells on successive transverse sections behind the interface showing the method of formation of a complete but coarser cellular array. ×200



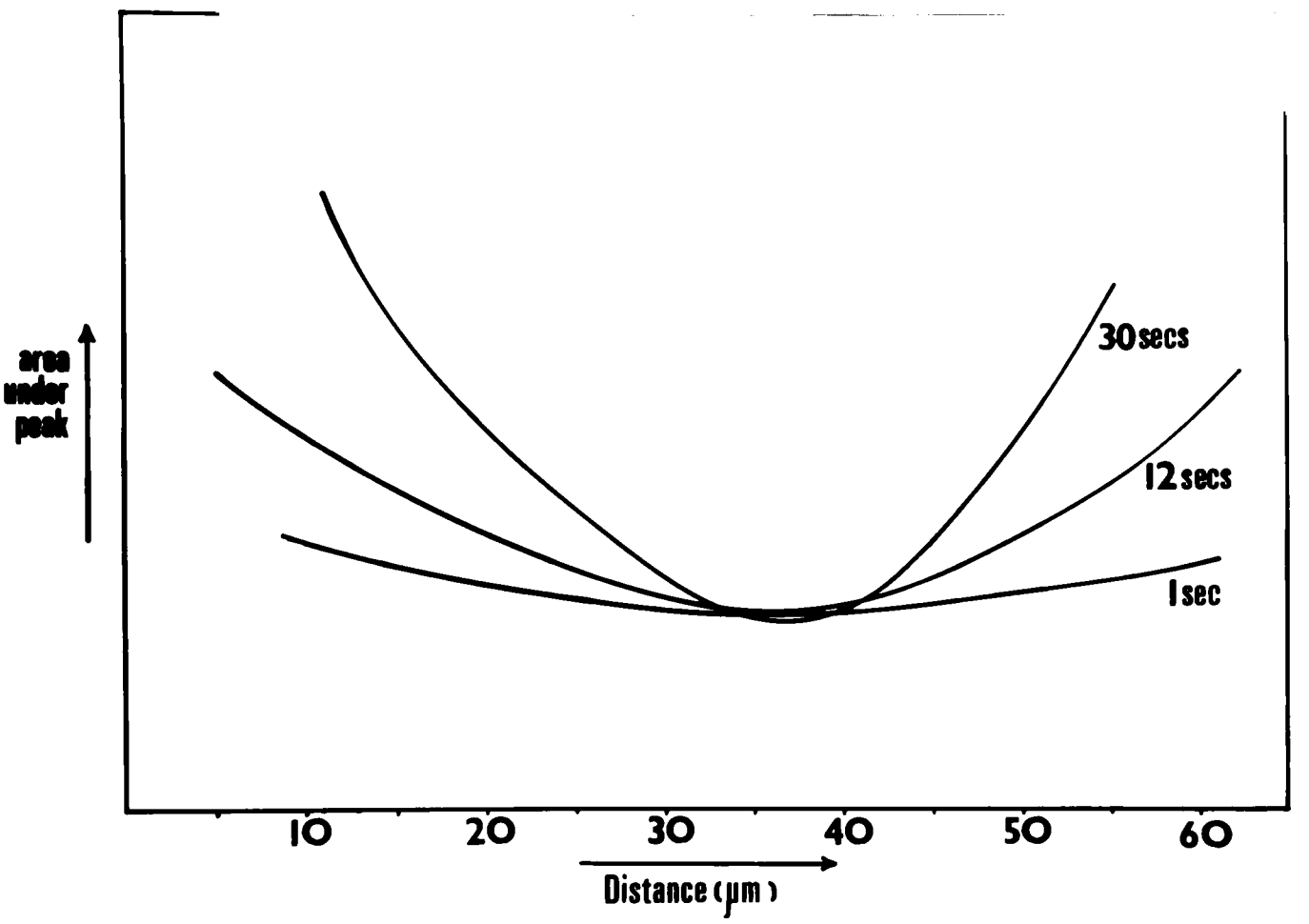
57. Cell size of the coarsened cellular structure plotted against the velocity of growth. Tip cell size is also shown.



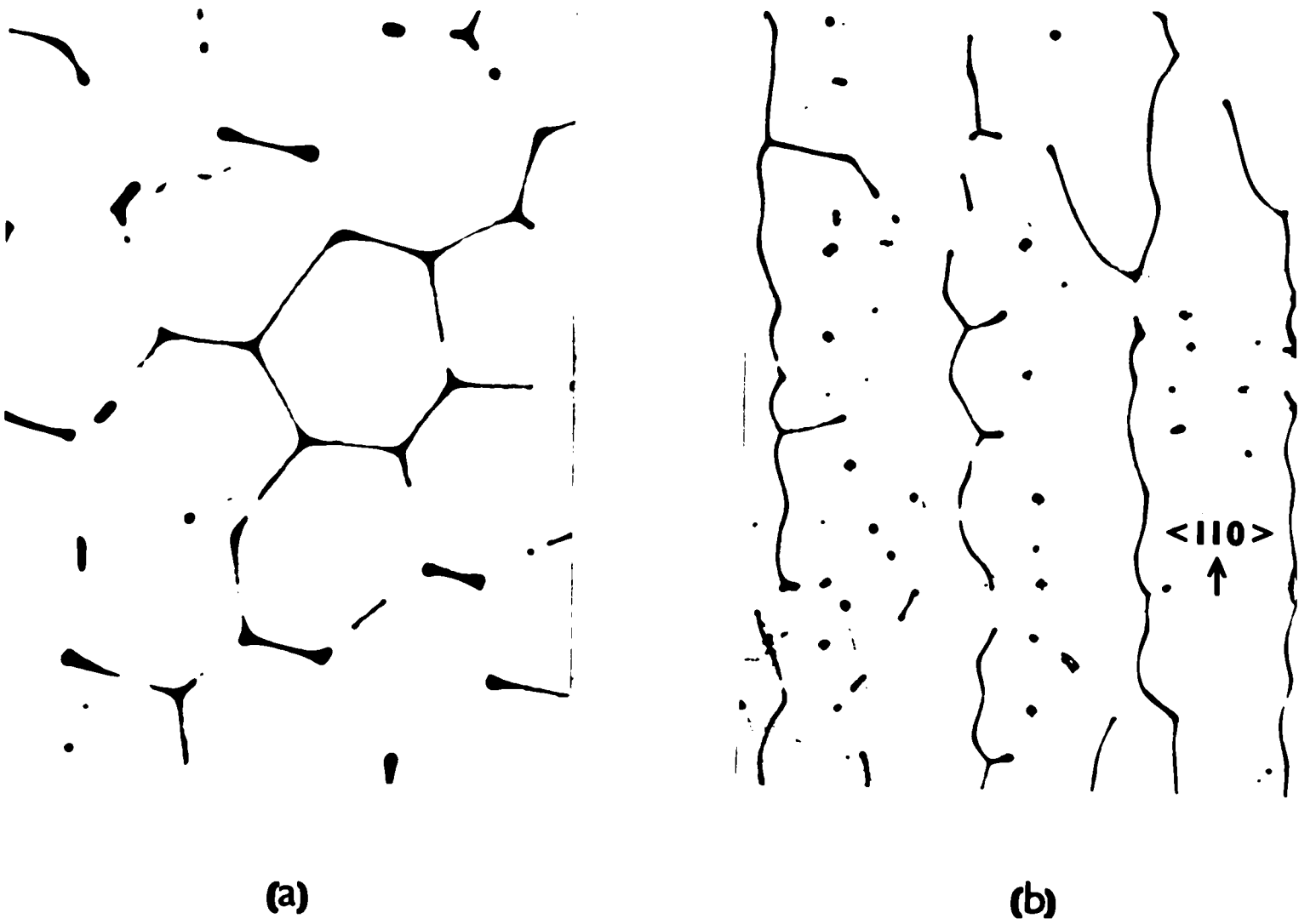
58. Cell size of the coarsened cellular structure plotted against the parameter $V^{-\frac{1}{2}}$.



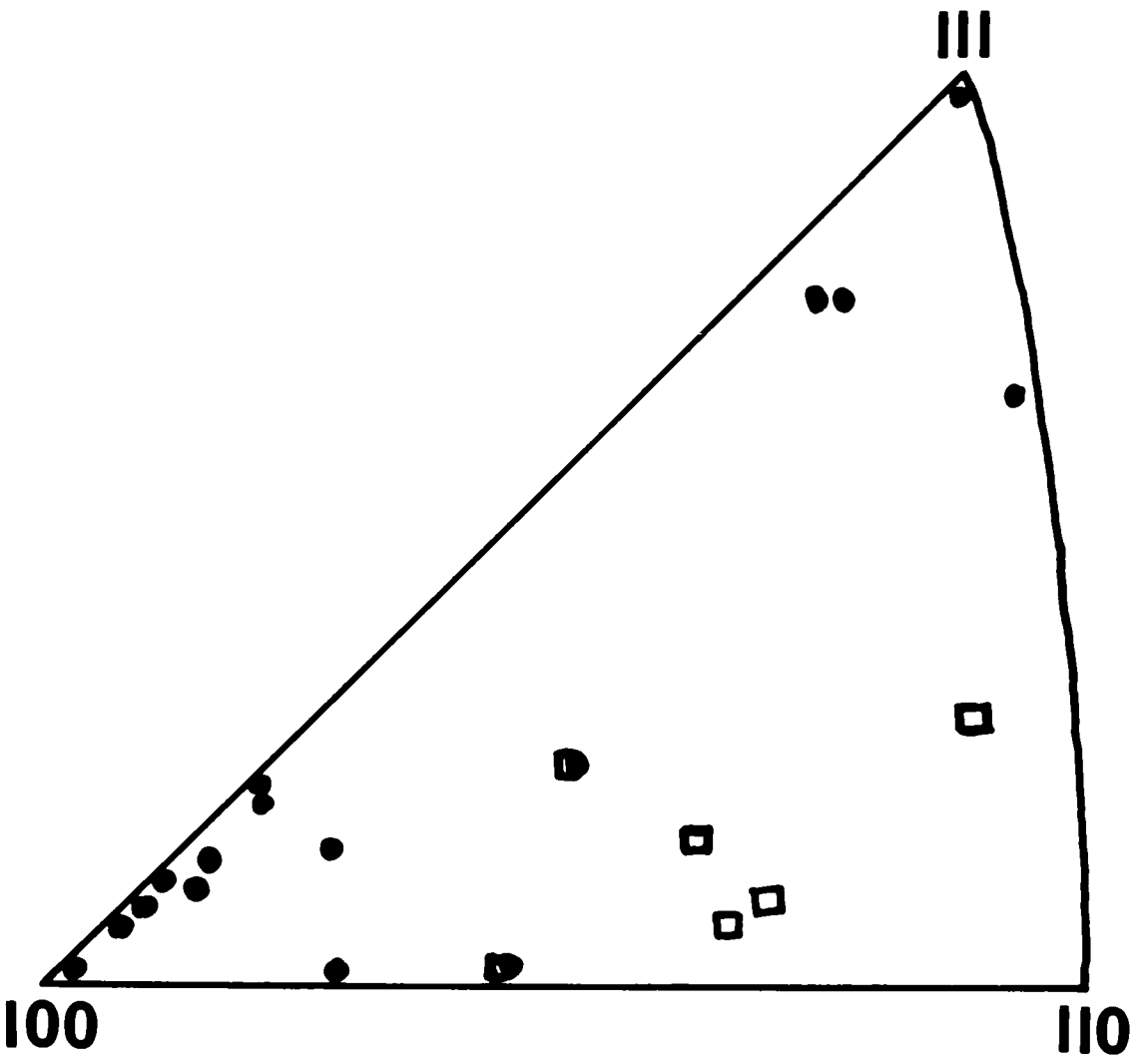
59. Showing how solute concentrations were measured from line scans over cell wells on transverse sections, (a) to give solute profiles, the areas under which changed on successive sections behind the interface as in (b).



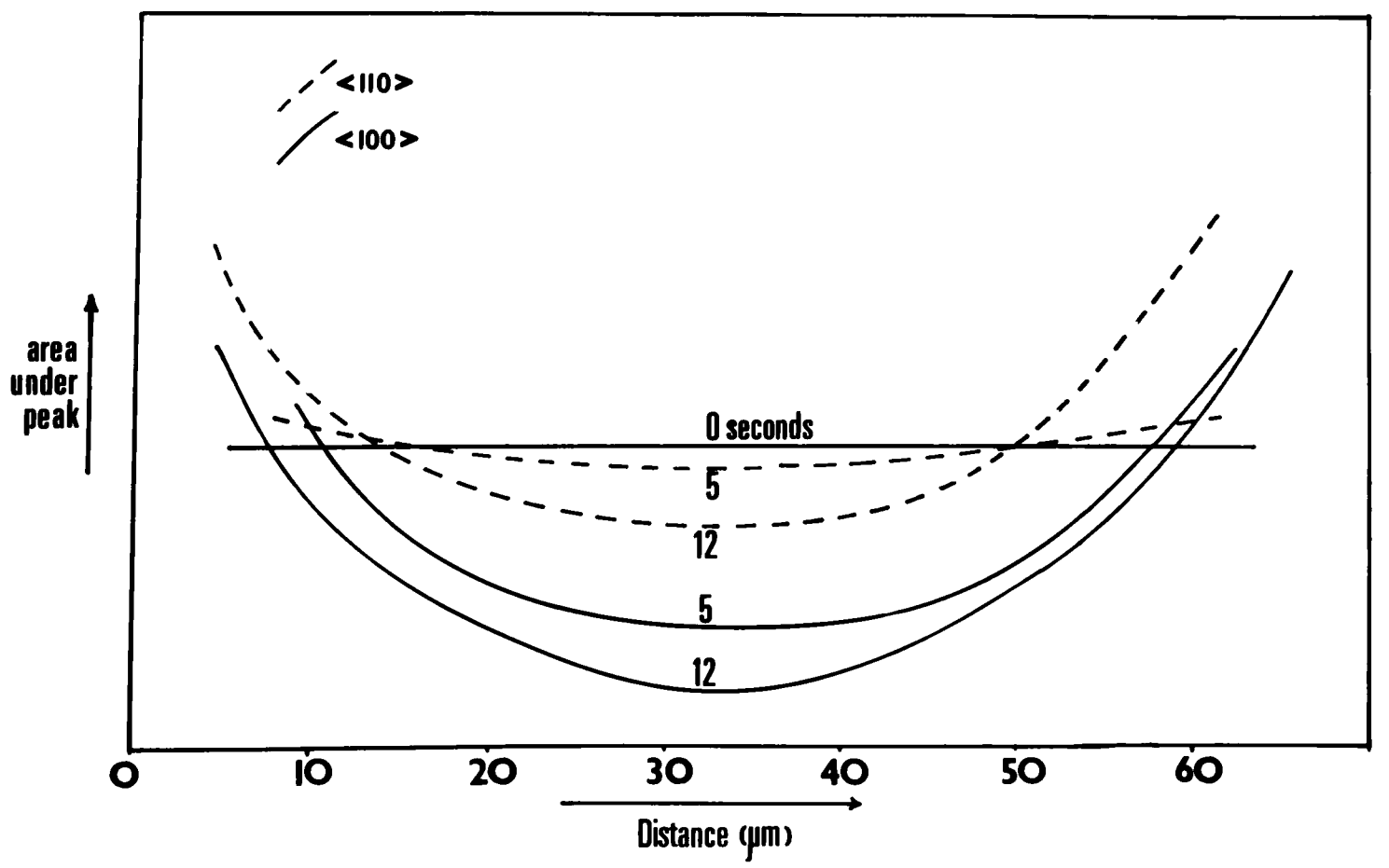
60. Equivalent diagram to fig 59 (b) except that in this case the width of the wall in the centre has not decreased significantly although the corners have still grown larger.



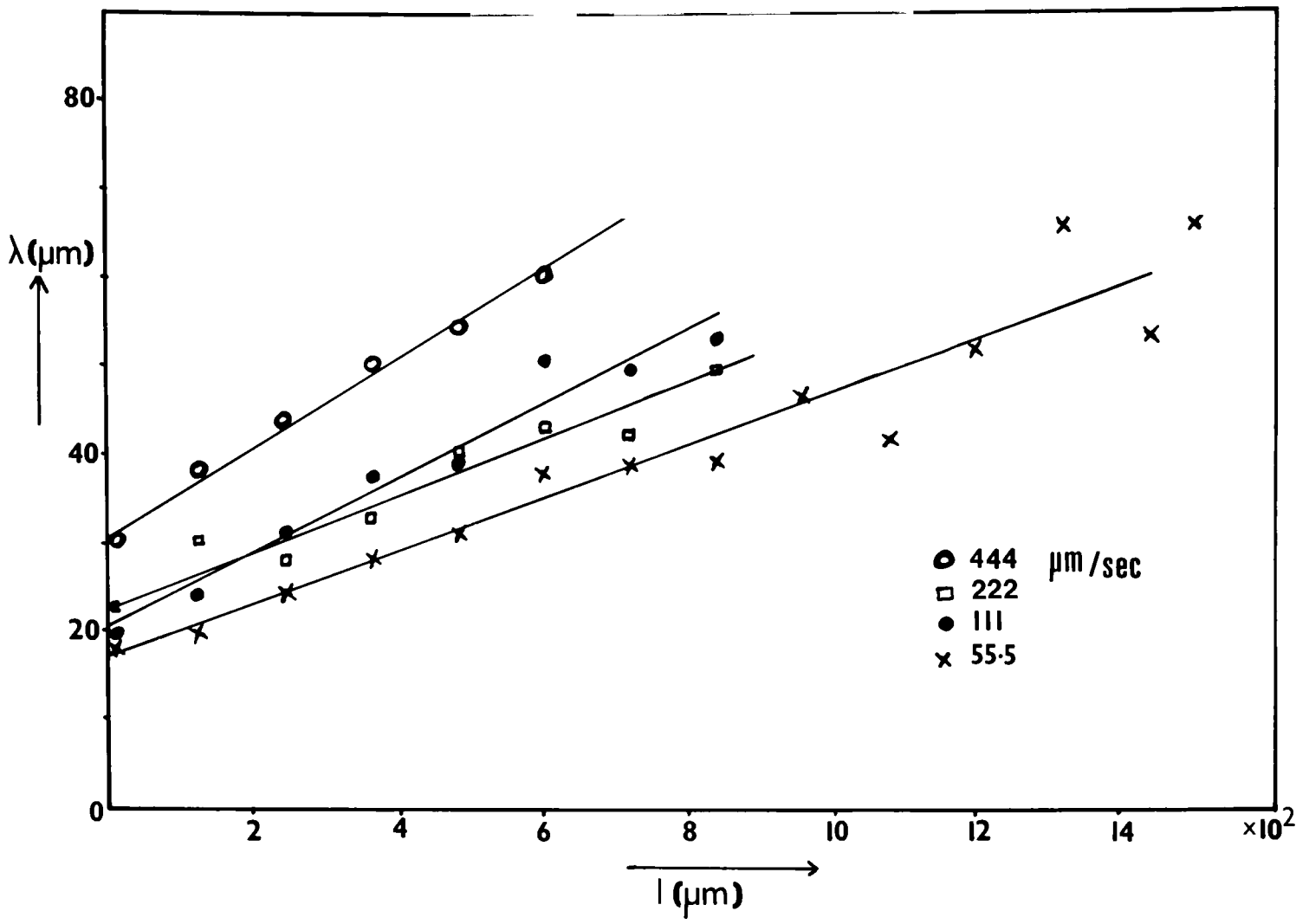
61. Transverse sections of coarsened cells (a) close to <100> and (b) close to <110>. x 140



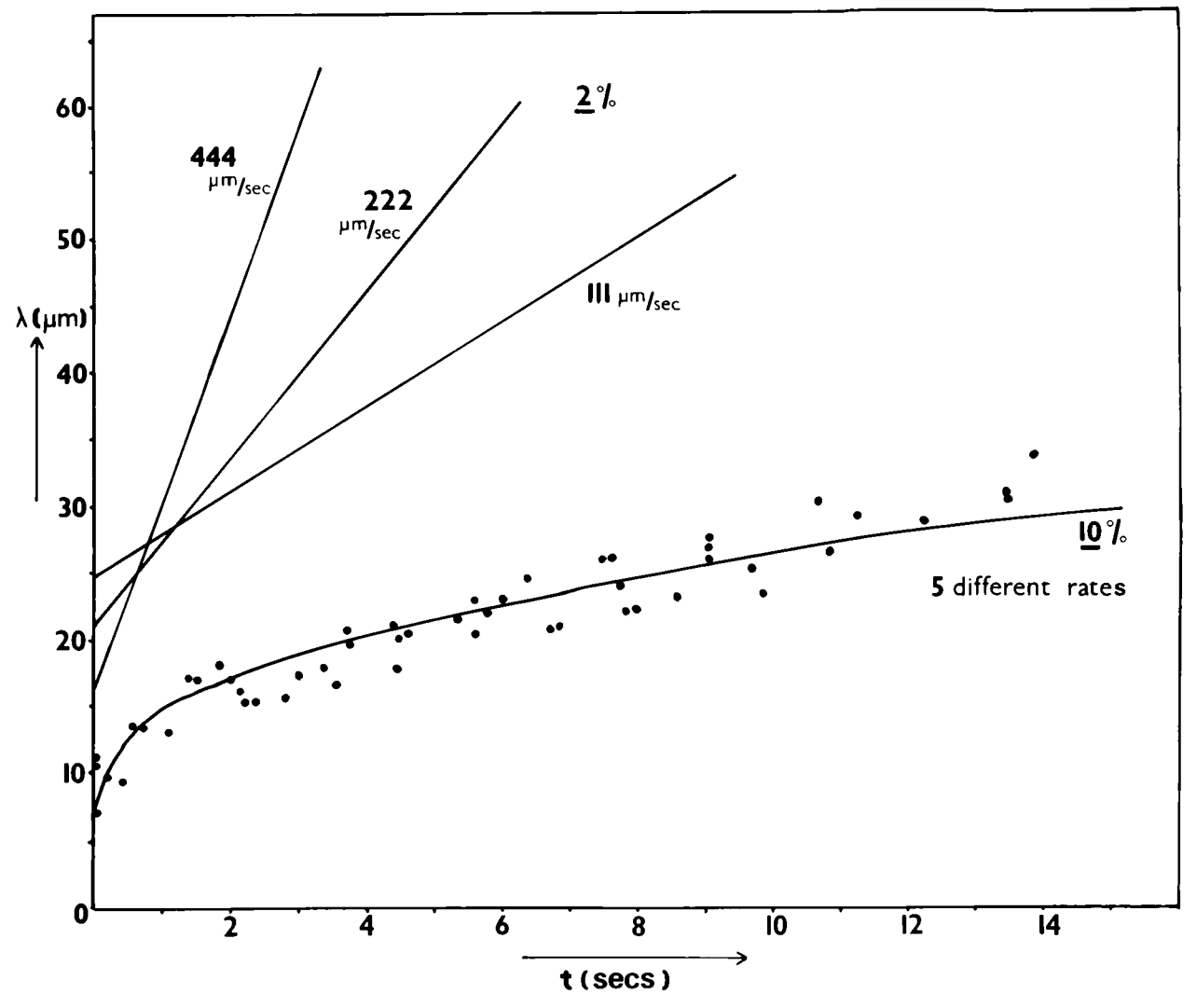
62. Distribution of growth directions on a standard projection. Those denoted by ● coarsened to give patterns as figure 6● (a) and by □ as in figure 6● (b). ◘ denotes that a combination of coarsened morphologies was observed.



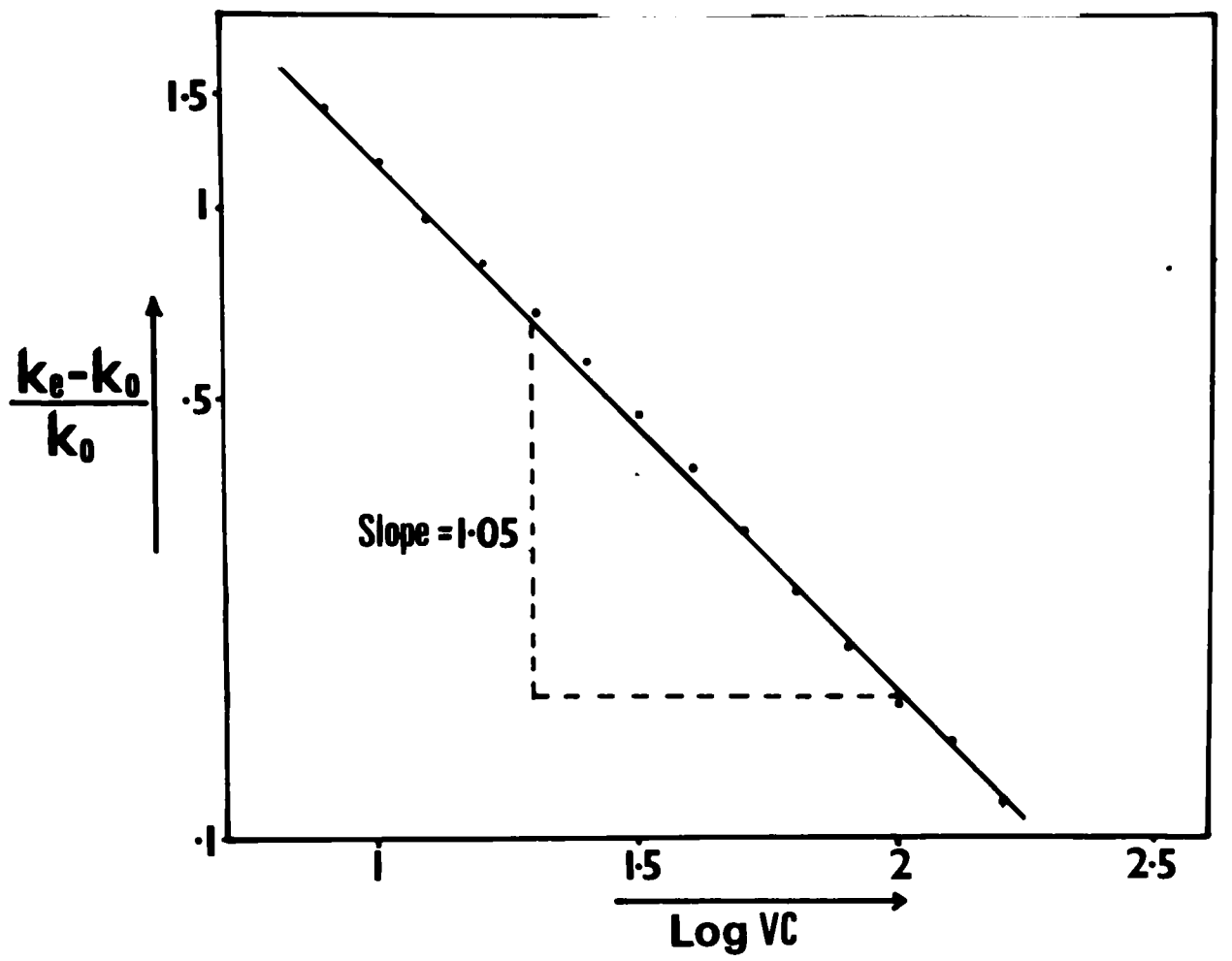
63. Solute concentration measured on successive transverse sections behind the interface, in two directions at right angles for the case of a specimen whose growth direction was close to <110>.



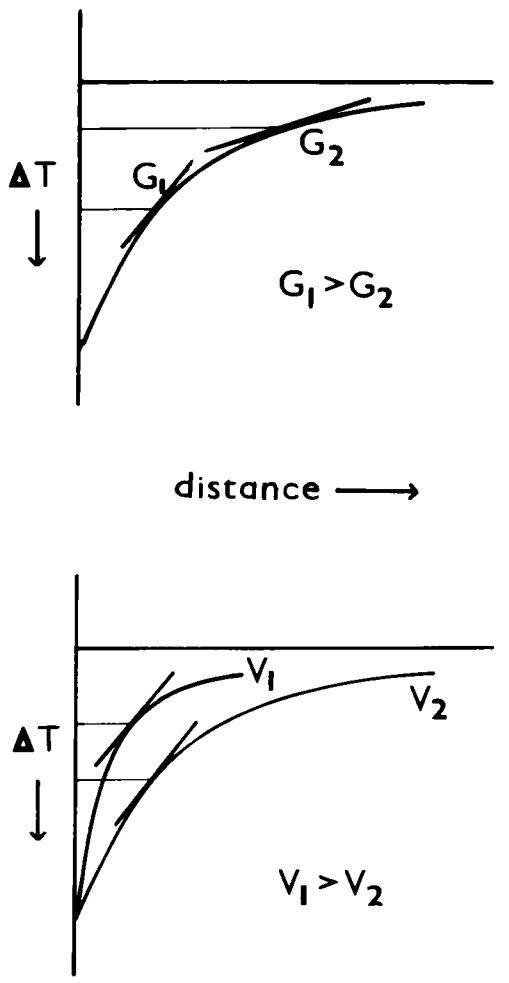
64. Spacings of branched cell arms plotted against distance behind the interface for alloys containing 3% copper.



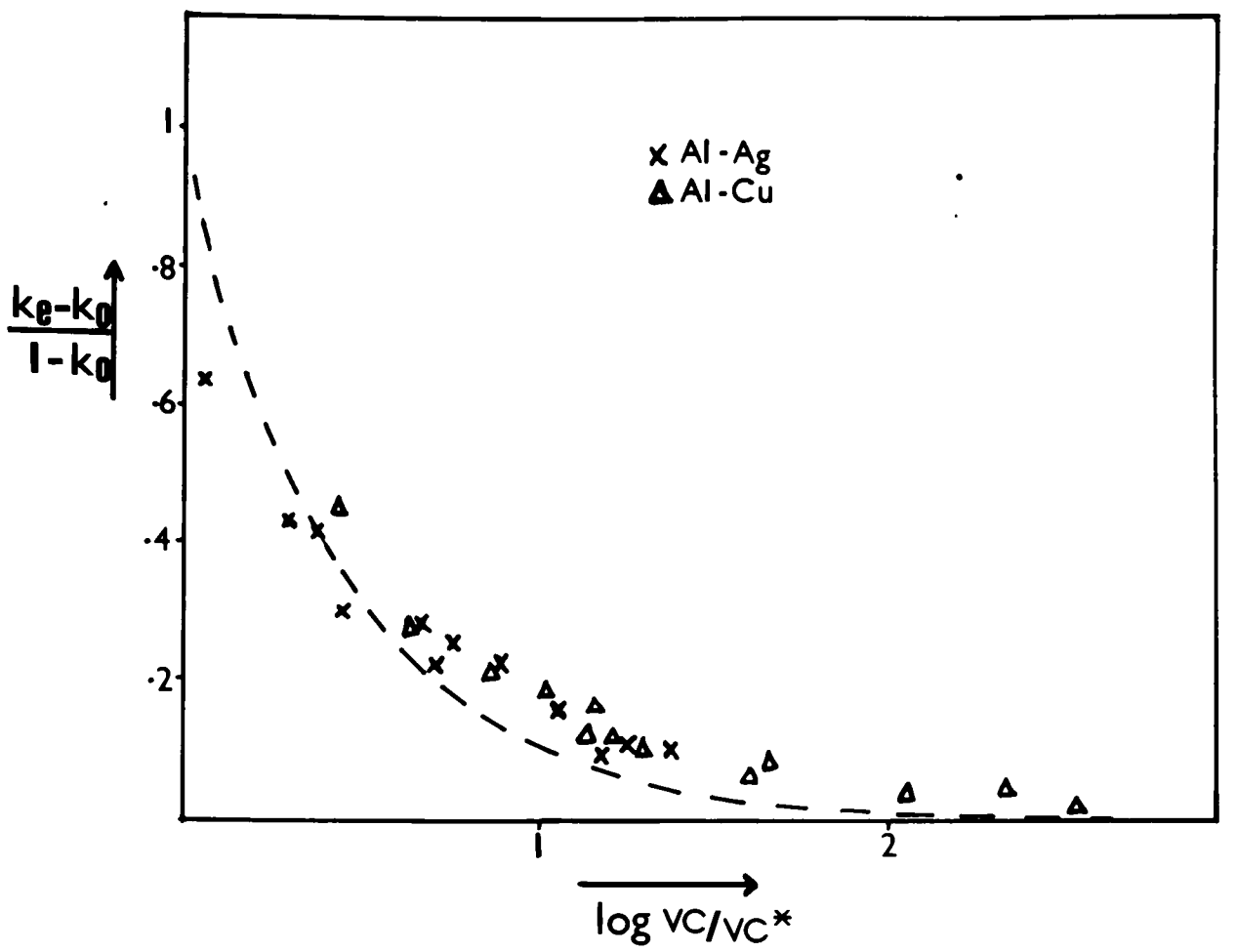
65. Spacings of branched cell and dendrite arms plotted against time available for coarsening for alloys containing 2% and 10% copper.



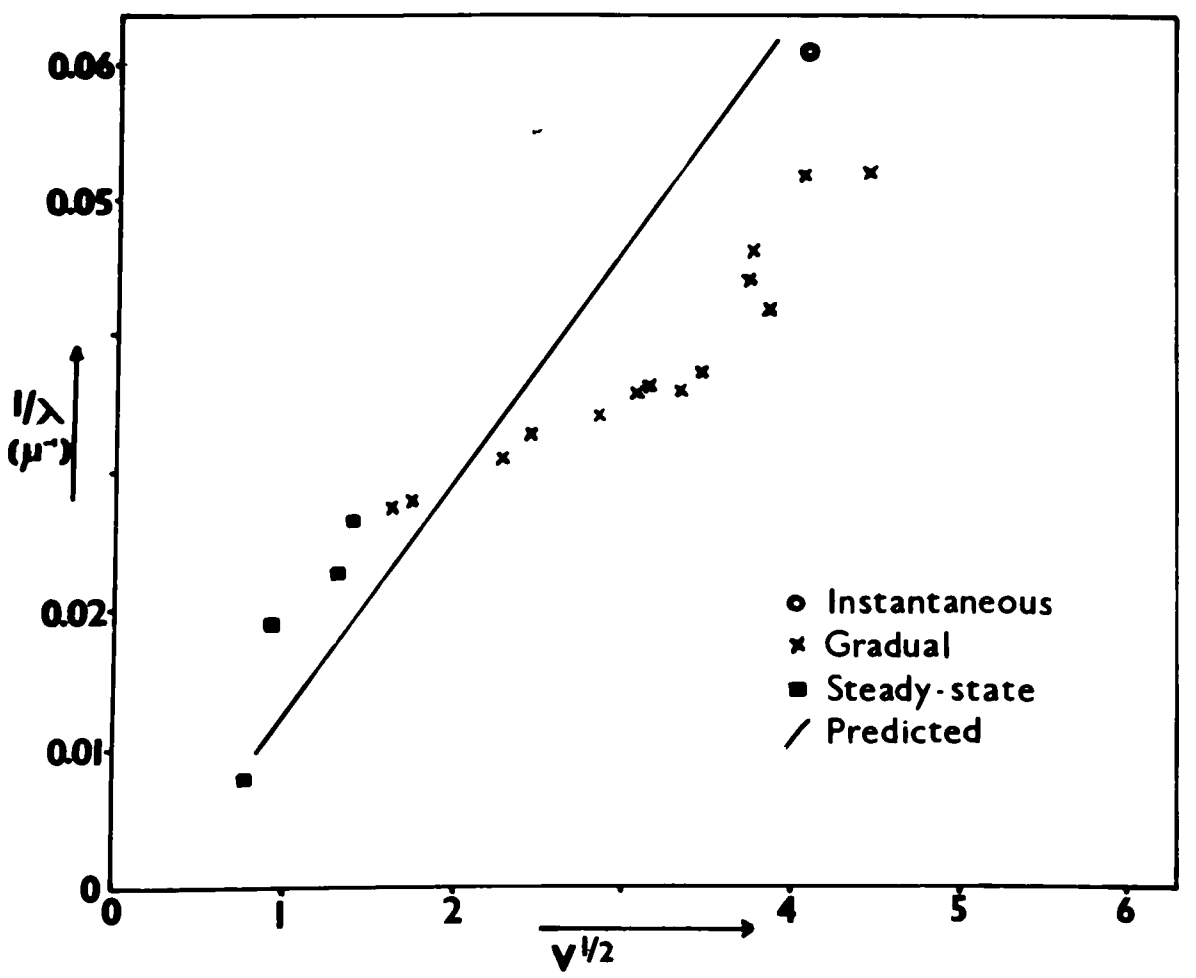
66. Log $(\frac{ke-ko}{ko})$ plotted against log VC for aluminium-copper alloys. ke values obtained from figure 40.



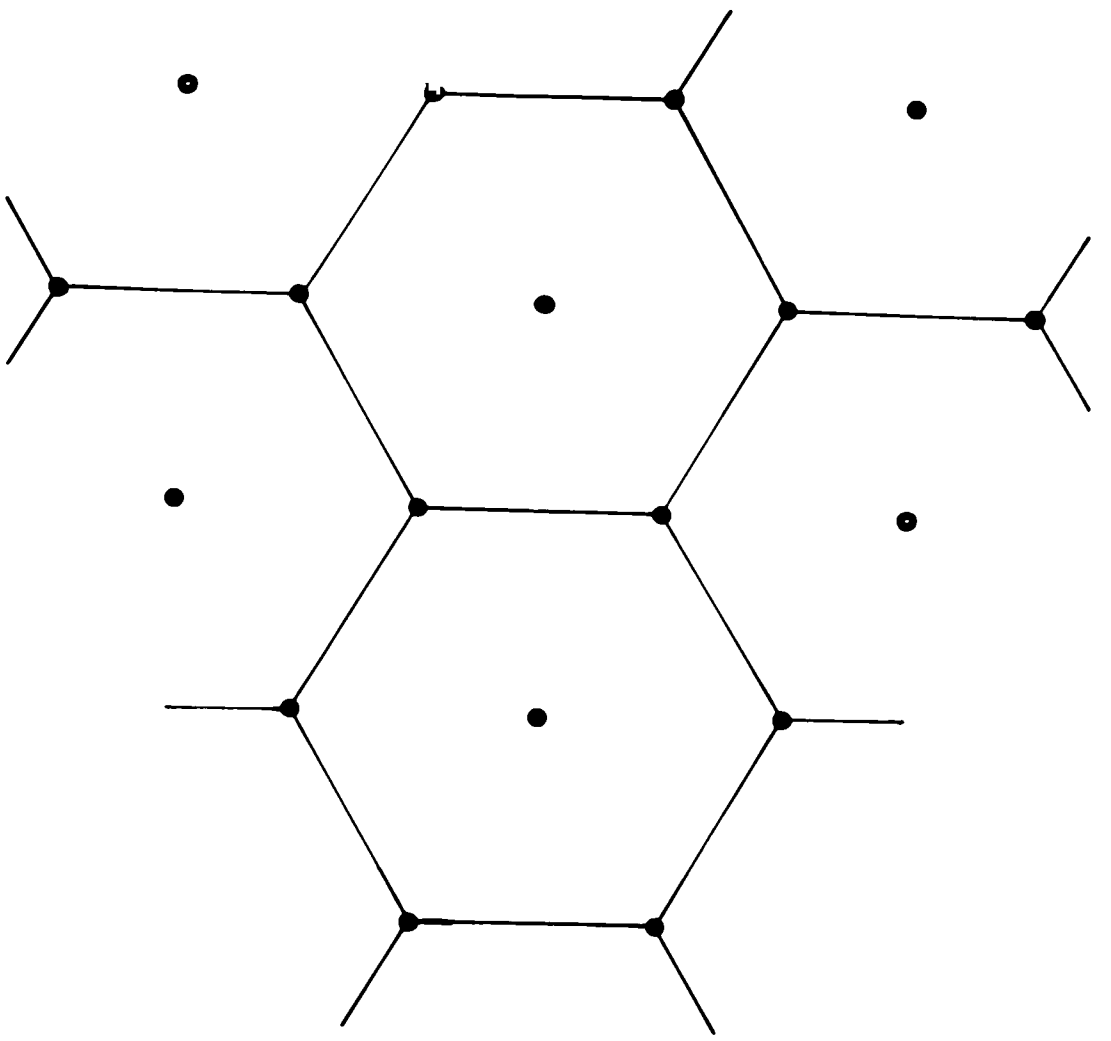
67. Diagram showing the dependence of undercooling on temperature gradients and growth rates, assuming that the liquidus gradient at the interface is equal to the imposed temperature gradient.



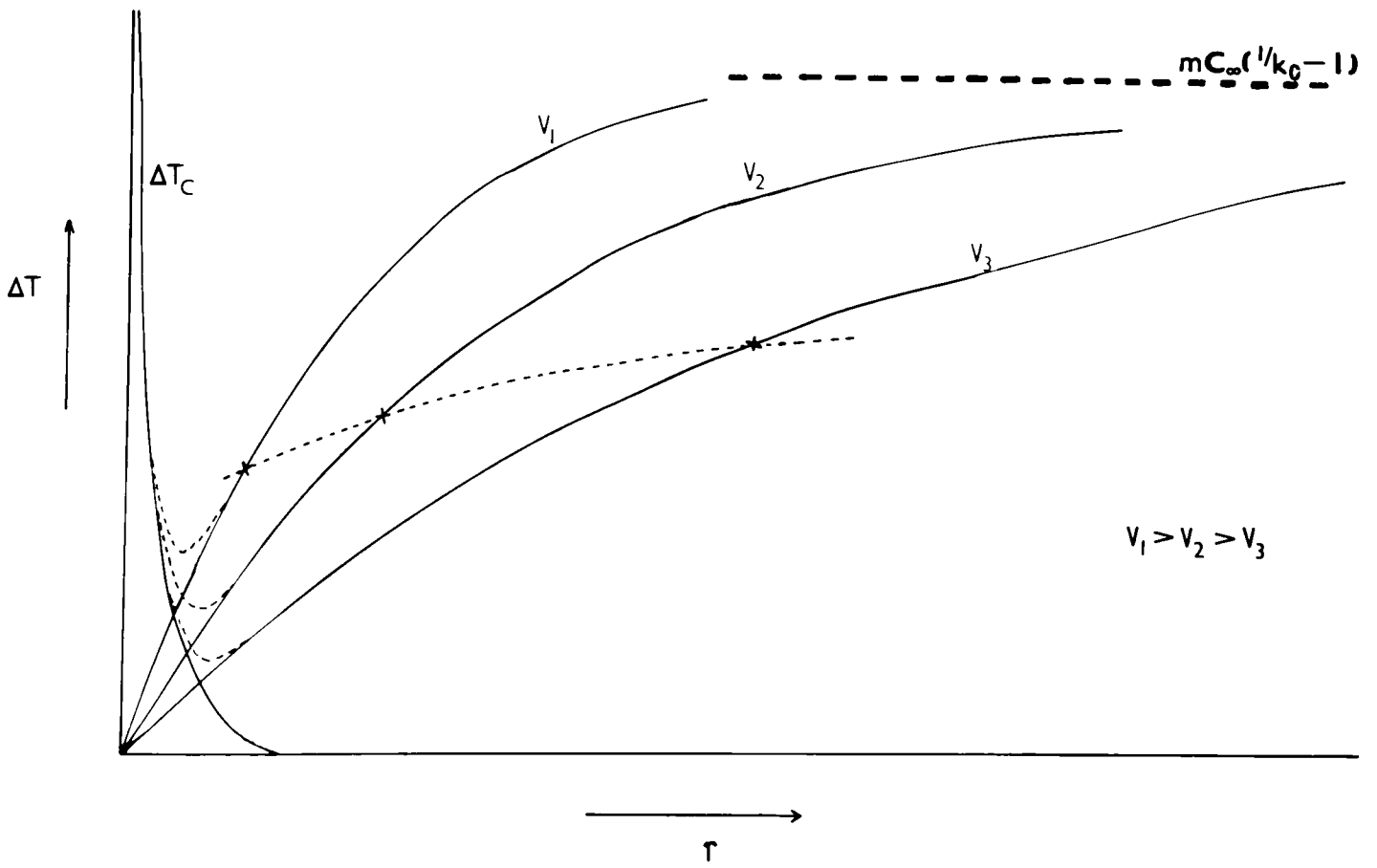
68. $(\frac{ke-ko}{1-ko})$ plotted against $^{(vc)}/(vc)^{*}$ for aluminium-copper and aluminium-silver alloys at a variety of concentrations, temperature gradients and growth rate.



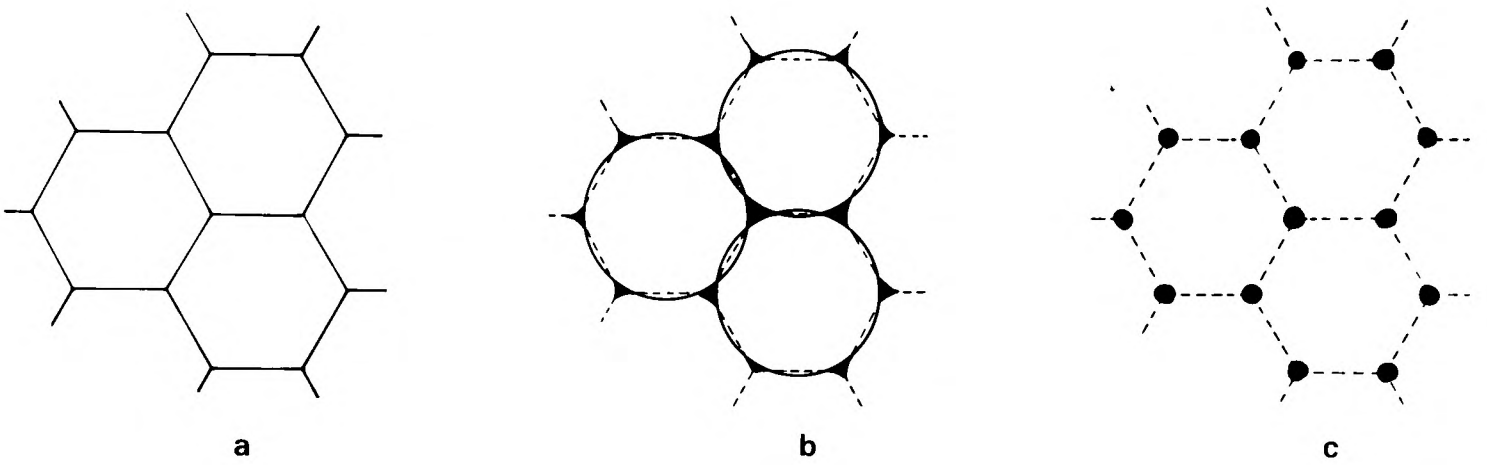
69. Results obtained from the computer solution of the central equation of Mullins and Sekerka (full line). The points represent experimentally measured cell spacings multiplied by a constant factor of 0.6.



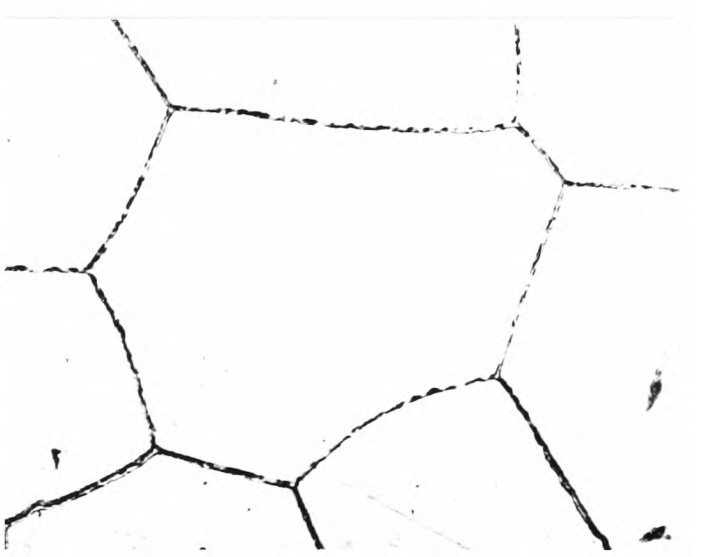
70. Showing a possible relation between an arrangement of close-packed holes and a cellular substructure.



71. Diagram illustrating the effect of curvature on the undercooling for three different growth rates. The maximum value of solute undercooling is that corresponding to a planar interface.

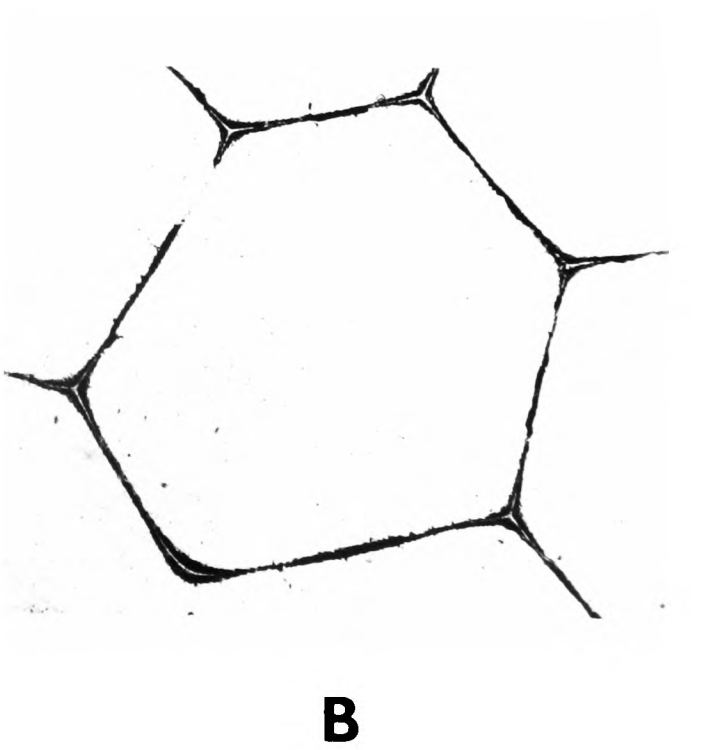


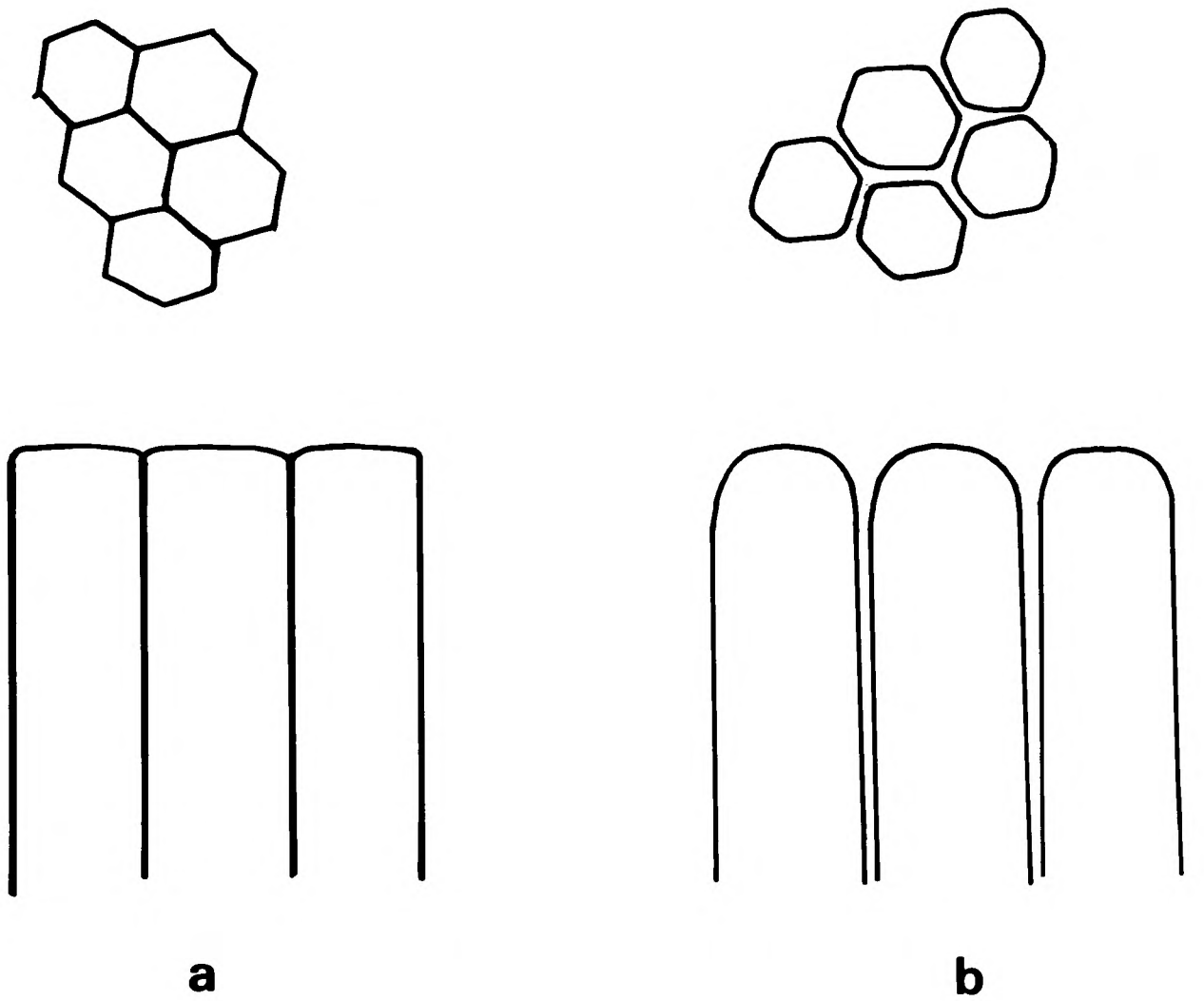
72. Diagram showing how the reduction of solid-liquid interface area might lead to enlargement of cell corners and eventually to the production of cylindrical channels of solute-rich liquid.



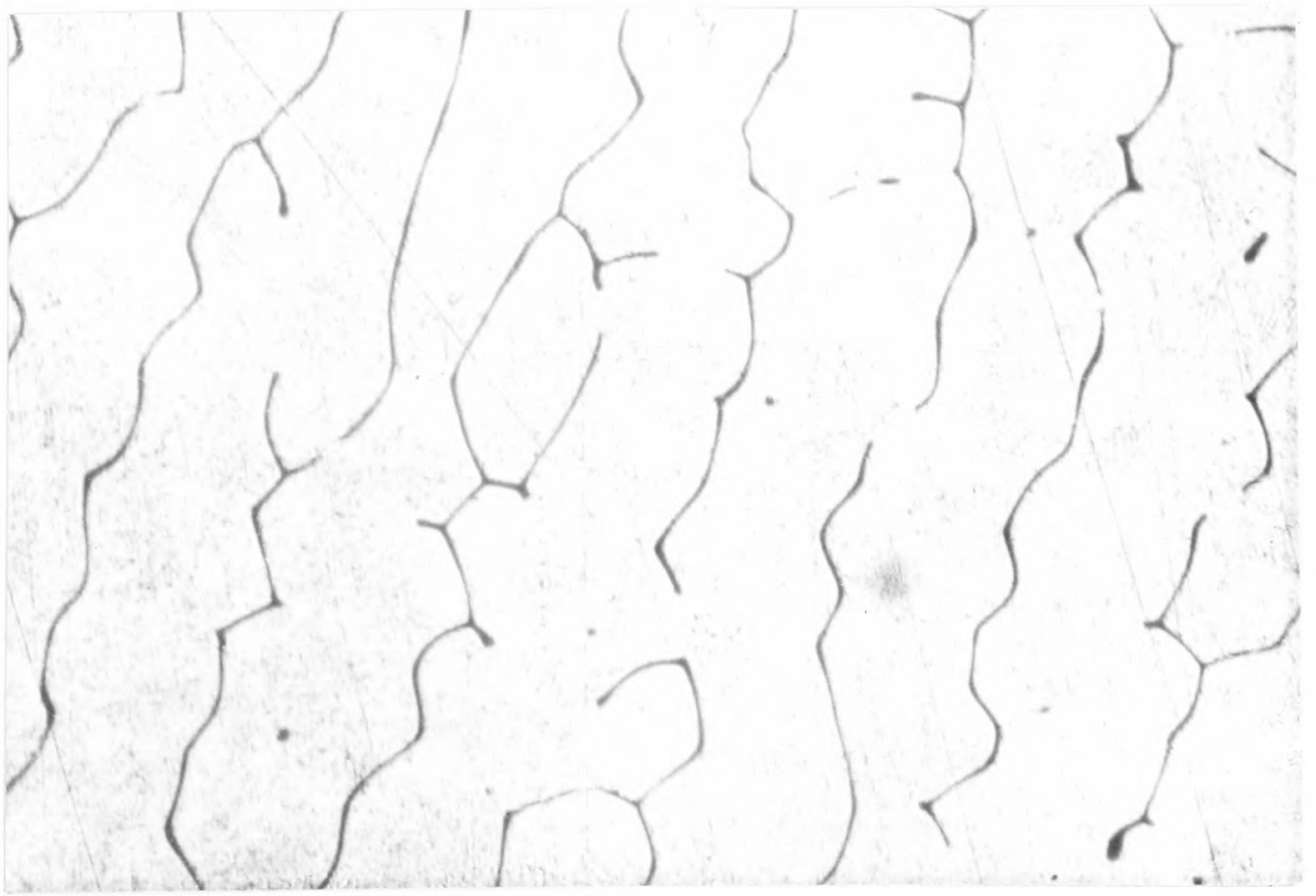
73. Thinning and breaking of an actual cell wall, showing the simultaneous enlargement of the cell corners.

x500

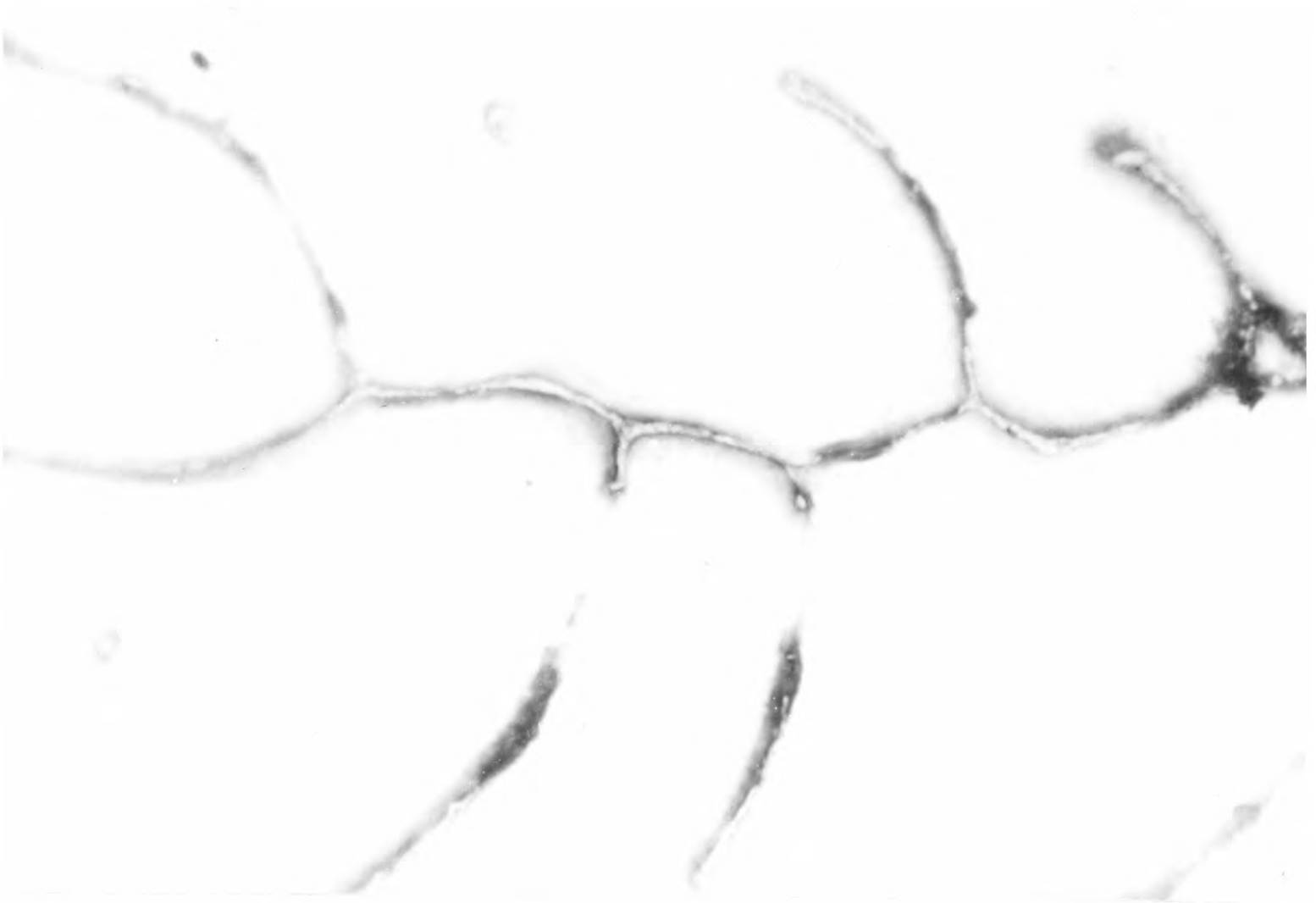




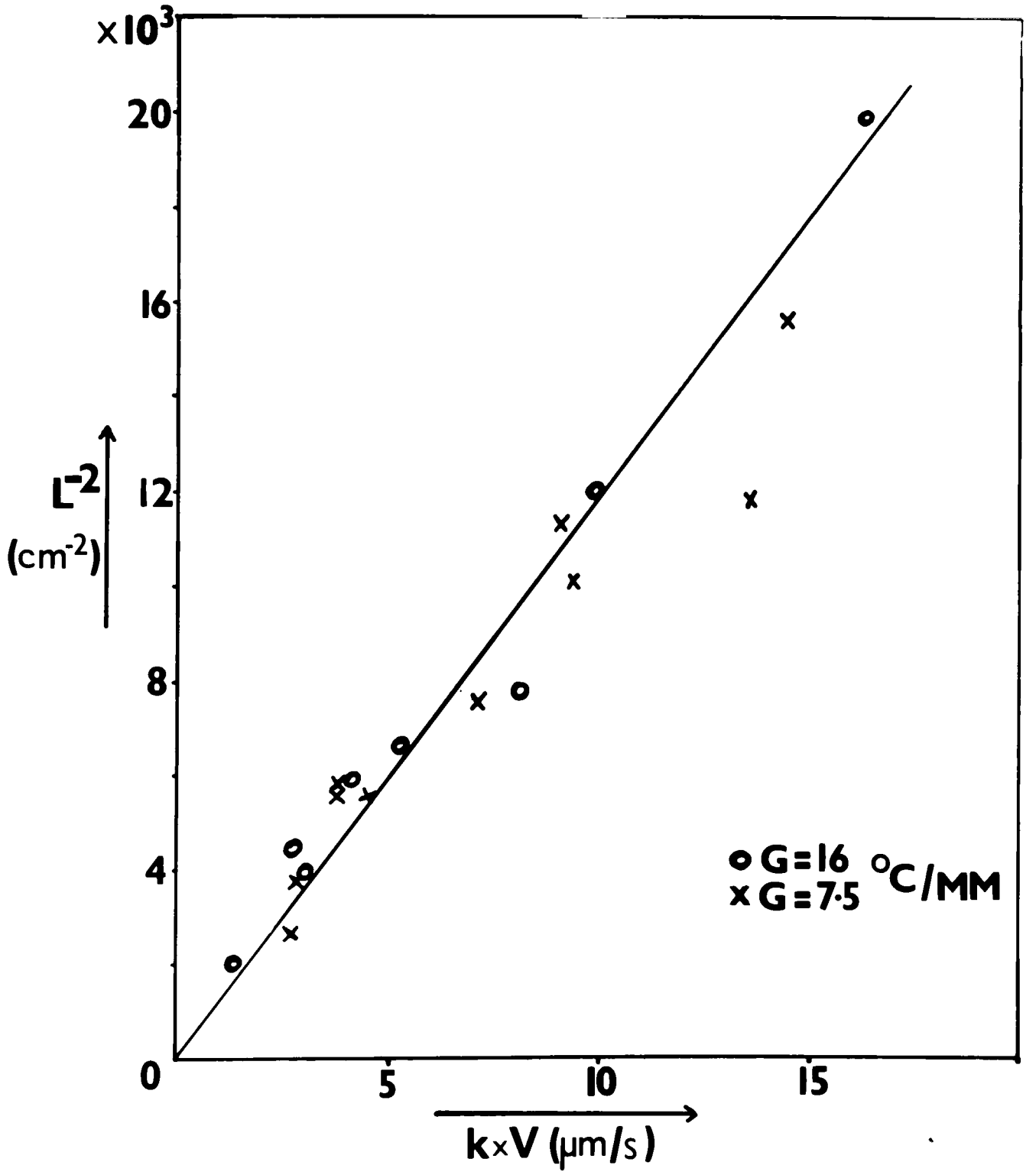
74. Showing the different profiles in longitudinal and transverse section of cells grown at slow (a) and fast (b) growth rates.



75. Photograph of a well-developed elongated cell structure formed by intercellular liquid rearrangement behind the interface. ×230



76. Showing channels of liquid in the branched cell structure being broken up into droplets and pulled out of the positions between the arms. ×1050



77. Variation of the proportionality constant k with the primary spacing of the branched cells.

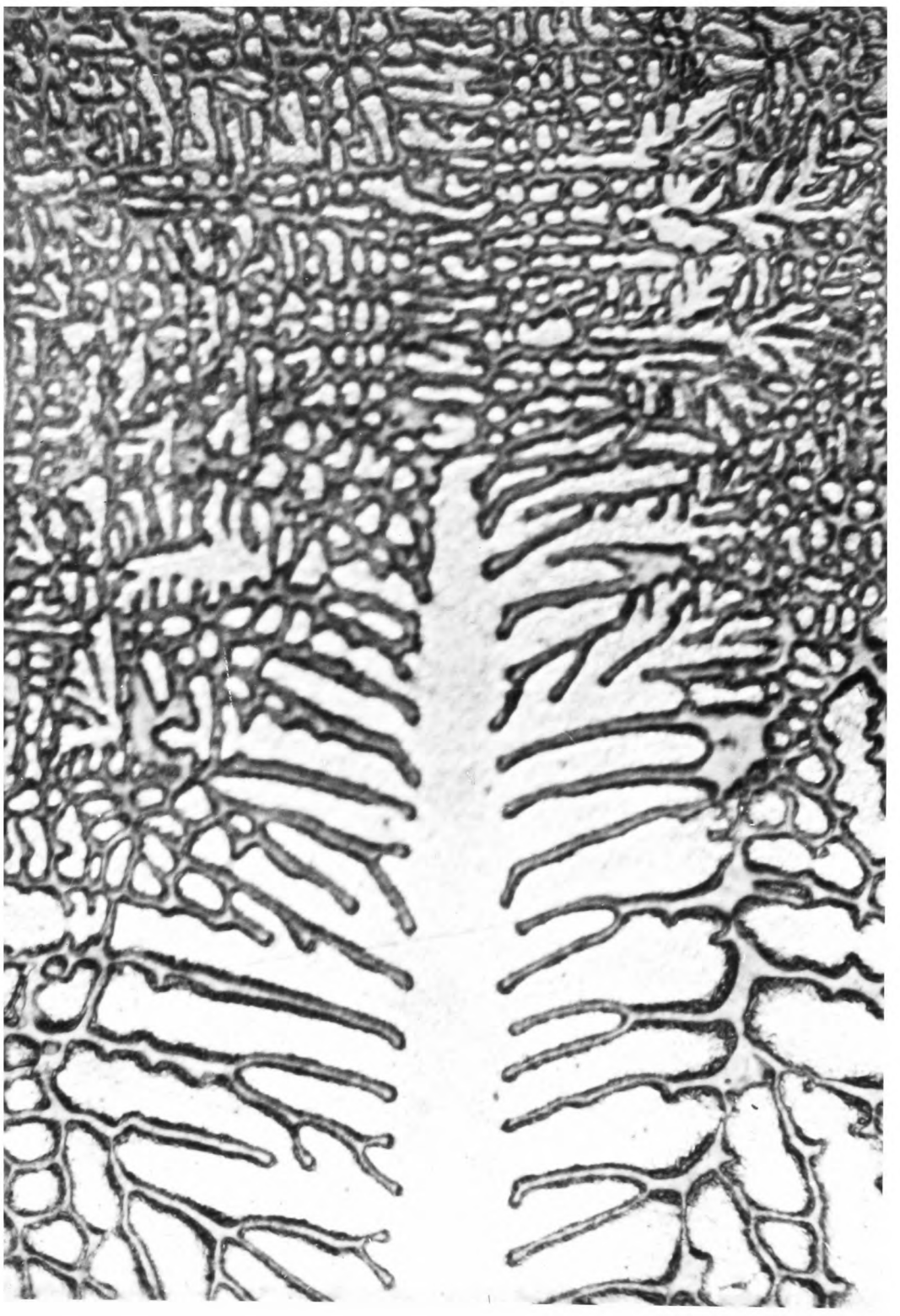


Fig 78 Quenched tip of a dendrite showing how the scale of the secondary arms at the tip is of the same order as the scale of the quenched structure. ×600